The Dissertation Committee for Dipesh Das Certifies that this is The Approved Version of the Following Dissertation:

Synthesis, Characterization and Aggregation Behavior of Carbon Nanotube-Metal Oxide Nanohybrids

Committee:

Navid B. Saleh, Supervisor

Lynn E. Katz

Mary J. Kirisits

Desmond F. Lawler

Jamie R. Lead

Marissa N. Rylander

Synthesis, Characterization and Aggregation Behavior of Carbon Nanotube-Metal Oxide Nanohybrids

by

Dipesh Das, B.S.; M.S.

Dissertation

Presented to the Faculty of the Graduate School of

The University of Texas at Austin

in Partial Fulfillment

of the Requirements

for the Degree of

Doctor of Philosophy

The University of Texas at Austin

May 2017

Dedication

My Late Grandfather, Gopal Chandra Sarkar

Acknowledgements

On my Journey to the finish line of my graduate studies, I have countless people to thank. The continuous support and well wishes of these people kept me going to achieve the ultimate goal in my graduate studies. These people have more contribution than mine towards this achievement.

First of all, I would like to express my deepest gratitude to my PhD supervisor, my mentor Dr. Navid Saleh. I cannot thank him enough for his invaluable guidance, tremendous patience, and extraordinary mentorship in the course of my dissertation research. I am indebted to him forever for letting me join his research group and trusting me with all his heart. He taught me how to write technical papers and how to present my research as a story. He has supported me not only on my academics but also in my personal life. He has always treated me as family and has always been a source of inspiration in the toughest times of my academic life. I could not have asked for more from him as my PhD advisor.

I would also like to thank all the members of my dissertation committee for their continuous support and amazing inputs in my research. Despite having super busy schedules, they have always been available for me whenever I asked them for their advice. I am grateful to Dr. Lynn Katz for her insights towards my research. Without her suggestions, it would have been difficult for me to design my research plan. In my final days, whenever I got stuck, I asked for her advice and she always pointed me to the right

direction. Her class “Water Pollution Chemistry” is one of my most favorite classes of all time. In that class, she taught me the coolest thing in environmental engineering that I could ever learn: “how to solve critical water chemistry problems in your head”. I also thank Dr. Desmond Lawler for his comments about my research in my proposal defense. He made me look at my research from a different angle which ultimately pushed me to expand my area of research. I also had the opportunity of taking his “Physico-chemical Treatment Processes” course which is, in my opinion, one of the best classes an environmental engineering student can ever have. I cannot describe how much I learnt from that class. His door was always open for me whenever I had any question regarding that course and the discussions we had about those questions was priceless. He has been and will always be a guardian to me as he is for all EWRE students. I thank Dr. Mary Jo Kirisits for her comments on my dissertation proposal as well as for being an amazing and dedicated teacher. Her ‘Environmental Microbiology’ course is one of the first courses I took at UT Austin and the experience made me realize what I had been missing all these years. The passion and dedication she had for that class is indescribable. She is also one of the kindest persons I have ever met. Her kind and inspirational words always boosted my self-confidence. I would also like to thank Dr. Nichole Rylander to take the time out of her busy schedule to serve as one of my dissertation committee members and giving valuable comments on my proposal defense. I am grateful to Dr. Jamie Lead for agreeing to be in my dissertation committee and carefully reviewing my dissertation proposal. I am grateful to him for allowing me to work in his lab for a semester. He was one of my earliest mentors along with Dr. Saleh and taught me how to think critically. I also thank Dr. Gerald Speitel

Jr. for teaching one of the most interesting and enjoyable courses “Biological Wastewater Treatment/Sludge Processing”. I learned a lot from him about environmental engineering in general while taking this course.

I intend to extend my gratitude to Dr. Karalee Jervis for training me at the HRTEM, STEM, EDS. I also thank Dr. Hugo Celio for helping me with XPS. I thank Dr. Shouliang Zhang for training me on the SEM and at times helping me with HRTEM, Dr. Steve Swinnea for XRD training and Dr. Damon Smith for clean room training. Many thanks to Ms. Velma Vela, Ms. Aurea G. Zegarra-Coronado, Ms. Melissa Pollard, Ms. RoseAnna Goewey, Ms. Griselda Trevino, Ms. Shamma Haque, Ms. Laura Klopfenstein, and Ms. Sharon Bernard for helping me with all the administrative issues. I also thank Mr. Charles Perego, Mr. Lamont Prosser, Mr. Danny Quiroz, Mr. Phil Tomlin, and Mr. Michael Williams to make my life easier at UT Austin.

I would like to express my deepest appreciation to the current and past members of SusNWaTr research group. I thank Dr. Iftheker Khan for his advice throughout my PhD life. I thank my friends Dr. Nabiul Afrooz and Dr. Nirupam Aich for their assistance, advice and suggestions from the very day I joined Dr. Saleh’s research group. Thanks to Jaime Plazas-Tuttle for being an amazing groupmate and above all for his friendship. I also thank him for his extraordinary graphical interpretation of one of my research projects. I thank Indu for working alongside me in a project and helping me in the lab. I thank Stetson, Christine, Allison, Anna and Craig for their friendship and support. I thank my undergraduate mentee Sneha, for helping me in my research. I also thank my other mentees Erica, Cindy, Sarah, and Rachel without whom working in the lab could not be as fun as it

was. I am also very grateful to Tongren Zhu from Dr. Lawler's research group who helped me in my research with his Matlab programming skills and Erin Burns who helped me with one of the critical experiments I had to perform for my research. I also thank all the members of EWRE research group, specifically Bryant, Sarah, Farith, Soyoon, Sungmin, Julien, Jim, Sarah, Shehzad, Justin, Joon, John, for making me feel EWRE as my second family.

Finally, I am grateful to my family, my parents and my sister, for their endless unconditional love, care and support. Without their love and encouragement, I wouldn't have been able to be anywhere near where I am right now in my life. I would like to thank my late grandparents and my extended family for their love and support. I would like to thank my friends back in Bangladesh and here for their friendship. Last, but not the least, very special thanks to my friend, Papu, for bearing with me for long 6 years in spite of living 1500 miles away. She was always there to lift my spirits up no matter how tough the situation might be.

Synthesis, Characterization, and Aggregation Behavior of Carbon Nanotube-Metal Oxide Nanohybrids

Dipesh Das, Ph.D.

The University of Texas at Austin, 2017

Supervisor: Navid B. Saleh

Extracting multifunctional benefits by combining multiple nano-scale materials has driven materials science to develop nano-heterostructures, which are known as nanohybrids (NHs). Many such composite materials have been researched for applications in the energy sector and in biomedical devices and processes. Among these NHs, carbon nanotubes combined with metal oxides (MOs) are one of the most studied materials that provide unique advantages as electrocatalyst supports, and are currently being commercialized as embedded electrodes for fuels cells. NHs are not only a new class of complex materials but also brings in novel physicochemical properties that most likely cannot be captured by the sum of the properties of their components materials. Thus, understanding the environmental health and safety (EHS) of this new class of composite NHs is imperative. The first challenge that the nano-EHS community faces is to synthesize these materials with a range of MO loadings or composition under a controlled and comparable set of experimental conditions.

In this dissertation, a set of carbonaceous-metal oxide NHs have been synthesized and characterized under comparable synthesis conditions. After synthesis, the underlying mechanisms of metal oxide formation on multiwalled carbon nanotubes (MWNT) surfaces has been enumerated, and finally, aggregation behavior of a select NH and its components has been assessed as a function of the metal oxide loading. A modified sol-gel technique has been developed to grow TiO_2, ZnO, Er_2O_3, and Pr_6O_{11} nanocrystals on MWNT surfaces. The novelty of this technique is that, by varying reagent composition, metal oxide content on the MWNT surfaces can be controlled, keeping all other parameters unchanged. The modified synthesis protocol has been successfully developed to produce a relatively large amount of NHs (100s of mg per batch of synthesis), adequate for systematic nano EHS studies. Following detailed characterization of the materials, underlying hybridization and MO crystal formation mechanism(s) have been enumerated. Furthermore, standard electron potential of the metal species (while considering electron transfer between their oxidized state to zero valent form) has been found to be the controlling factor for the formation of metal or metal oxide crystals from the precursors on MWNT surfaces, using the sol-gel synthesis technique.

Self-aggregation, one of the dominant environmental processes that particles undergo upon release into aquatic environment, has been assessed for one of the most used and commercialized NHs MWNT-TiO_2 and its components. This study investigated the role of TiO_2 loading on the aggregation behavior, MWNT-TiO_2 NH with three different TiO_2 loadings. Results suggested that TiO_2 loading on MWNT surfaces control aggregation behavior of the composite NHs. NHs with all TiO_2 loading demonstrated strong

dependence on electrokinetics. Deoxygenation of the NHs with decreased TiO_2 loading due to the NH synthesis process appeared to be a key contributor on the electrokinetics of the NHs. The van der Waals interaction forces of the NHs decreased with decrease in TiO_2 loading. This study also concluded that classical DLVO theory may be inadequate to capture the aggregation behavior of the NHs.

The controlled synthesis technique developed during this research, as well as the mechanisms of metal vs. metal oxide formation identified will be valuable to prepare a large set of NHs for nano-EHS studies. Aggregation behavior of the composites can be very complex in nature and cannot be predicted form the sum of the behavior of their component materials. The deviation of DLVO prediction from the experimental aggregation data calls for further investigation on direct measurement of other complex surface properties of the NHs upon hybridization such as surface roughness and surface charge heterogeneity.

Table of Contents

List of Tables

List of Figures

Chapter 1: Introduction

1.1 INTRODUCTION

Unique chemical and physical properties that arise as the material size is decreased to nanometer scale encouraged research and development of nanomaterials (NMs) over the past three decades. Since the discovery of Fullerene C_{60} in 1985[1], NMs have become an intrinsic part of our everyday life and are being used in personal care products[2], electronics,[3] conventional and renewable energy sources,[4] catalyst based industrial production,[5] infrastructure,[6] transportation,[7] food,[8] textile,[9] biomedical imaging and medicine,[10] environmental remediation and water treatment[11] and so on. Commercialization of nano-enabled products is ever increasing and grosses more than $1trillion dollars per year worldwide. Recently, material synthesis has progressed from singular NMs to multicomponent nano-heterostructures, which are known as nanohybrids (NHs) [15,16]. Such a shift in materials design has taken place to extract multifunctional benefits from the composite materials.

Nanohybrids (NHs) are conjugates of two or more singular nanostructures of unique chemical origin or are composites of nanostructures and organic macromolecules[12]. They can be categorized based on the origin of the singular materials; i.e., carbon-carbon, carbon-metal, metal-metal, and organic molecule coated carbon/metal NHs[12]. MOs supported on carbon NM are one such composite nanomaterial that has not only been studied as a research-grade material but also has been incorporated into a number of applications. Carbon nanotube-TiO_2, one of the most prominent carbonaceous-metal oxide NHs, is used as catalyst supports (for Pt catalyst) in the fuel cell industry. Due to an unprecedented growth in the fuel cell industry (86% increase over the past decade) and with an allocated Senate approved budget of $147.8M for this sector, it is anticipated that millions of kg of carbon nanotube supported metal oxide electrocatalysts will be in the market

or in use by 2050[13, 14]. Thus, this new class of NHs is highly relevant for release and interaction in the environment.

One of the major challenges with the environmental health and safety (EHS) studies of NHs is synthesis of these materials for a wide range of MO loading or composition, under a controlled and comparable set of experimental conditions. Numerous hybridization techniques have been reported for producing CNT-MO NHs, which can be divided into two categories- *ex situ* and *in situ*. For the *ex situ* methods, MOs are synthesized separately prior to hybridization with CNTs, aided by a linker between the MOs and the CNTs. For the *in situ* methods, appropriate precursors are used to grow the MO nanocrystals on the CNT backbone. The *in situ* methods include sol-gel[15-23], hydrothermal[24-27], solvothermal[28], chemical[29] and physical[30] vapor deposition, electrochemical[31], electrodeposition[32], thermal decomposition[33], direct deposition[34, 35], direct mixing[36], microwave irradiation[37], and atomic layer deposition[32], among others. The synthesis conditions for these different methods vary widely; e.g., use of different chemicals to functionalize CNTs, use of different solvents, variations in pH, temperature, and pressure, etc. As most of these synthesis processes focus on the application of the NHs, the material homogeneity and reproducibility aspect is generally overlooked, which are of paramount importance for NH EHS studies. Furthermore, a common synthesis technique (that can synthesize these NHs using any metal species) with comparable experimental conditions across the material class needs to be developed to enable systematic nano-EHS studies. It is thus imperative to develop such a technique as well as to understand the underlying mechanisms of nanocrystal formation on nanotube surfaces to assess potential applicability of the developed method to synthesize a wide variety of metal/MO.

A wide range of MOs can be hybridized on MWNTs using a variety of different synthesis techniques (Table 1.1). Key synthesis conditions, i.e., solvent type, reaction time, temperature, and

pressure, and calcination temperature vary among the techniques. Sol-gel and hydrothermal synthesis processes have been reported to hybridize the most metal oxides on CNTs. These two synthesis processes utilize wet chemical approaches and do not require expensive and elaborate experimental setup as required in electrodeposition and in chemical and physical vapor deposition (Table 1.1). So-gel technique is also preferred due to the continuous stirring conditions during formation of the nanocrystals, which allow for achieving better homogeneity in terms of size and distribution of the formed crystals. Furthermore, this technique does not require high pressure during synthesis, which simplifies the process and facilitates adjustment and modification of the method. Due to the stated advantages of the sol-gel process, it has been chosen as the preferred synthesis technique in this research.

Table 1.1: Key parameters and advantages and disadvantages of MWNT-MO Synthesis Processes

Synthesis Technique	Metal oxides	Synthesis Parameters	Advantages	Disadvantages
Sol-gel	Al_2O_3[38], CeO_2[39], Co_3O_4[40], NiO[41], RuO_2[42], SiO_2[43], SnO_2[44], TiO_2[45], ZnO[46]	-Reaction temperature: room temperature to 140 °C - Reaction time: few hours to days -Pressure: ambient -pH: low to high, depending on the material -Solvents: alcohols, other water miscible organic solvents	-Simple, wet chemical process -Continuous mixing enables achieving better particle distribution on CNT surfaces - MO nanocrystal size can be controlled -A range of MOs can be hybridized with CNTs	-CNTs needs to be acid etched to have surface binding groups
Hydrothermal	Al_2O_3[47], CeO_2[48], Cu_2O[49], Eu_2O_3[50], Fe_xO_y[51], RuO_2[52], SnO_2[53], TiO_2[54], ZnO[55], ZrO_2[56]	-Reaction temperature: 50 °C to 200 °C -Reaction time: several hours -Solvents: water and organic solvents -Can also be used at supercritical CO_2 environment at very high pressure Pressure: 0.5 MPa to 9 MPa	-Relatively simple, wet chemical method - A range of MOs can be hybridized with CNTs	-Reaction takes place in a stagnant condition resulting in unattached MO crystal growth -Requires high pressure -May result in large, undesirable MO size -Not as simple and scalable as sol-gel process

Table 1.1: Key parameters and advantages and disadvantages of MWNT-MO Synthesis Processes (Cont.)

Solvothermal	TiO_2[57], CeO_2[58]	-Similar parameters as hydrothermal process -Reaction only with organic solvents	-Adjustable parameters for desired MO nanocrystal size	- Reaction takes place in a stagnant condition resulting in unattached MO crystal growth -Not designed to be used with water as a solvent
Chemical vapor deposition	Al_2O_3[59], Co_3O_4[41], MnO_2[60], NiO[61], RuO_2[62], SnO_2[63], TiO_2[64], ZrO_2[65]	-MO deposition from the vapor phase -Reaction temperature: room temperature -Reaction time: few seconds to hours	-Claimed to have achieved uniform MO coating on CNT surfaces -Works well for pristine CNTs	-Requires expensive and elaborate experimental setup -Not ideal for aqueous suspension preparation
Physical vapor deposition	Al_2O_3[66], HfO_2[30], MgO[67], RuO_2[68], SiO_2[69], ZnO[70]	-MOs are laser deposited or sputter coated	-Claimed to have uniform MO coatings -Works well for pristine CNTs	-Requires expensive and elaborate experimental setup -Not ideal for aqueous suspension preparation
Direct mixing	TiO_2[36]	-Mechanical mixing of pre-synthesized MO crystals and CNTs	-Simple technique	-Severe lack of uniformity and reproducibility -Co-association may be achieved, but not hybridization

Table 1.1: Key parameters and advantages and disadvantages of MWNT-MO Synthesis Processes (Cont.)

Microwave irradiation	TiO_2[71], SnO_2[72]	-Reaction time: few seconds -No additional heat required other than heat generated from microwave irradiation	-Simple technique -Can be energy efficient due to short reaction time	-Particle size can widely vary depending on the microwave power -Lack of mixing resulting in compromised material uniformity
Noncovalent bonding	Al_2O_3[73], Eu_2O_3[74], TiO_2[75], ZrO_2[76]	-Reaction time: several minutes to hours -Reaction temperature: room temperature	-Uniform MO coverage on the MWNT surface -Calcination may not be necessary for crystal growth	-Surfactant or polymer addition necessary -Toxic solvents utilized to facilitate π-π stacking
Ex situ: covalent	SiO_2[77], TiO_2[78]	-MO are produced separately and then linked with CNTs functionalized with different functional groups -Temperature: ambient Reaction time: several hours	-Calcination may not be necessary -Stronger bond between MWNT and MO nanocrystals	-Linker molecules needed, which can create bonds with both MWNTs and MO nanocrystals -Low material yield
Electrodeposition	Fe_xO_y[79], MnO_2[80], RuO_2[81], TiO_2[82]	-High ionic strength -Constant voltage application necessary	-Claimed to produce large quantity of material	-Requires expensive and elaborate experimental setup -Not ideal for aqueous suspension preparation

Table 1.1: Key parameters and advantages and disadvantages of MWNT-MO Synthesis Processes (Cont.)

Microemulsion	TiO_2[83], ZnO[84]	-Reaction Temperature: room temperature to 110 °C -Surfactants with aromatic groups and non-aqueous phase used	-Well distributed MO crystals	-Use of surfactants (often toxic) and oil for emulsification

Assessing EHS of NMs can involve a large set of studies where fate, transport, and toxicity of the NMs will need to be studied systematically for different aquatic conditions. Self-aggregation is one of the predominant environmental processes that particles undergo upon release into aquatic environment, and this process also dictates subsequent fate of the particulates[85, 86]. Particle aggregation of singular nanostructures has been studied extensively[87-92]. Surface potential, responsible for electrostatic double layer repulsion and the intrinsic van der Waals attraction forces of NMs are considered as the most important nanomaterial properties that influence their aggregation behavior[87-92]. However, there is a major data gap in understanding the aggregation behavior of composite NMs. Such studies on composite NHs may not be necessary if the exhibited behavior of the composites can be predicted as the sum of the behaviors of the parts. However, upon hybridization, the NH surfaces not only alter its chemical identity but can also introduce complex attributes that are highly relevant to aggregation processes of these materials. Hybridization of a singular nanomaterial with a secondary nano-scale entity of unique chemical origin will alter the surface properties (e.g., surface potential, roughness) as well as alter van der Waals interaction energy[93] and thus will strongly influence this dominant environmental process (of aggregation)[94]. Such changes in surface properties and a variable van der Waals interaction energy presented at the interface of the composite materials can be responsible to dismiss the linear superposition rule in predicting EHS of these composite materials.

1.2 OBJECTIVES AND SCOPE

This dissertation aims to develop a simple, common synthesis technique for hybridizing a wide range of metal oxide (MO) nanocrystals with multiwalled carbon nanotubes (MWNTs) by modifying a sol-gel NH synthesis process, propose dominant mechanism of crystal formation on MWNT surfaces (thus enumerate the utility of the developed method), and finally assess aggregation behavior of an already commercialized NH, namely, MWNT-TiO_2, as a function of TiO_2 hybridization (% loading) on MWNT surfaces.

In this dissertation, a modified sol-gel synthesis technique has been utilized to hybridize MWNTs with TiO_2, ZnO, Er_2O_3, and Pr_2O_3. Possible hybridization mechanism(s) describing formation of the nanocrystals has also been proposed. The role of standard electrode potential of the metal species on formation of metal vs. metal oxide nanocrystals under comparable synthesis conditions has also been evaluated. Finally, a set of MWNT-TiO_2 NHs with a wide range of TiO_2 loading (C to Ti molar ratio of 1:0.1, 1:0.05 and 1:0.033) onto the MWNTs has been synthesized and characterized.

It is to be noted that the modification of the sol-gel technique and experimental setup was first prepared, which were followed by subsequent environmental implications research reported in this dissertation and an environmental application research reported elsewhere[95]. The synthesis and characterization of the materials reported herein were performed with an objective of understanding mechanisms of crystal formation and assessing aggregation behavior of these complex heterostructures. The parallel dissertation work utilized the modified sol-gel method developed within the scope of this dissertation

and prepared a set of MWNT-Er_2O_3 NHs with an objective of exploring MWNTs' ability to harness microwave radiation and Er_2O_3's spectral conversion capacity to inactivate waterborne pathogens[95].

1.3 Research Hypotheses

Hypothesis 1: Sol-gel synthesis process can be modified to synthesize a wide range of MWNT-MO NHs with comparable physicochemical properties; i.e., size, surface charge, and MO crystallinity.

Hypothesis 2: Metal or metal oxide nano-crystal formation on MWNT surfaces (utilizing a sol-gel method) will be a function of the standard electrode potential of the metal species.

Hypothesis 3: The aggregation propensity of the MWNT-TiO_2 NHs will decrease with decreasing TiO_2 nanocrystal content in the NH and aggregation behavior of the components may not capture the aggregation of the composite NH.

1.4 Approach and Methodology

The proposed research is accomplished by completing of the following tasks.

Task 1: Synthesis and characterization of MWNT-MO NHs for a wide range of metal species.

Task 2: Mechanistic assessment of MO crystal formation on MWNT surfaces and evaluation of the role of standard electrode potential in metal vs. metal oxide growth during the sol-gel synthesis.

Task 3: Assessment of aggregation behavior of MWNT-TiO_2 NHs and its components as

a function of TiO_2 loading.

1.5 Organization of the Dissertation

The dissertation is organized in five chapters and three appendices. Chapter 1 presents the introduction to this dissertation with problem statement and significance, research objectives, hypotheses, and approach and methodology. The experimental details and results are compiled in chapters 2, 3, and 4. These chapters are either published (Chapter 2) or are being prepared for publication (Chapters 3 and 4) in peer-reviewed journals. Chapter 5 presents the summary of key findings and includes recommendations for future work.

Chapter 2 presents the details of the synthesis technique and results on materials characterization for the synthesized MWNT-MO NHs. NHs synthesized using this method include MWNT-TiO_2, MWNT-ZnO, MWNT-Er_2O_3, and MWNT-Pr_6O_{11}, which have been characterized with a suite of characterization tools to evaluate the physical morphology, crystallinity, chemical composition, chemical bonding between the MO and the MWNT surface, and reproducibility of the synthesis technique. This work was led by the candidate and co-authored by Jaime Plazas Tuttle, Indu Venu Sabaraya, Sneha S. Jain, Tara Sabo-Attwood, and Navid B. Saleh and appears as a peer-reviewed article in *Environmental Science: Nano* (January 2017) with the title: "An Elegant Method for Large Scale Synthesis of Metal Oxide-Carbon Nanotube Nanohybrids for Nano-environmental Application and Implication Studies"[88].

Chapter 3 presents experimental results and discussion to enumerate the crystal formation mechanism (with X-ray characterization) for the metal oxides synthesized in Chapter 2. To assess the applicability of sol-gel method for hybridizing metal vs. metal oxides with MWNTs, two other metal species, Cu and Ag were chosen. Formation of metal crystals (not metal oxides) with these metals partially validated hypothesis 2. This work was led by the candidate and is now in preparation for publication with the following proposed title: " Insights on Metal Oxide and Metal Nanocrystal Formation During the Sol-gel Hybridization Process".

Chapter 4 presents results on aggregation behavior of MWNT-TiO_2 NHs with three different TiO_2 loadings. Aggregation study was performed with dynamic light scattering (DLS) for the NHs and the component materials in a wide range of chemical conditions. This work was led by the candidate and is currently in preparation for publication with the following proposed title: "Aggregation behavior of multiwalled carbon nanotube-titanium dioxide nanohybrids: Role of titanium dioxide loading".

The final chapter (Chapter 5) presents the summary, conclusions, environmental implications, and future recommendations relevant to the synthesis of MWNT-MO NHs and their EHS studies.

1.6 LITERATURE CITED

1. Smalley, R. E., Discovering the fullerenes. *Reviews of Modern Physics* **1997,** *69*, (3), 723.
2. Keller, A. A.; Vosti, W.; Wang, H.; Lazareva, A., Release of engineered nanomaterials from personal care products throughout their life cycle. *Journal of nanoparticle research* **2014,** *16*, (7), 2489.
3. Jariwala, D.; Sangwan, V. K.; Lauhon, L. J.; Marks, T. J.; Hersam, M. C., Carbon nanomaterials for electronics, optoelectronics, photovoltaics, and sensing. *Chemical Society Reviews* **2013,** *42*, (7), 2824-2860.
4. Chambers, B. A.; Afrooz, A. R. M. N.; Bae, S.; Aich, N.; Katz, L.; Saleh, N. B.; Kirisits, M. J., Effects of Chloride and Ionic Strength on Physical Morphology, Dissolution, and Bacterial Toxicity of Silver Nanoparticles. *Environmental science & technology* **2014,** *48*, (1), 761-769.
5. Serp, P.; Philippot, K., *Nanomaterials in catalysis*. Wiley: 2012.
6. Zohhadi, N. Functionalized graphitic nanoreinforcement for cement cmposites. University of South Carolina, Columbia, SC, 2014.
7. Khattak, M. J.; Khattab, A.; Rizvi, H. R.; Zhang, P., The impact of carbon nano-fiber modification on asphalt binder rheology. *Construction and Building Materials* **2012,** *30*, 257-264.
8. Arora, A.; Padua, G., Review: nanocomposites in food packaging. *Journal of Food science* **2010,** *75*, (1), R43-R49.
9. Dastjerdi, R.; Montazer, M., A review on the application of inorganic nano-structured materials in the modification of textiles: focus on anti-microbial properties. *Colloids and Surfaces B: Biointerfaces* **2010,** *79*, (1), 5-18.
10. Zhang, L.; Gu, F.; Chan, J.; Wang, A.; Langer, R.; Farokhzad, O., Nanoparticles in medicine: therapeutic applications and developments. *Clinical Pharmacology & Therapeutics* **2007,** *83*, (5), 761-769.
11. Mauter, M. S.; Elimelech, M., Environmental applications of carbon-based nanomaterials. *Environ. Sci. Technol.* **2008,** *42*, (16), 5843-5859.
12. Aich, N.; Plazas-Tuttle, J.; Lead, J.; Saleh, N., A Critical Review of Nanohybrids: Synthesis, Applications, and Environmental Implications. *Environmental Chemistry* **2014,** *11*, 609-623.
13. Usui, T. *World budget of platinum*; Stanford University: 2010.
14. Wilburn, D. R.; Bleiwas, D. I. *Platinum-group metals-world supply and demand* U.S. Geological Survey: 2004.
15. Nguyen, M. T.; Nguyen, C. K.; Vu, T. M. P.; Van Duong, Q.; Pham, T. L.; Nguyen, T. C., A study on carbon nanotube titanium dioxide hybrids: experiment and calculation. *Advances in Natural Sciences: Nanoscience and Nanotechnology* **2014,** *5*, (4), 045018.
16. Eder, D.; Windle, A. H., Carbon–inorganic hybrid materials: the carbon-nanotube/TiO2 interface. *Advanced Materials* **2008,** *20*, (9), 1787-1793.

17. Yang, C.-F.; Hsu, W.-C.; Wu, S.-M.; Su, C.-C., Elucidating how surface functionalization of multiwalled carbon nanotube affects nanostructured MWCNT/titania hybrid materials. *Journal of Nanomaterials* **2015,** *2015*.
18. Haldorai, Y.; Rengaraj, A.; Lee, J.-B.; Huh, Y. S.; Han, Y.-K., Highly efficient hydrogen production via water splitting using Pt@ MWNT/TiO 2 ternary hybrid composite as a catalyst under UV–visible light. *Synth. Met.* **2015,** *199*, 345-352.
19. Jitianu, A.; Cacciaguerra, T.; Berger, M.-H.; Benoit, R.; Béguin, F.; Bonnamy, S., New carbon multiwall nanotubes–TiO 2 nanocomposites obtained by the sol–gel method. *Journal of non-crystalline solids* **2004,** *345*, 596-600.
20. Ding, M.; Sorescu, D. C.; Star, A., Photoinduced Charge Transfer and Acetone Sensitivity of Single-Walled Carbon Nanotube–Titanium Dioxide Hybrids. *Journal of the American Chemical Society* **2013,** *135*, (24), 9015-9022.
21. Zarezade, M.; Ghasemi, S.; Gholami, M. R., The effect of multiwalled carbon nanotubes and activated carbon on the morphology and photocatalytic activity of TiO 2/C hybrid materials. *Catalysis Science & Technology* **2011,** *1*, (2), 279-284.
22. Khanderi, J.; Hoffmann, R. C.; Gurlo, A.; Schneider, J. J., Synthesis and sensoric response of ZnO decorated carbon nanotubes. *Journal of Materials Chemistry* **2009,** *19*, (28), 5039-5046.
23. Song, W.-L.; Cao, M.-S.; Wen, B.; Hou, Z.-L.; Cheng, J.; Yuan, J., Synthesis of zinc oxide particles coated multiwalled carbon nanotubes: Dielectric properties, electromagnetic interference shielding and microwave absorption. *Materials Research Bulletin* **2012,** *47*, (7), 1747-1754.
24. Byrappa, K.; Dayananda, A.; Sajan, C.; Basavalingu, B.; Shayan, M.; Soga, K.; Yoshimura, M., Hydrothermal preparation of ZnO: CNT and TiO2: CNT composites and their photocatalytic applications. *Journal of Materials Science* **2008,** *43*, (7), 2348-2355.
25. Dai, K.; Zhang, X.; Fan, K.; Peng, T.; Wei, B., Hydrothermal synthesis of single-walled carbon nanotube–TiO 2 hybrid and its photocatalytic activity. *Applied Surface Science* **2013,** *270*, 238-244.
26. Liu, C.; Chen, H.; Dai, K.; Xue, A.; Chen, H.; Huang, Q., Synthesis, characterization, and its photocatalytic activity of double-walled carbon nanotubes-TiO 2 hybrid. *Materials Research Bulletin* **2013,** *48*, (4), 1499-1505.
27. Saleh, T. A.; Gondal, M.; Drmosh, Q., Preparation of a MWCNT/ZnO nanocomposite and its photocatalytic activity for the removal of cyanide from water using a laser. *Nanotechnology* **2010,** *21*, (49), 495705.
28. Tian, L. H.; Ye, L. Q.; Deng, K. J.; Zan, L., TiO2/carbon nanotube hybrid nanostructures: Solvothermal synthesis and their visible light photocatalytic activity. *Journal of Solid State Chemistry* **2011,** *184*, (6), 1465-1471.
29. Gomathi, A.; Vivekchand, S.; Govindaraj, A.; Rao, C., Chemically bonded ceramic oxide coatings on carbon nanotubes and inorganic nanowires. *Advanced Materials* **2005,** *17*, (22), 2757-2761.
30. Ikuno, T.; Yasuda, T.; Honda, S.-i.; Oura, K.; Katayama, M.; Lee, J.-G.; Mori, H., Coating carbon nanotubes with inorganic materials by pulsed laser deposition. *Journal of applied physics* **2005,** *98*, (11), 114305.

31. Xie, X.; Gao, L., Characterization of a manganese dioxide/carbon nanotube composite fabricated using an in situ coating method. *Carbon* **2007,** *45*, (12), 2365-2373.
32. Green, J. M.; Dong, L.; Gutu, T.; Jiao, J.; Conley Jr, J. F.; Ono, Y., ZnO-nanoparticle-coated carbon nanotubes demonstrating enhanced electron field-emission properties. *Journal of applied physics* **2006,** *99*, (9), 094308.
33. Guo, G.; Guo, J.; Tao, D.; Choy, W.; Zhao, L.; Qian, W.; Wang, Z., A Simple method to prepare multi-walled carbon nanotube/ZnO nanoparticle composites. *Applied Physics A* **2007,** *89*, (2), 525-528.
34. Kim, B. C.; Kim, S.; Chung, J.; Chen, J.; Park, S.; Wallace, G. G., Charge storage in carbon nanotube–TiO 2 hybrid nanoparticles. *Synth. Met.* **2012,** *162*, (7), 650-654.
35. Yan, X. M.; Pan, D. Y.; Li, Z.; Zhao, B.; Zhang, J. C.; Wu, M. H., Facile synthesis of solution-disposable carbon nanotube-TiO2 hybrids in organic media. *Materials Letters* **2010,** *64*, (15), 1694-1697.
36. Ueda, T.; Takahashi, K.; Mitsugi, F.; Ikegami, T., Preparation of single-walled carbon nanotube/TiO 2 hybrid atmospheric gas sensor operated at ambient temperature. *Diamond and Related Materials* **2009,** *18*, (2), 493-496.
37. Du, Y.; Hao, C.; Wang, G., Preparation of floral-patterned ZnO/MWCNT heterogeneity structure using microwave irradiation heating method. *Materials Letters* **2008,** *62*, (1), 30-32.
38. Mo, C. B.; Cha, S. I.; Kim, K. T.; Lee, K. H.; Hong, S. H., Fabrication of carbon nanotube reinforced alumina matrix nanocomposite by sol–gel process. *Materials Science and Engineering: A* **2005,** *395*, (1), 124-128.
39. Li, Y.; Ding, J.; Chen, J.; Xu, C.; Wei, B.; Liang, J.; Wu, D., Preparation of ceria nanoparticles supported on carbon nanotubes. *Materials Research Bulletin* **2002,** *37*, (2), 313-318.
40. Wu, R.-J.; Wu, J.-G.; Yu, M.-R.; Tsai, T.-K.; Yeh, C.-T., Promotive effect of CNT on Co 3 O 4–SnO 2 in a semiconductor-type CO sensor working at room temperature. *Sensors and Actuators B: Chemical* **2008,** *131*, (1), 306-312.
41. Fan, Z.; Chen, J.; Cui, K.; Sun, F.; Xu, Y.; Kuang, Y., Preparation and capacitive properties of cobalt–nickel oxides/carbon nanotube composites. *Electrochimica Acta* **2007,** *52*, (9), 2959-2965.
42. Kahram, M.; Asnavandi, M.; Dolati, A., Synthesis and electrochemical characterization of sol–gel-derived RuO2/carbon nanotube composites. *Journal of Solid State Electrochemistry* **2014,** *18*, (4), 993-1003.
43. Attari, S. G.; Bahrami, A.; Shahna, F. G.; Heidari, M., Single-walled carbon nanotube/silica composite as a novel coating for solid-phase microextraction fiber based on sol-gel technology. *Journal of analytical chemistry* **2015,** *70*, (10), 1192-1198.
44. Gong, J.; Sun, J.; Chen, Q., Micromachined sol–gel carbon nanotube/SnO 2 nanocomposite hydrogen sensor. *Sensors and Actuators B: Chemical* **2008,** *130*, (2), 829-835.
45. Abbas, N.; Shao, G. N.; Haider, M. S.; Imran, S. M.; Park, S. S.; Jeon, S.-J.; Kim, H. T., Inexpensive sol-gel synthesis of multiwalled carbon nanotube-TiO 2 hybrids for high

performance antibacterial materials. *Materials Science and Engineering: C* **2016,** *68*, 780-788.
46. Köse, H.; Karaal, Ş.; Aydın, A. O.; Akbulut, H., A facile synthesis of zinc oxide/multiwalled carbon nanotube nanocomposite lithium ion battery anodes by sol–gel method. *Journal of Power Sources* **2015,** *295*, 235-245.
47. Bi, S.; Su, X.; Hou, G.; Gu, G.; Xiao, Z., Microstructural characterization of alumina-coated multi-walled carbon nanotubes synthesized by hydrothermal crystallization. *Physica B: Condensed Matter* **2010,** *405*, (16), 3312-3315.
48. Kalubarme, R. S.; Kim, Y.-H.; Park, C.-J., One step hydrothermal synthesis of a carbon nanotube/cerium oxide nanocomposite and its electrochemical properties. *Nanotechnology* **2013,** *24*, (36), 365401.
49. Yu, Y.; Ma, L.-L.; Huang, W.-Y.; Du, F.-P.; Jimmy, C. Y.; Yu, J.-G.; Wang, J.-B.; Wong, P.-K., Sonication assisted deposition of Cu 2 O nanoparticles on multiwall carbon nanotubes with polyol process. *Carbon* **2005,** *43*, (3), 670-673.
50. Chen, C.-S.; Chen, X.-H.; Yi, B.; Zhang, G.-B.; Li, F.-J.; Luo, H.-S., Modified multi-walled carbon nanotubes with nano-europium oxide. *Transactions of Nonferrous Metals Society of China* **2007,** *17*, (s1B), s704-s707.
51. Matsui, K.; Kyotani, T.; Tomita, A., Hydrothermal synthesis of nano-sized iron oxide crystals in the cavity of carbon nanotubes. *Molecular Crystals and Liquid Crystals* **2002,** *387*, (1), 1-5.
52. Sun, Z.; Liu, Z.; Han, B.; Miao, S.; Du, J.; Miao, Z., Microstructural and electrochemical characterization of RuO 2/CNT composites synthesized in supercritical diethyl amine. *Carbon* **2006,** *44*, (5), 888-893.
53. Liu, H.; Huang, J.; Li, X.; Liu, J.; Zhang, Y., One-step hydrothermal synthesis of flower-like SnO2/carbon nanotubes composite and its electrochemical properties. *Journal of Sol-Gel Science and Technology* **2012,** *63*, (3), 569-572.
54. Wang, A.; Wang, Y.; Yu, W.; Huang, Z.; Fang, Y.; Long, L.; Song, Y.; Cifuentes, M. P.; Humphrey, M. G.; Zhang, L., TiO 2–multi-walled carbon nanotube nanocomposites: hydrothermal synthesis and temporally-dependent optical properties. *Rsc Advances* **2016,** *6*, (24), 20120-20127.
55. Li, H.; Zhang, X.; Zhu, Y.; Li, R.; Chen, H.; Gao, P.; Zhang, Y.; Li, T.; Liu, Y.; Li, Q., Hydrothermal deposition of a zinc oxide nanorod array on a carbon nanotube film as a piezoelectric generator. *Rsc Advances* **2014,** *4*, (82), 43772-43777.
56. Garmendia, N.; Bilbao, L.; Muñoz, R.; Imbuluzqueta, G.; García, A.; Bustero, I.; Calvo-Barrio, L.; Arbiol, J.; Obieta, I., Zirconia coating of carbon nanotubes by a hydrothermal method. *Journal of Nanoscience and Nanotechnology* **2008,** *8*, (11), 5678-5683.
57. Zhao, L.; Chen, X.; Wang, X.; Zhang, Y.; Wei, W.; Sun, Y.; Antonietti, M.; Titirici, M. M., One-Step Solvothermal Synthesis of a Carbon@ TiO2 Dyade Structure Effectively Promoting Visible-Light Photocatalysis. *Advanced Materials* **2010,** *22*, (30), 3317-3321.
58. Zhang, D.; Pan, C.; Zhang, J.; Shi, L., Solvothermal synthesis of necklace-like carbon nanotube/ceria composites. *Materials Letters* **2008,** *62*, (23), 3821-3823.

59. Keshri, A. K.; Huang, J.; Singh, V.; Choi, W.; Seal, S.; Agarwal, A., Synthesis of aluminum oxide coating with carbon nanotube reinforcement produced by chemical vapor deposition for improved fracture and wear resistance. *Carbon* **2010,** *48*, (2), 431-442.
60. Fan, Z.; Chen, J.; Wang, M.; Cui, K.; Zhou, H.; Kuang, Y., Preparation and characterization of manganese oxide/CNT composites as supercapacitive materials. *Diamond and Related Materials* **2006,** *15*, (9), 1478-1483.
61. Yu, K.-l.; Zou, J.-j.; Ben, Y.-h.; Zhang, Y.-p.; Liu, C.-j., Synthesis of NiO-embedded carbon nanotubes using corona discharge enhanced chemical vapor deposition. *Diamond and Related Materials* **2006,** *15*, (9), 1217-1222.
62. Min, Y. S.; Bae, E. J.; Jeong, K. S.; Cho, Y. J.; Lee, J. H.; Choi, W. B.; Park, G. S., Ruthenium oxide nanotube arrays fabricated by atomic layer deposition using a carbon nanotube template. *Advanced Materials* **2003,** *15*, (12), 1019-1022.
63. Turano, S.; Flicker, J.; Ready, W., Nanoscale coaxial cables produced from vertically aligned carbon nanotube arrays grown via chemical vapor deposition and coated with indium tin oxide via ion assisted deposition. *Carbon* **2008,** *46*, (5), 723-728.
64. Zhang, R.; Zhang, Y.; Zhang, Q.; Xie, H.; Wang, H.; Nie, J.; Wen, Q.; Wei, F., Optical visualization of individual ultralong carbon nanotubes by chemical vapour deposition of titanium dioxide nanoparticles. *Nature communications* **2013,** *4*, 1727.
65. Javey, A.; Kim, H.; Brink, M.; Wang, Q.; Ural, A.; Guo, J.; McIntyre, P.; McEuen, P.; Lundstrom, M.; Dai, H., High-κ dielectrics for advanced carbon-nanotube transistors and logic gates. *Nature materials* **2002,** *1*, (4), 241-246.
66. Ikuno, T.; Katayama, M.; Kamada, K.; Honda, S.-i.; Lee, J.-G.; Mori, H.; Oura, K., Insulator-coated carbon nanotubes synthesized by pulsed laser deposition. *Japanese journal of applied physics* **2003,** *42*, (11B), L1356.
67. Pan, L.; Konishi, Y.; Tanaka, H.; Chakrabarti, S.; Hokushin, S.; Akita, S.; Nakayama, Y., Effect of MgO coating on field emission of a stand-alone carbon nanotube. *Journal of Vacuum Science & Technology B* **2007,** *25*, (5), 1581-1583.
68. Fang, W.-C.; Chyan, O.; Sun, C.-L.; Wu, C.-T.; Chen, C.-P.; Chen, K.-H.; Chen, L.-C.; Huang, J.-H., Arrayed CN x NT–RuO 2 nanocomposites directly grown on Ti-buffered Si substrate for supercapacitor applications. *Electrochemistry Communications* **2007,** *9*, (2), 239-244.
69. Fan, W.; Gao, L., Silica nanobeads-decorated multi-walled carbon nanotubes by vapor-phase method. *Chemistry Letters* **2005,** *34*, (7), 954-955.
70. Borkar, T.; Chang, W. S.; Hwang, J. Y.; Shepherd, N. D.; Banerjee, R., Microstructural and optical properties of nanocrystalline ZnO deposited onto vertically aligned carbon nanotubes by physical vapor deposition. *Materials Research Bulletin* **2012,** *47*, (10), 2756-2759.
71. Nguyen, V. H.; Ren, Y.; Lee, Y. R.; Tuma, D.; Min, B.-K.; Shim, J.-J., Microwave-Assisted Synthesis of Carbon Nanotube-TiO2 Nanocomposites in Ionic Liquid for the Photocatalytic Degradation of Methylene Blue. *Synthesis and Reactivity in Inorganic, Metal-Organic, and Nano-Metal Chemistry* **2012,** *42*, (2), 296-301.

72. Motshekga, S. C.; Pillai, S. K.; Sinha Ray, S.; Jalama, K.; Krause, R. W. M., Recent Trends in the Microwave-Assisted Synthesis of Metal Oxide Nanoparticles Supported on Carbon Nanotubes and Their Applications. *Journal of Nanomaterials* **2012,** *2012*, 15.
73. Hernadi, K.; Couteau, E.; Seo, J. W.; Forró, L., Al (OH) 3/multiwalled carbon nanotube composite: homogeneous coverage of Al (OH) 3 on carbon nanotube surfaces. *Langmuir* **2003,** *19*, (17), 7026-7029.
74. Georgakilas, V.; Tzitzios, V.; Gournis, D.; Petridis, D., Attachment of magnetic nanoparticles on carbon nanotubes and their soluble derivatives. *Chemistry of Materials* **2005,** *17*, (7), 1613-1617.
75. Eder, D.; Windle, A. H., Morphology control of CNT-TiO2 hybrid materials and rutile nanotubes. *J. Mater. Chem.* **2008,** *18*, (17), 2036-2043.
76. Sun, Z.; Zhang, X.; Na, N.; Liu, Z.; Han, B.; An, G., Synthesis of ZrO2− Carbon Nanotube Composites and Their Application as Chemiluminescent Sensor Material for Ethanol. *The Journal of Physical Chemistry B* **2006,** *110*, (27), 13410-13414.
77. Bottini, M.; Tautz, L.; Huynh, H.; Monosov, E.; Bottini, N.; Dawson, M. I.; Bellucci, S.; Mustelin, T., Covalent decoration of multi-walled carbon nanotubes with silica nanoparticles. *Chemical Communications* **2005**, (6), 758-760.
78. Sainsbury, T.; Fitzmaurice, D., Templated assembly of semiconductor and insulator nanoparticles at the surface of covalently modified multiwalled carbon nanotubes. *Chemistry of Materials* **2004,** *16*, (19), 3780-3790.
79. Mahajan, S.; Hasan, S.; Cho, J.; Shaffer, M.; Boccaccini, A.; Dickerson, J., Carbon nanotube–nanocrystal heterostructures fabricated by electrophoretic deposition. *Nanotechnology* **2008,** *19*, (19), 195301.
80. Chou, S.-L.; Wang, J.-Z.; Chew, S.-Y.; Liu, H.-K.; Dou, S.-X., Electrodeposition of MnO 2 nanowires on carbon nanotube paper as free-standing, flexible electrode for supercapacitors. *Electrochemistry Communications* **2008,** *10*, (11), 1724-1727.
81. Nørskov, J. K.; Bligaard, T.; Logadottir, A.; Kitchin, J.; Chen, J. G.; Pandelov, S.; Stimming, U., Trends in the exchange current for hydrogen evolution. *Journal of the Electrochemical Society* **2005,** *152*, (3), J23-J26.
82. Jiang, L. C.; Zhang, W. D., Electrodeposition of TiO2 nanoparticles on multiwalled carbon nanotube arrays for hydrogen peroxide sensing. *Electroanalysis* **2009,** *21*, (8), 988-993.
83. Moriguchi, I.; Hidaka, R.; Yamada, H.; Kudo, T.; Murakami, H.; Nakashima, N., A Mesoporous Nanocomposite of TiO2 and Carbon Nanotubes as a High-Rate Li-Intercalation Electrode Material. *Advanced Materials* **2006,** *18*, (1), 69-73.
84. Sun, J.; Gao, L.; Iwasa, M., Noncovalent attachment of oxide nanoparticles onto carbon nanotubes using water-in-oil microemulsions. *Chemical Communications* **2004**, (7), 832-833.
85. Lowry, G. V.; Gregory, K. B.; Apte, S. C.; Lead, J. R., Transformations of nanomaterials in the environment. In ACS Publications: 2012.
86. Nowack, B.; Ranville, J. F.; Diamond, S.; Gallego-Urrea, J. A.; Metcalfe, C.; Rose, J.; Horne, N.; Koelmans, A. A.; Klaine, S. J., Potential scenarios for nanomaterial release

and subsequent alteration in the environment. *Environmental Toxicology and Chemistry* **2012,** *31*, (1), 50-59.
87. Afrooz, A. N.; Khan, I. A.; Hussain, S. M.; Saleh, N. B., Mechanistic heteroaggregation of gold nanoparticles in a wide range of solution chemistry. *Environmental science & technology* **2013,** *47*, (4), 1853-1860.
88. Afrooz, A. R. M. N.; Sivalapalan, S. T.; Murphy, C. J.; Hussain, S. M.; Schlager, J. J.; Saleh, N. B., Spheres vs. rods: the shape of gold nanoparticles influences aggregation and deposition behavior. *Chemosphere* **2013,** *91*, (1), 93-98.
89. Aich, N.; Boateng, L. K.; Sabaraya, I. V.; Das, D.; Flora, J. R.; Saleh, N. B., Aggregation kinetics of higher order fullerene clusters in aquatic systems. *Environmental science & technology* **2016,** *50*, (7), 3562-3571.
90. Khan, I. A.; Afrooz, A. R. M. N.; Flora, J. R. V.; Schierz, P. A.; Ferguson, P. L.; Sabo-Attwood, T.; Saleh, N. B., Chirality affects aggregation kinetics of single-walled carbon nanotubes. *Environmental science & technology* **2013,** *47*, (4), 1844-1852.
91. Saleh, N. B.; Pfefferle, L. D.; Elimelech, M., Aggregation kinetics of multiwalled carbon nanotubes in aquatic systems: measurements and environmental implications. *Environmental Science & Technology* **2008,** *42*, (21), 7963-7969.
92. Saleh, N. B.; Pfefferle, L. D.; Elimelech, M., Influence of biomacromolecules and humic acid on the aggregation kinetics of single-walled carbon nanotubes. *Environmental Science & Technology* **2010,** *44*, (7), 2412-2418.
93. Hua, Z.; Zhang, J.; Bai, X.; Ye, Z.; Tang, Z.; Liang, L.; Liu, Y., Aggregation of TiO 2–graphene nanocomposites in aqueous environment: Influence of environmental factors and UV irradiation. *Science of the Total Environment* **2016,** *539*, 196-205.
94. Saleh, N. B.; Aich, N.; Lead, J.; Plazas-Tuttle, J.; Lowry, G. V., Research strategy to determine when novel nanohybrids pose unique environmental risks. *Environmental Science: Nano* **2015,** *2*, 11-18 (Cover Article).
95. Plazas-Tuttle, J. Nano-Enabled Water Disinfection Technology Development that Harnesses the Power of Microwaves. The University of Texas at Austin, Austin, Texas, 2017.

Chapter 2: An Elegant Method for Large Scale Synthesis of Metal Oxide-Carbon Nanotube Nanohybrids for Nano-environmental Application and Implication Studies[1]

[1] Das, D.; Plazas-Tuttle, J.; Sabaraya, I. V.; Jain, S. S.; Sabo-Attwood, T.; Saleh, N. B., An elegant method for large scale synthesis of metal oxide-carbon nanotube nanohybrids for nano-environmental application and implication studies. *Environmental Science: Nano* **2017,** *4*, (1), 60-68.
Note: All the experiments for this article have been either performed or supervised by Dipesh Das.

2.1 INTRODUCTION

Materials engineering has moved on from passive nanostructures to hierarchical nanohybrids[1, 2] (NHs) in quest of achieving multifunctionality and improved efficiency. One of the major classes of such complex heterostructures is carbon nanotube-metal oxide (CNT-MO) NHs. These heterostructures have shown improved performance compared to their component materials when integrated as electro- and photo-catalysts[3], and into electronics[4], gas sensing[5], biosensing[6], and laser technology[7]. With such a wide range of application possibilities, commercialization of these heterostructures is on the rise, especially with an incredible growth in the fuel cell industry in recent years[8]. CNT-MOs, such as CNT-TiO_2 and CNT-ZnO are mostly used as anodes as well as catalyst supports in fuel cells and are likely to result in environmental release during the end of life processing for resource recovery (e.g., Pt recovery)[9]. Once released into the environment, the environmental health and safety (EHS) of these multicomponent heterostructures with emergent properties will likely differ from those of their component materials, resulting in new unpredictable environmental risks[2, 10-12]. To determine if linear superposition of the environmental behavior of the components will adequately capture the heterostructure EHS, gaining control over the synthesis process from their component materials becomes necessary.

Electronic band engineering of MO nanocrystals allows their efficient use in microelectronic circuits, sensors, piezoelectric devices, fuel cells, and as corrosion resistant coating and catalysts[13]. With recent advances in nanotechnology and a constant need for improvement in the energy sector, researchers have emphasized hybridizing MOs with a

secondary element or nanostructure in order to achieve synergistic advantages[14]. CNTs with unique mechanical, thermal, physicochemical, and optoelectronic properties have been used as a nano-scale support for the MOs[14]. The ballistic electron conductivity and high surface area of the CNTs also enhance the catalytic and optoelectronic efficiency of the MOs upon hybridization[15]. We posit that these advantageous NHs with novel properties will manifest new and unknown environmental risks.

Multiwalled carbon nanotubes (MWNTs) and several MO nanocrystals have displayed toxicity when introduced to a wide range of microorganisms and aquatic species[16-18]. MWNTs have been reported to generate reactive oxygen species (ROS), exhibit physical perturbation to cell walls[21], and even compromise membrane integrity[19, 20]. Nano ZnO and TiO_2 are example nano-MOs that have shown antimicrobial properties by ROS generation[21]. ZnO NPs have also demonstrated dissolution mediated toxicity[22]. The toxicological manifestation of the nano-MOs is not only a function of the chemical composition and band architecture of the materials[23] but also is strongly dependent on their size,[24] shape and morphology,[25] surface chemistry,[26] and crystallinity.[27] As hybridization or chemical attachment of MO nanocrystals to CNT surfaces develops novel heterostructures following is the critical question for the nano-EHS community: will the hybrid CNT-MO attain new properties and exhibit environmental behavior unique to its components? The answer likely lies in potentially emergent material characteristics of these NHs.

Hybridization of CNTs with nano-MOs has been known to modulate their physicochemical properties[1, 2]. For example, the photocatalytic activity of TiO_2 (visible

photoactivation) enhances when TiO_2 is hybridized onto CNTs; lowering of the band gap is known to be behind such enhancement[28]. CNTs hybridized with ZnO show enhanced photocatalytic activity than that of CNTs and ZnO, separately (when UV irradiated)[29]. Hybridization is also known to alter van der Waals interaction energy[30], likely resulting in unknown interaction of the NHs with environmental interfaces (i.e., aggregation and deposition in porous media). Determination of property changes in a systematic way from components to nano-heterostructures is key to better predict the EHS of the NHs, where controlled synthesis in a large enough quantity becomes essential.

Several methods have been employed to synthesize CNT-MO NHs including sol-gel[3, 31-38], hydrothermal[39-42], solvothermal[43], thermal decomposition[44], direct deposition[45, 46], direct mixing[47], microwave irradiation[48], and atomic layer deposition[49], among others. Some of these techniques are fairly simple and can be used to achieve on-demand MO composition and loading. However, a simple technique, where varying reagent composition and/or amount yields a large amount of hybrid materials with on-demand hybrid composition, is yet to be developed. Such a technique will not only strengthen the synthesis capability by widening the heterostructure chemical composition space but will also facilitate performing comparable EHS studies on a large set of CNT-MOs.

The objective of this study is to develop an elegant method to synthesize CNT-MOs in large quantities (100s of mg), where MOs of different chemical composition can be conjugated with the MWNTs by merely changing the precursor type. In order to do so, an already published sol-gel synthesis process[8] to hybridize MWNT-TiO_2 NH has been modified to grow MO nanocrystals of two transitional metals (Ti and Zn) and two

Lanthanide series metals (Er and Pr) *in situ* onto acid-etched MWNTs. The oxides of Ti and Zn are chosen for their excellent antimicrobial and catalytic properties[50], while those of the Er and Pr for their superior optical properties.[51] Precursors with relevant chemical composition are utilized to form these MO nanocrystals. Physical morphology and elemental distribution of these NHs are characterized by employing electron microscopy techniques. To identify if the grown MOs on MWNT surfaces are crystalline, X-ray diffraction (XRD) is performed. To ensure that reproducibility has been achieved between batches, X-ray photoelectron spectroscopy (XPS) is used to determine the material composition. One of the key questions in hybridization is whether these MO nanocrystals are chemically bound to the MWNTs or are physically associated to the tubules. Peak oxidation temperature, which is a strong function of the MWNT chemical bond structure, is determined with thermal gravimetric analysis (TGA). Furthermore, a synthesized NP is only useful for environmental studies if it possesses appreciable colloidal stability in water. A common suspension technique has been employed for all the NHs and their stability is determined with dynamic light scattering (DLS). The elegance of this synthesis technique lies in the simplicity of changing MO type by merely changing the precursor composition as well as in the large yield of the synthesized materials. Such large material yield is essential to perform detailed nano-EHS studies of any synthesized NP.

2.2 MATERIALS AND METHODS FOR SYNTHESIS OF NHS

2.2.1 Chemicals and Reagents

Pristine MWNTs (O.D. 8-15 nm) were procured from Cheap Tubes Inc. (Brattleboro, VT). Concentrated nitric acid, sulfuric acid, titanium (IV) isopropoxide (TTIP), erbium (III) nitrate pentahydrate, and praseodymium (III) nitrate hexahydrate were purchased from Sigma Aldrich (St. Louis, MO). Isopropanol was obtained from Fisher Scientific (Pittsburgh, PA) while zinc (II) nitrate hexahydrate was purchased from J.T Baker (Center Valley, PA). For preparing all aqueous suspensions and solutions, 18.2 mΩ (Milli-Q) water was used unless otherwise stated.

2.2.2 Synthesis of MWNT-MO NHs

MWNTs (1 g) were acid-etched by ultrasonication (Qsonica LLC, Newtown, CT) in 300 mL of concentrated nitric and sulfuric acid mixture (1:1 volume basis). Upon sonication, the mixture was refluxed at 100 °C for 3 h under continuous stirring. The oxidized MWNTs were subsequently filtered until the pH of the filtrate reached >5.5 and then were dried for 48 h in a desiccator. Once dried, 50 mg of the oxidized MWNTs were re-suspended in 100 mL isopropanol with an ultrasonic dismembrator (Qsonica, Newtown, CT) and transferred into a round bottom flask. Appropriate amount of precursors (10:1 carbon to precursor molar ratio for MWNT-TiO_2 and MWNT-ZnO and 16:1 carbon to carbon to precursor molar ratio for MWNT-Er_2O_3 and MWNT-Pr_6O_{11} synthesis) were added to 10 mL of isopropanol and introduced dropwise to the MWNT-isopropanol suspension at 0.301 mL/min with a peristaltic pump (Ismatec, Wertheim, Germany). The

slow rate of precursor addition was maintained to provide sufficient mixing time. The entire suspension was refluxed at 80 °C for 3 h in a nitrogen environment. For MWNT-TiO_2 NH, 5 mL of water was added dropwise into the reaction vessel to promote TiO_2 crystal formation on the MWNT backbone via a hydrolysis process over 1 h. Hydrolysis was necessary for the MWNT-TiO_2 NH only; the precursors used for the other NHs were already in hydrated form. Afterwards, the refluxed mixture was washed 4 times with isopropanol (as a purification step), which removed any unreacted reagent. Finally, isopropanol was evaporated, the dry materials were powdered using a mortar and pestle, and the resultant materials were calcined at 400 °C for 3 h under nitrogen to facilitate crystal formation. Synthesis of all four NHs was triplicated using the same method to ensure reproducibility. The synthesis setup is shown in Figure A1.

2.3 Material Characterization

2.3.1 Physical Morphology

The physical morphology of the NMs was determined using a JEOL 2010F high resolution transmission electron microscopy (HRTEM, JEOL, Japan) equipped with energy dispersive spectroscopy (EDS). Electron micrographs were obtained at an acceleration voltage of 200 kV. High annular angle dark field scanning transmission electron microscopy (STEM) images were obtained with the same equipment, where EDS was employed to obtain elemental mapping for the NHs. The details of the HRTEM and EDS methodology are described elsewhere[52-58]. In brief, drops of aqueous dispersions of NHs were placed on lacey carbon coated copper TEM grids (SPI Supplies, West Chester,

PA) and air-dried over a few minutes. Several micrographs were taken to obtain representative images.

2.3.2 Crystallinity and Chemical Composition

The crystallinity of the MO on the NH surfaces was evaluated with an XRD. A 600 W Rigaku MiniFlex 600 (Rigaku, Japan) with a Cu-Kα irradiator (0.154 nm wavelength) and a graphite monochromator was used at a step width of 0.02° (between 2θ values of 20° to 60°) and a scanning rate of 2°/min. To eliminate extensive noise for the MWNT-Pr_2O_3 NH XRD spectra, a step width of 0.5° was used. The scattering was detected using a scintillation counter.

To determine the elemental composition of the dry MWNT and NH samples, a Kratos X-ray Photoelectron Spectrometer-Axis Ultra DLD, equipped with a monochromated Al K_α X-ray source (1.486 KeV) and a concentric hemispherical analyzer was employed. A thin layer of powdered sample was placed on a double-sided copper taped stainless steel bar. The bar was then placed in the analysis chamber and degassed for at least 3 h. The X-ray photoelectron spectroscopy (XPS) analysis was then performed to obtain the survey spectra as well as the spatial high-resolution spectra and the data was analyzed by fitting the high-resolution element specific peaks with CasaXPS (Casa Software Ltd., Japan). To ensure reproducibility and overall homogeneity, a total of 9 samples for each material (MWNT and four NHs) were analyzed (3 samples each in triplicate batches for all NHs).

2.3.3 Thermal Gravimetric Analysis (TGA)

TGA and differential thermogravimetric analysis (DTG) were performed by a Mettler Thermogravimetric Analyzer TGA/DSC 1 (Mettler Toledo, Columbus, OH). A dry NH or MWNT mass of 3-5 mg was placed in an alumina crucible and heated at 10 °C/min ramp up to 800 °C in presence of air (flow rate 50 mL/min). The TGA data was analysed to determine percent mass loss and peak oxidation temperature[59]. Mass of the grown MOs on the MWNT surfaces were determined from the residual mass at the completion of the oxidation reaction. TGA and DTG analysis were performed in triplicates for each of the NHs to ensure reproducibility in synthesized composition.

2.3.4 Size Analysis of Stable Aqueous Suspensions

To prepare an aqueous suspension of the NHs, 2.5 mg of the samples were added to 50 mL of Milli-Q water and sonicated with the ultrasonic dismembrator for 30 min (2 min pulse with a 24 s pause). The suspension was further diluted to 10 mg/L and sonicated for an additional 15 min to achieve a stable suspension. This stable suspension was diluted to 2 mg/L for size measurement with DLS. The sizes of the suspended colloids were measured with a highly sensitive ALV/CGS-3 compact goniometer system (ALV-Laser GmbH, Langen/Hessen, Germany), equipped with a 22 mW HeNe 632.8 nm laser and a high QE APD detector with photomultipliers of 1:25 sensitivity. The experimental details of size measurement have been described elsewhere[53, 55, 57, 58, 60, 61]. In brief, 2 mL of the 2 mg/L of suspensions were injected into pre-cleaned borosilicate glass vials[53, 55, 57, 58, 60, 61] and inserted into the toluene-filled goniometer sample housing. The scattered laser was

collected every 15 s for at least 25 min at 90°. A cumulant fit was used to analyze the collected data and the average hydrodynamic radii (HDR) were obtained for every 15 s segment during the entire duration of the experiments.

2.3.5 Electrokinetic Properties

The electrophoretic mobility (EPM) of the aqueous suspensions was measured with a Malvern Zetasizer (Malvern Instruments Ltd., Worcestershire, UK) at 20 °C to assess the electrokinetic properties. For each measurement, 900 µL of the aqueous suspension of the samples was introduced into a disposable capillary cell (DTS 1070). Five independent cells were used for the oxidized MWNTs and the four NH samples to avoid cross contamination. Measurements were performed in triplicates following a well-established protocol[52-58].

2.4 Results and Discussions

2.4.1 Physical Morphology

Representative TEM (Figure A2) micrographs of the MWNTs show that the tubes are mostly debundled with an average shell thickness of 21.3±2.6 nm. The HRTEM images illustrate presence of catalyst-metal free MWNTs. TEM and STEM micrographs with elemental mapping of the NHs (Figure 2.1) confirm the presence of the metal atoms (Ti, Zn, Er and Pr), which are distributed throughout the MWNT backbone. These micrographs and the elemental mapping of the MWNT-TiO_2 NH suggest that TiO_2 nanocrystals (HRTEMs show lattice fringes) have successfully been grown throughout the MWNT surfaces. Similarly, TEMs of the other NHs (i.e., MWNT-ZnO, MWNT-Er_2O_3, and MWNT-Pr_6O_{11}) exhibit distinct nanocrystalline MO features on the MWNTs. It is also to

be noted that though most of MONPs are observed to be at the exterior of the MWNTs, some of the nanocrystals might have been encapsulated within the tube interior. Further experimentation is necessary to determine and analyze the encapsulation ratio. It was also observed that the spatial distribution of the MOs was not uniform throughout the MWNT surfaces for all NHs. This most likely has occurred due to a lack of homogeneity in distribution of the oxygen-containing surface binding sites on the MWNT backbone at the first place. Presence of lattice fringes, as observed in the HRTEMs, confirms crystalline growth of TiO_2, ZnO, Er_2O_3, and Pr_6O_{11}.

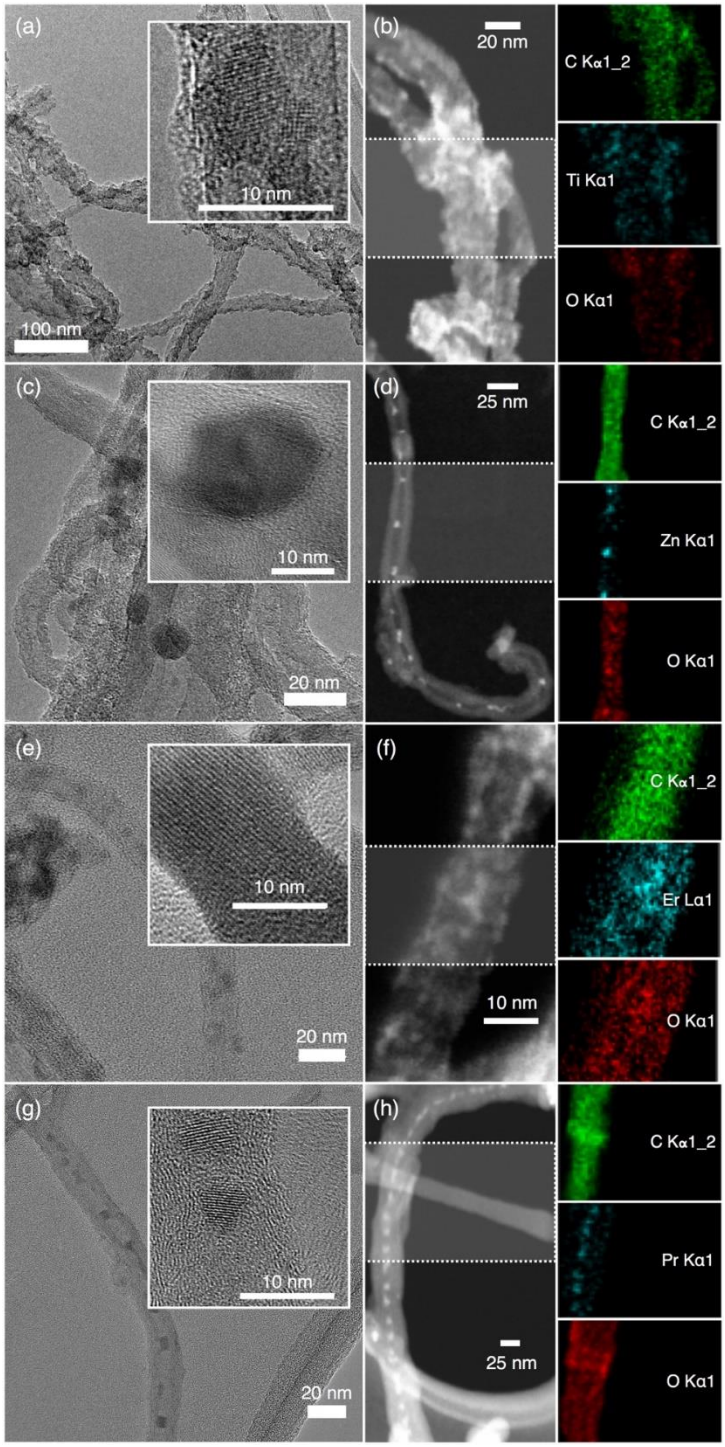

Figure 2.1: Representative TEM micrographs of (a) MWNT-TiO_2, (c) MWNT-ZnO, (e) MWNT-Er_2O_3, and (g) MWNT-Pr_6O_{11}. HRTEMs with lattice fringes of MOs are shown in the insets. Representative STEM micrographs and elemental mapping of (b) MWNT-TiO_2, (d) MWNT-ZnO, (f) MWNT-Er_2O_3, and (h) MWNT-Pr_6O_{11}.

2.4.2 Crystallinity and Chemical Composition

The XRD patterns of the MWNTs and the NHs are presented in Figure 2.2. The lattice planes corresponding to the grown MO nanocrystals possess signature XRD peaks and are in excellent agreement with previously reported XRD patterns of oxidized MWNT[62], MWNT-TiO_2[62] and MWNT-ZnO NHs[29]. Since there are no literature report on XRD patterns of MWNT-Er_2O_3 and MWNT-Pr_6O_{11} NHs, spectral patterns for these materials were compared to those of Er_2O_3[63] and Pr6O_{11}[64] nanocrystals (Figure A3).

MWNTs and the NHs display strong graphitic carbon peak at 25.7º. The MWNT-TiO_2 NHs exhibited a major peak for the lattice plane (101), typical to anatase crystalline phase. Although weaker, the peak occurrences at 37.5º, 48º, and 55.5º correspond to (004), (200), (211), crystalline planes, respectively[62], which further confirm dominance of anatase phase in the grown TiO_2. MWNT-ZnO NHs show strong peaks corresponding to (100), (002), (101), (102), and (110) planes, which are consistent with ZnO nanocrystal structure[29]. The XRD spectrum of MWNT-Er_2O_3 NH (Figure 2.2 and A3 a) and the MWNT-Pr_6O_{11} NH (Figure 2.2 and A3 b) indicates that MOs in both these hybrids have amorphous content. However, both NHs also demonstrate crystalline peaks which match certain MO crystalline planes when compared to Er_2O_3 and Pr_6O_{11} nanocrystals. For the MWNT-Er_2O_3 NH, the crystalline planes match with Er_2O_3 were (222), (400), (431), (440), and (622)[63]. For the MWNT-Pr_6O_{11} NHs, lattice planes of (111), (200), and (220) have been identified[64]. Further insight on the amorphous nature content of the MOs in MWNT-Er_2O_3 and MWNT-Pr_6O_{11} NHs have been provided in chapter 2.

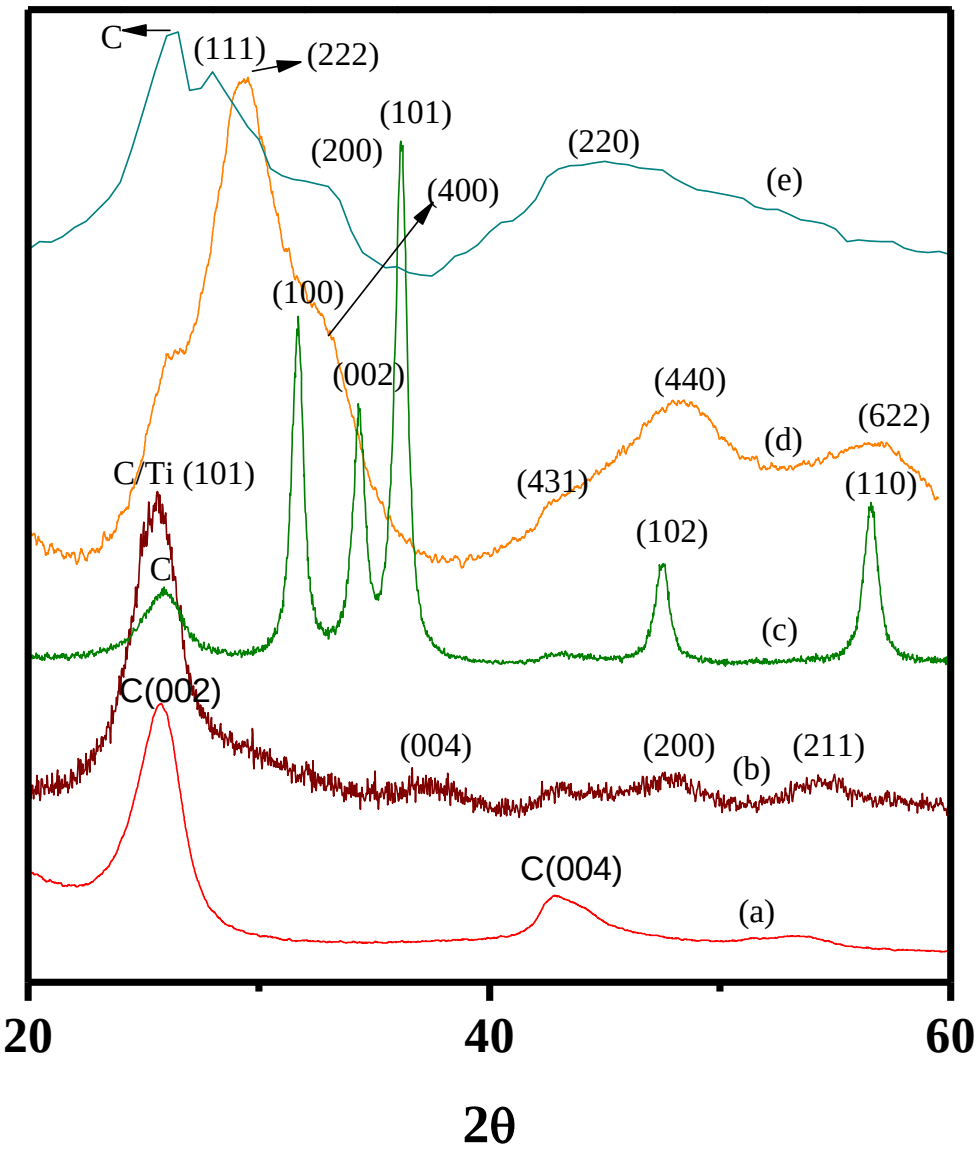

Figure 2.2: Representative XRD spectra of (a) oxidized MWNTs, (b) MWNT-TiO_2, (c) MWNT-ZnO, (d) MWNT-Er_2O_3, and (e) MWNT-Pr_6O_{11} NH. Numbers in parentheses indicate the lattice planes of CNT (a) and MOs in the respective NHs (b-e).

The chemical composition of the NHs has been further analyzed with XPS. Figure A4 presents the XPS spectra for C 1s in the oxidized MWNTs. The peak positions of the deconvoluted spectrum indicate presence of multiple oxygen containing moieties on the MWNT surfaces, which is in agreement with previously reported XPS data on acid-treated MWNTs[65]. Percent oxidation of the MWNTs was determined to be 10.8±1.5%. Survey spectra of the oxidized MWNTs (Figure 2.3) show that these are free from any catalyst metal, while, those of the NHs (Figure 2.3) confirm presence of the respective metals with no traces of other metal impurities. XPS peaks, corresponding to different orbitals of the metal atoms as well as the Auger peaks, have been identified (Figure 2.3) from CasaXPS library and the National Institute of Standards and Technology X-ray photoelectron spectroscopy database[66]. High-resolution XPS spectra of the metal atoms in all the NHs have been shown in Figure A4. The MWNT-TiO_2 NH show peaks at 458.3 and 464.3 eV, which are characteristic to Ti 2p3/2 and Ti 2p1/2 on anatase phase TiO_2[67]. For the other NHs, characteristic ZnO peak for Zn 2p3/2 at 1022.3 eV[29] , Er_2O_3 peak for Er 4d at 168.8 eV[66], and Pr_6O_{11} peak for Pr 3d at 933.3 eV[66] have been located on MWNT-ZnO, MWNT-Er_2O_3 and MWNT-Pr_6O_{11}, respectively. The deconvoluted spectrum for Pr3d (Figure A4 e) confirms presence of multiple oxidation states (i.e., III and IV) of Pr[64].

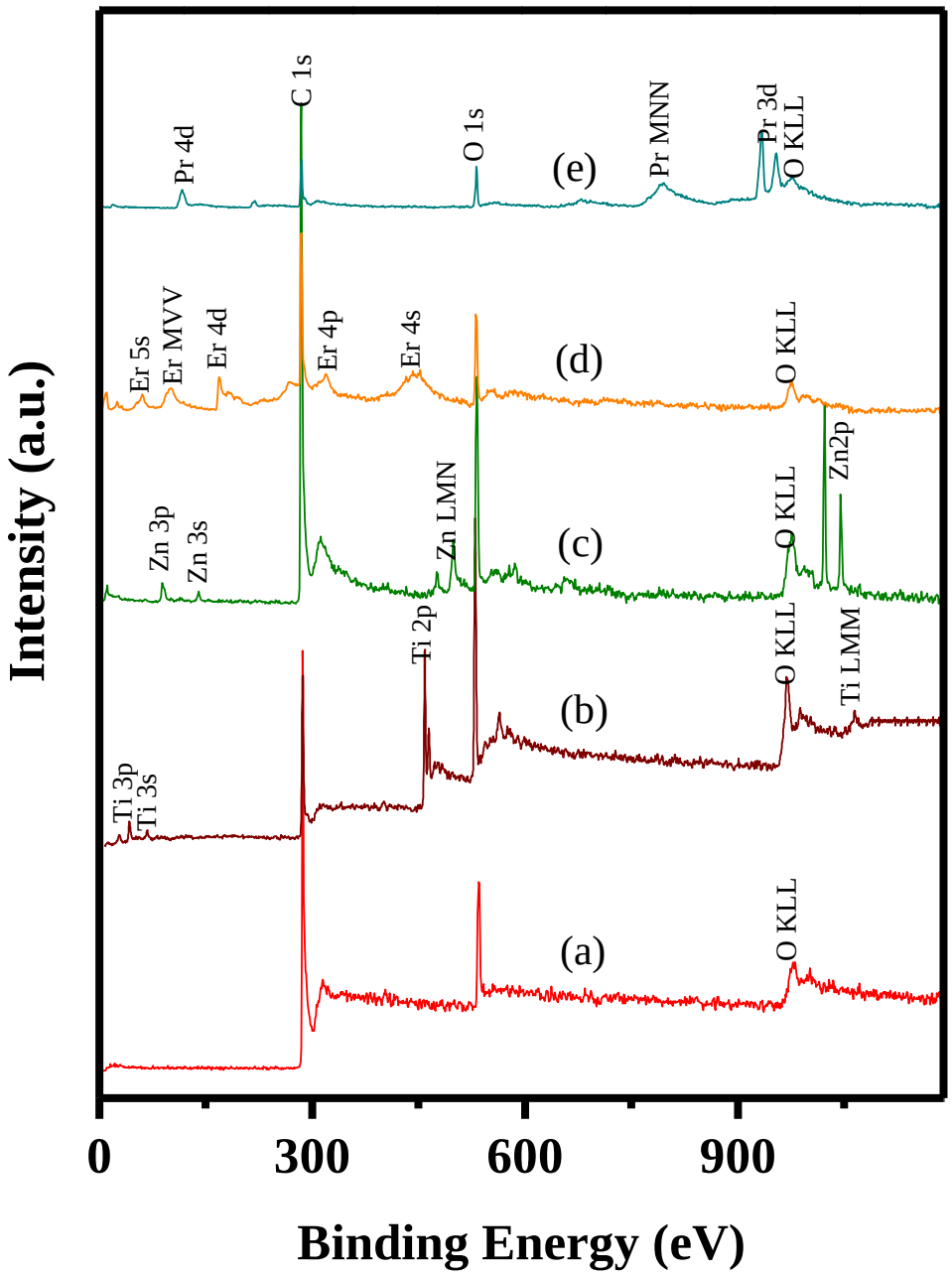

Figure 2.3: Representative XPS survey spectra of (a) oxidized MWNTs, (b) MWNT-TiO_2, (c) MWNT-ZnO, (d) MWNT-Er_2O_3, and (e) MWNT-Pr_6O_{11} NH. The peak labels indicate the atomic orbitals associated with the binding energies at the respective peak positions.

Table 2.1 presents the carbon and metal percentages on the NHs. The %MOs have been calculated using the %metal values and metal equivalence (i.e., 1 eq. of Ti on TiO_2, 1 eq. of Zn in ZnO, 2 eq. of Er in Er_2O_3, and 6 eq. of Pr in Pr_6O_{11}). Table 1 shows that MWNT-TiO_2 NHs contain maximum MO percentage (~8.5%), while MWNT-Pr_6O_{11} NHs have the lowest (~0.7%) among all NH types. The XPS results show ~6.2% molar ratio of zinc in the MWNT-ZnO NHs. This value appears to be lower than that of the MWNT-TiO_2 NHs (~8.5%), though similar molar ratio of carbon to precursor (10:1) was used for both the NHs. Similarly, the metal content in MWNT-Pr_6O_{11} and MWNT-Er_2O_3 are similar between each other (~4.7% for MWNT-Er_2O_3 and ~4.2% for MWNT-Pr_6O_{11}) but vary with other NHs, in spite of using a carbon to precursor molar ratio (16:1) for synthesizing these lanthanide oxide NHs. It is to be noted that XPS is a highly surface sensitive method with a maximum X-ray penetration depth of 10 nm. This might have caused the observed differences in the metal content for the NHs with similar carbon to precursor molar ratio. The highlight of the XPS results is the low standard deviation (<10%) of the mean values for all the NHs, which confirms achieving reproducibility between different batches of the synthesized NHs. Figure A5 further demonstrates the reproducibility of different NHs among triplicates for each of the materials.

Table 2.1: Atomic percentages and molar ratio of carbon:metal estimated from the XPS spectra using CasaXPS software.

Sample	%C	%Metal	%Metal Oxide in the NHs
MWNT-TiO_2	63.9±0.7	8.5±0.6	~8.5
MWNT-ZnO	78.5±1.0	6.2±0.5	~6.2
MWNT-Er_2O_3	81.4±0.9	4.7±0.4	~2.35
MWNT-Pr_6O_{11}	79.5±1.2	4.2±0.4	~0.7

2.4.3 Evidence of Chemical Hybridization

Thermal oxidation of materials, i.e., TGA (Figure 2.4 and Table A1) assesses nature of hybridization by providing insight into the oxidation of carbonaceous materials[68]. The peak oxidation temperature for MWNTs has been determined as 635.4±0.6 °C by plotting the rate of mass loss over the temperature range. Oxidation temperatures for the NHs show a significant leftward shift for all NHs, when compared to the oxidized MWNTs; i.e., the peak oxidation temperatures are 74.9, 48.3, 161.4 and 197.9 °C lower for TiO_2-MWNT, ZnO-MWNT, Er_2O_3-MWNT, and Pr_2O_3-MWNT, respectively. Lowering in the peak oxidation temperature for hybridized CNTs has been reported earlier, where MOs were found to have caused enhancement in oxidation reaction[68, 69]. The change in the oxidation temperature is also reported to vary based on the degree of MO crystallinity and concentration of defects on the MWNT surfaces[68].

The residual mass for the oxidized MWNTs is determined to be 1.4±0.2%, which can be attributed to any metal impurities in the oxidized MWNTs. However, the other characterization techniques (i.e., TEM, HRTEM, XRD, and XPS) did not find any trace impurities in the oxidized MWNTs. Other likely sources of the residual mass are possible incomplete combustion of MWNTs or measurement sensitivity issues. The residual mass

for the MWNT-TiO_2 NHs and MWNT-ZnO NHs is ~40.3% and ~46.1%, respectively while those for the MWNT-Er_2O_3 and MWNT-Pr_6O_{11} is found to be ~47.3% and 51.8%, respectively. The maximum difference in the aforementioned residual masses among the NHs is (~11.5%). This difference can be lowered by changing the carbon to precursor ratio at the beginning of the synthesis process. It is important to note that differences in determined MO mass using TGA and XPS cannot be equated; since the former is a mass-based bulk technique while the latter is a surface technique. However, similar to the XPS results, the low standard deviation for the percent mass loss (Table A1) and similar oxidation temperatures among triplicates for each of the NHs (Figure A6) further highlight the reproducibility between synthesized batches.

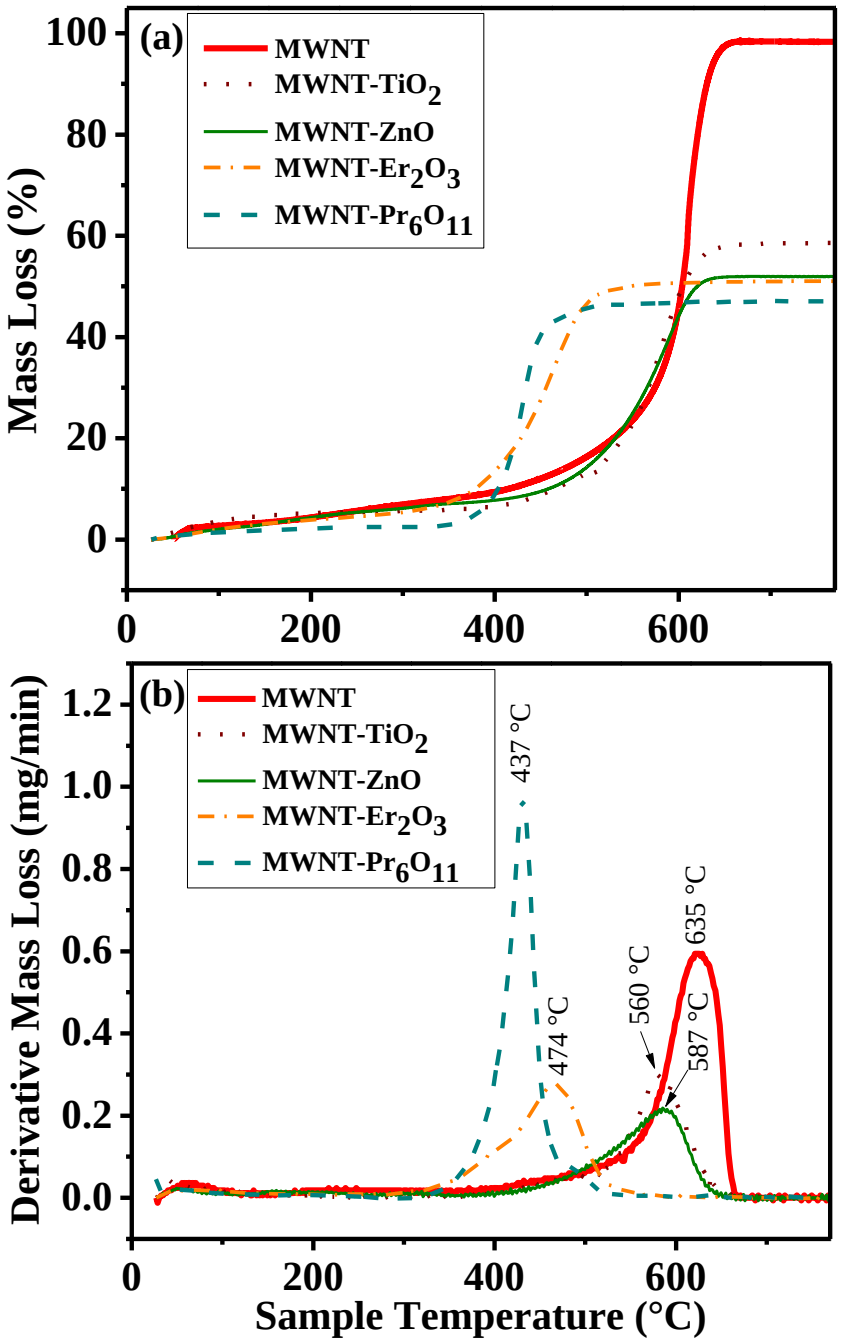

Figure 2.4: TGA mass loss profiles as a function of oxidation temperature; (a) percent mass loss and (b) derivative mass loss. The peak oxidation temperatures of the oxidized MWNTs and the NHs are labeled.

2.4.4 Suspension Stability

The oxidized MWNTs and the NHs can be suspended in water with high degree of stability as (Figure A7). The hydrodynamic radius (HDR) of the oxidized MWNT clusters is determined to be 75±2.4 nm (Figure 2.5 a), which increases upon hybridization; i.e. 101±2, 128±8, 185±11, and 150±17, for MWNT-TiO2, MWNT-ZnO, MWNT-Er_2O_3 and MWNT-Pr_6O_{11}, respectively (Figure 2.5 a). The higher HDR of the NHs is likely due to altered physical properties of the MWNTs, which has influenced the packing of the clusters. No significant settling of the aqueous suspensions of oxidized MWNTs and the MWNT-TiO_2 NHs has been observed for more than 30 d at a concentration of 10 mg/L; while the other NHs (i.e., MWNT-ZnO, MWNT-Er_2O_3 and MWNT-Pr_6O_{11}) at the same concentration started to settle after 48 h from the time of suspension preparation. The difference is likely caused by variation in van der Waals attractive interaction among ZnO, Er_2O_3 and Pr_6O_{11} nanocrystals or due to altered electrokinetic behavior. To achieve higher colloidal stability of the MWNT-ZnO, MWNT-Er_2O_3 and MWNT-Pr_6O_{11} NHs, surface functionalization (with polymers/surfactants) may be applied[70, 71].

2.4.5 Electrokinetic Properties

Oxidized MWNTs as well as all the NHs (Figure 2.5 b) exhibit negative surface potential. The EPM values are found to be -3.15±0.1, -2.94±0.3, -2.27±0.3 -2.24±0.1, and -2.33±0.2 $m^2V^{-1}S^{-1}$ for oxidized MWNT, MWNT-TiO_2 NHs, MWNT-ZnO NHs, MWNT-Er_2O_3 NHs, and MWNT-Pr_6O_{11} NHs, respectively. The measured EPM values of the MWNTs agree with previously reported EPMs for oxidized MWNTs (-3.5 to -2.4 m^2 V^{-1}

S^{-1} with high and low oxygen content, respectively at low ionic strength)[72], which likely originated from the oxygen containing moieties on the MWNT surfaces via acid-etching[72-74]. Other carbon allotropes such as single-walled carbon nanotubes (-2.8 m^2 V^{-1} S^{-1} to -1.25 m^2 V^{-1} S^{-1})[55, 75, 76] and graphene[77, 78] have shown similar surface potential upon oxidation. The EPM values of the MWNT-ZnO, MWNT-Er_2O_3, and MWNT-Pr_6O_{11} NHs are significantly lower than those of the oxidized MWNTs and the MWNT-TiO_2 NHs. Hence the relative instability of the MWNT-ZnO, MWNT-Er_2O_3, and MWNT-Pr_6O_{11} NHs, as discussed earlier, may have been dominated by electrokinetics of these materials.

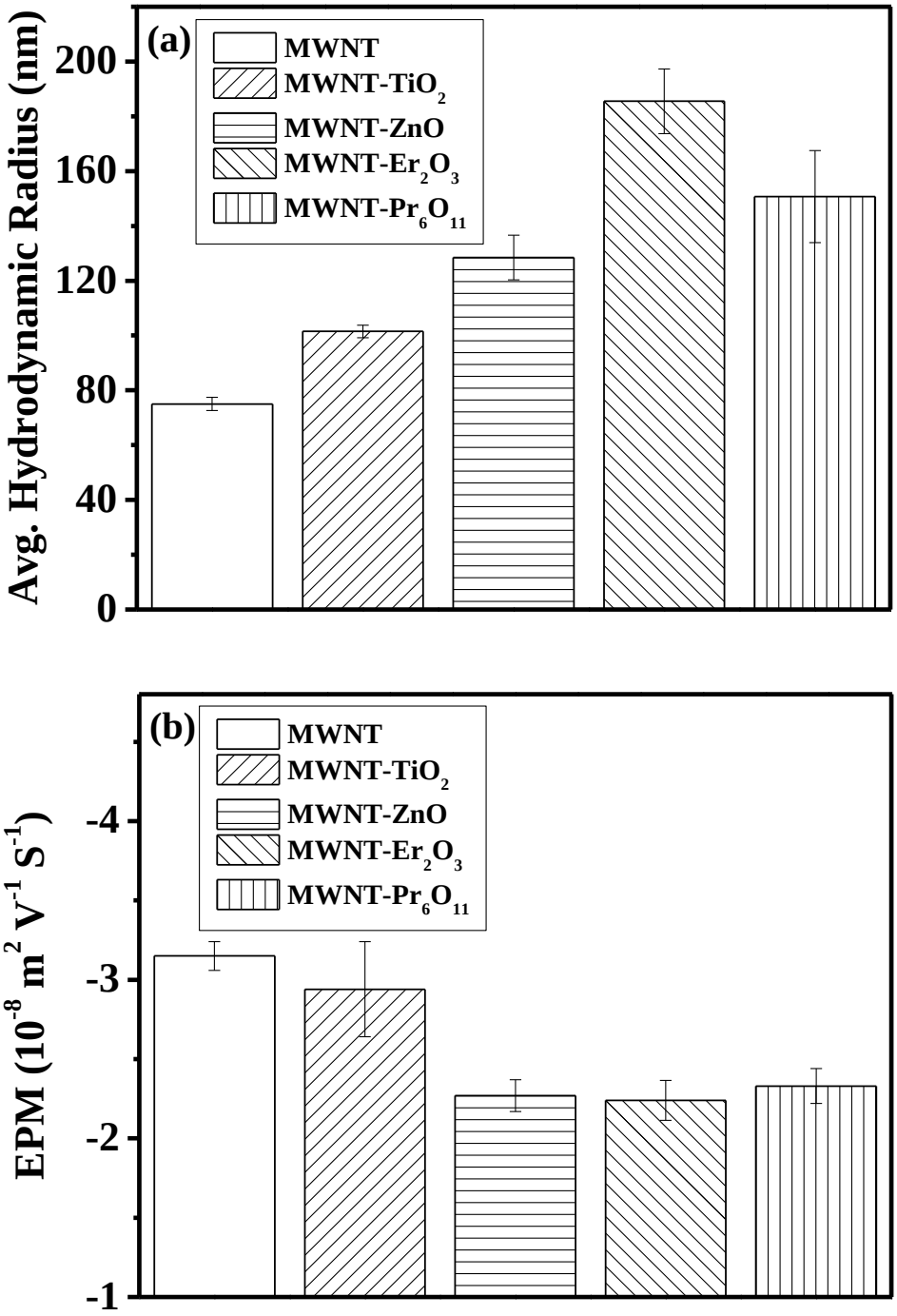

Figure 2.5: (a) Average hydrodynamic radius and (b) electrophoretic mobility of MWNTs and the NHs. All measurements were carried out at pH of 6.9±0.2 and at 25 °C. The bars indicate mean values while the error bars indicate standard deviations.

2.5 SUMMARY

A large-scale, elegant, and facile synthesis process has been developed by modifying a wet-chemical based sol-gel hybridization process in order to synthesize four CNT-MO NHs. The novelty of this study lies in this synthesis technique being a singular standardized method synthesizing carbonaceous-metallic nanohybrids with a wide range of MOs including new nanohybrids that involves lanthanide series metals; and that this method has allowed for synthesizing at least 100s of mg of nanohybrids in a single synthesis cycle while achieving high degree of reproducibility. The synthesized NHs were characterized to identify their physical morphology, crystallinity, chemical composition as well as to demonstrate proper hybridization and reproducibility of the NHs. The characterization results demonstrate successful preparation of CNT-MO NHs with a wide range of MO composition, which are highly reproducible between batches. One of the limitations of this method is in limited homogeneity in the spatial distribution of the MONPs on the MWNT surfaces. However, it is important to note that these NHs will interact with other environmental entities as a cluster rather than as individual tubules. Hence, the overall homogeneity in MO distribution may not play a significant role in their manifested EHS. The strength of this synthesis technique lies in large material yield with high reproducibility between synthesized batches. The simplicity in tuning MO composition by merely changing the reagent type widens the materials choice, which can be extremely useful to perform nano-EHS studies on carbon-metal oxide heterostructures. This study also concludes that although the synthesis process produced multiple MWNT-MO NHs with high degree of overall homogeneity and reproducibility, other parameters,

i.e., particle sizes, surface charge, and degree of crystallinity, showed variation between the NHs.

2.6 LITERATURE CITED

1. Aich, N.; Plazas-Tuttle, J.; Lead, J.; Saleh, N., A Critical Review of Nanohybrids: Synthesis, Applications, and Environmental Implications. *Environmental Chemistry* **2014,** *11*, 609-623.
2. Saleh, N. B.; Aich, N.; Lead, J.; Plazas-Tuttle, J.; Lowry, G. V., Research strategy to determine when novel nanohybrids pose unique environmental risks. *Environmental Science: Nano* **2015,** *2*, 11-18 (Cover Article).
3. Eder, D.; Windle, A. H., Carbon–inorganic hybrid materials: the carbon-nanotube/TiO2 interface. *Advanced Materials* **2008,** *20*, (9), 1787-1793.
4. Alley, N. J.; Liao, K. S.; Andreoli, E.; Dias, S.; Dillon, E. P.; Orbaek, A. W.; Barron, A. R.; Byrne, H. J.; Curran, S. A., Effect of carbon nanotube-fullerene hybrid additive on P3HT:PCBM bulk-heterojunction organic photovoltaics. *Synth. Met.* **2012,** *162*, (1-2), 95-101.
5. Llobet, E.; Espinosa, E.; Sotter, E.; Ionescu, R.; Vilanova, X.; Torres, J.; Felten, A.; Pireaux, J.-J.; Ke, X.; Van Tendeloo, G., Carbon nanotube–TiO2 hybrid films for detecting traces of O2. *Nanotechnology* **2008,** *19*, (37), 375501.
6. Liu, Z.; Wang, J.; Xie, D.; Chen, G., Polyaniline-Coated Fe3O4 Nanoparticle–Carbon-Nanotube Composite and its Application in Electrochemical Biosensing. *Small* **2008,** *4*, (4), 462-466.
7. Zhu, Y.; Elim, H. I.; Foo, Y. L.; Yu, T.; Liu, Y.; Ji, W.; Lee, J. Y.; Shen, Z.; Wee, A. T.-S.; Thong, J. T.-L., Multiwalled carbon nanotubes beaded with ZnO nanoparticles for ultrafast nonlinear optical switching. *Advanced Materials* **2006,** *18*, (5), 587-592.
8. Rigdon, W. A.; Huang, X., Carbon monoxide tolerant platinum electrocatalysts on niobium doped titania and carbon nanotube composite supports. *Journal of Power Sources* **2014,** *272*, (0), 845-859.
9. Pehnt, M., Life-cycle analysis of fuel cell system components. *Handbook of Fuel Cells* **2003**.
10. Saleh, N. B.; Afrooz, A.; Bisesi Jr, J. H.; Aich, N.; Plazas-Tuttle, J.; Sabo-Attwood, T., Emergent properties and toxicological considerations for nanohybrid materials in aquatic systems. *Nanomaterials* **2014,** *4*, (2), 372-407.
11. Saleh, N. B.; Aich, N.; Plazas-Tuttle, J.; Lead, J. R.; Lowry, G. V., Research strategy to determine when novel nanohybrids pose unique environmental risks. *Environmental Science: Nano* **2015,** *2*, (1), 11-18.
12. Aich, N.; Plazas-Tuttle, J.; Lead, J. R.; Saleh, N. B., A critical review of nanohybrids: synthesis, applications and environmental implications. *Environmental Chemistry* **2014,** *11*, (6), 609-623.
13. Fernández-García, M.; Rodriguez, J. A., Metal oxide nanoparticles. *Encyclopedia of Inorganic and Bioinorganic Chemistry* **2011**.
14. Eder, D., Carbon Nanotube−Inorganic Hybrids. *Chemical Reviews* **2010,** *110*, (3), 1348-1385.
15. Lee, S. H.; Lee, D. H.; Lee, W. J.; Kim, S. O., Tailored assembly of carbon nanotubes and graphene. *Advanced Functional Materials* **2011,** *21*, (8), 1338-1354.

16. Bergin, I. L.; Witzmann, F. A., Nanoparticle toxicity by the gastrointestinal route: evidence and knowledge gaps. *J Biomedical Nanosci and Nanotechnol* **2013,** *3*, 163-210.
17. Cheng, J.; Cheng, S. H., Influence of carbon nanotube length on toxicity to zebrafish embryos. *Int J Nanomedicine* **2012,** *7*, 3731-3739.
18. Diniz, M. S.; de Matos, A. P.; Lourenço, J.; Castro, L.; Peres, I.; Mendonça, E.; Picado, A., Liver alterations in two freshwater fish species (Carassius auratus and Danio rerio) following exposure to different TiO_2 nanoparticle concentrations. *Microsc Microanal* **2013,** *19*, 1131-1140.
19. Chen, H.; Wang, B.; Gao, D.; Guan, M.; Zheng, L.; Ouyang, H.; Chai, Z.; Zhao, Y.; Feng, W., Broad-Spectrum Antibacterial Activity of Carbon Nanotubes to Human Gut Bacteria. *Small* **2013,** *9*, (16), 2735-2746.
20. Kang, S.; Herzberg, M.; Rodrigues, D. F.; Elimelech, M., Antibacterial Effects of Carbon Nanotubes: Size Does Matter! *Langmuir* **2008,** *24*, (13), 6409-6413.
21. Adams, L. K.; Lyon, D. Y.; Alvarez, P. J., Comparative eco-toxicity of nanoscale TiO 2, SiO 2, and ZnO water suspensions. *Water research* **2006,** *40*, (19), 3527-3532.
22. Xia, T.; Kovochich, M.; Liong, M.; Mädler, L.; Gilbert, B.; Shi, H.; Yeh, J. I.; Zink, J. I.; Nel, A. E., Comparison of the Mechanism of Toxicity of Zinc Oxide and Cerium Oxide Nanoparticles Based on Dissolution and Oxidative Stress Properties. *ACS nano* **2008,** *2*, (10), 2121-2134.
23. Saleh, N. B.; Milliron, D. J.; Aich, N.; Katz, L. E.; Liljestrand, H. M.; Kirisits, M. J., Importance of Doping, Dopant Distribution, and Nano-Scale Defects on Electronic Band Structure
Alteration of Metal Oxide Nanoparticles: Implications for Reactive Oxygen Species Generation. *Science of the Total Environment (In Press)* **2016**.
24. Xiong, D.; Fang, T.; Yu, L.; Sima, X.; Zhu, W., Effects of nano-scale TiO2, ZnO and their bulk counterparts on zebrafish: Acute toxicity, oxidative stress and oxidative damage. *Science of the Total Environment* **2011,** *409*, (8), 1444-1452.
25. Balázs, N.; Mogyorósi, K.; Srankó, D. F.; Pallagi, A.; Alapi, T.; Oszkó, A.; Dombi, A.; Sipos, P., The effect of particle shape on the activity of nanocrystalline TiO2 photocatalysts in phenol decomposition. *Applied Catalysis B: Environmental* **2008,** *84*, (3–4), 356-362.
26. Mogyorosi, K.; Balazs, N.; Sranko, D. F.; Tombacz, E.; Dekany, I.; Oszko, A.; Sipos, P.; Dombi, A., The effect of particle shape on the activity of nanocrystalline TiO2 photocatalysts in phenol decomposition. Part 3: The importance of surface quality. *Applied Catalysis B-Environmental* **2010,** *96*, (3-4), 577-585.
27. Sayes, C. M.; Wahi, R.; Kurian, P. A.; Liu, Y.; West, J. L.; Ausman, K. D.; Warheit, D. B.; Colvin, V. L., Correlating Nanoscale Titania Structure with Toxicity: A Cytotoxicity and Inflammatory Response Study with Human Dermal Fibroblasts and Human Lung Epithelial Cells. *Toxicological Sciences* **2006,** *92*, (1), 174-185.
28. Jung, K.-h.; Hong, J. S.; Vittal, R.; Kim, K.-J., Enhanced Photocurrent of Dye-Sensitized Solar Cells by Modification of TiO2 with Carbon Nanotubes. *Chemistry Letters* **2002**, (8), 864-865.

29. Dai, K.; Dawson, G.; Yang, S.; Chen, Z.; Lu, L., Large scale preparing carbon nanotube/zinc oxide hybrid and its application for highly reusable photocatalyst. *Chemical Engineering Journal* **2012,** *191*, 571-578.
30. Hua, Z.; Zhang, J.; Bai, X.; Ye, Z.; Tang, Z.; Liang, L.; Liu, Y., Aggregation of TiO 2–graphene nanocomposites in aqueous environment: Influence of environmental factors and UV irradiation. *Science of the Total Environment* **2016,** *539*, 196-205.
31. Nguyen, M. T.; Nguyen, C. K.; Vu, T. M. P.; Van Duong, Q.; Pham, T. L.; Nguyen, T. C., A study on carbon nanotube titanium dioxide hybrids: experiment and calculation. *Advances in Natural Sciences: Nanoscience and Nanotechnology* **2014,** *5*, (4), 045018.
32. Yang, C.-F.; Hsu, W.-C.; Wu, S.-M.; Su, C.-C., Elucidating how surface functionalization of multiwalled carbon nanotube affects nanostructured MWCNT/titania hybrid materials. *Journal of Nanomaterials* **2015,** *2015*.
33. Haldorai, Y.; Rengaraj, A.; Lee, J.-B.; Huh, Y. S.; Han, Y.-K., Highly efficient hydrogen production via water splitting using Pt@ MWNT/TiO 2 ternary hybrid composite as a catalyst under UV–visible light. *Synth. Met.* **2015,** *199*, 345-352.
34. Jitianu, A.; Cacciaguerra, T.; Berger, M.-H.; Benoit, R.; Béguin, F.; Bonnamy, S., New carbon multiwall nanotubes–TiO 2 nanocomposites obtained by the sol–gel method. *Journal of non-crystalline solids* **2004,** *345*, 596-600.
35. Ding, M.; Sorescu, D. C.; Star, A., Photoinduced Charge Transfer and Acetone Sensitivity of Single-Walled Carbon Nanotube–Titanium Dioxide Hybrids. *Journal of the American Chemical Society* **2013,** *135*, (24), 9015-9022.
36. Zarezade, M.; Ghasemi, S.; Gholami, M. R., The effect of multiwalled carbon nanotubes and activated carbon on the morphology and photocatalytic activity of TiO 2/C hybrid materials. *Catalysis Science & Technology* **2011,** *1*, (2), 279-284.
37. Khanderi, J.; Hoffmann, R. C.; Gurlo, A.; Schneider, J. J., Synthesis and sensoric response of ZnO decorated carbon nanotubes. *Journal of Materials Chemistry* **2009,** *19*, (28), 5039-5046.
38. Song, W.-L.; Cao, M.-S.; Wen, B.; Hou, Z.-L.; Cheng, J.; Yuan, J., Synthesis of zinc oxide particles coated multiwalled carbon nanotubes: Dielectric properties, electromagnetic interference shielding and microwave absorption. *Materials Research Bulletin* **2012,** *47*, (7), 1747-1754.
39. Byrappa, K.; Dayananda, A.; Sajan, C.; Basavalingu, B.; Shayan, M.; Soga, K.; Yoshimura, M., Hydrothermal preparation of ZnO: CNT and TiO2: CNT composites and their photocatalytic applications. *Journal of Materials Science* **2008,** *43*, (7), 2348-2355.
40. Dai, K.; Zhang, X.; Fan, K.; Peng, T.; Wei, B., Hydrothermal synthesis of single-walled carbon nanotube–TiO 2 hybrid and its photocatalytic activity. *Applied Surface Science* **2013,** *270*, 238-244.
41. Liu, C.; Chen, H.; Dai, K.; Xue, A.; Chen, H.; Huang, Q., Synthesis, characterization, and its photocatalytic activity of double-walled carbon nanotubes-TiO 2 hybrid. *Materials Research Bulletin* **2013,** *48*, (4), 1499-1505.
42. Saleh, T. A.; Gondal, M.; Drmosh, Q., Preparation of a MWCNT/ZnO nanocomposite and its photocatalytic activity for the removal of cyanide from water using a laser. *Nanotechnology* **2010,** *21*, (49), 495705.

43. Tian, L. H.; Ye, L. Q.; Deng, K. J.; Zan, L., TiO2/carbon nanotube hybrid nanostructures: Solvothermal synthesis and their visible light photocatalytic activity. *Journal of Solid State Chemistry* **2011,** *184*, (6), 1465-1471.
44. Guo, G.; Guo, J.; Tao, D.; Choy, W.; Zhao, L.; Qian, W.; Wang, Z., A Simple method to prepare multi-walled carbon nanotube/ZnO nanoparticle composites. *Applied Physics A* **2007,** *89*, (2), 525-528.
45. Kim, B. C.; Kim, S.; Chung, J.; Chen, J.; Park, S.; Wallace, G. G., Charge storage in carbon nanotube–TiO 2 hybrid nanoparticles. *Synth. Met.* **2012,** *162*, (7), 650-654.
46. Yan, X. M.; Pan, D. Y.; Li, Z.; Zhao, B.; Zhang, J. C.; Wu, M. H., Facile synthesis of solution-disposable carbon nanotube-TiO2 hybrids in organic media. *Materials Letters* **2010,** *64*, (15), 1694-1697.
47. Ueda, T.; Takahashi, K.; Mitsugi, F.; Ikegami, T., Preparation of single-walled carbon nanotube/TiO 2 hybrid atmospheric gas sensor operated at ambient temperature. *Diamond and Related Materials* **2009,** *18*, (2), 493-496.
48. Du, Y.; Hao, C.; Wang, G., Preparation of floral-patterned ZnO/MWCNT heterogeneity structure using microwave irradiation heating method. *Materials Letters* **2008,** *62*, (1), 30-32.
49. Green, J. M.; Dong, L.; Gutu, T.; Jiao, J.; Conley Jr, J. F.; Ono, Y., ZnO-nanoparticle-coated carbon nanotubes demonstrating enhanced electron field-emission properties. *Journal of applied physics* **2006,** *99*, (9), 094308.
50. Jassby, D.; Farner Budarz, J.; Wiesner, M., Impact of aggregate size and structure on the photocatalytic properties of TiO2 and ZnO nanoparticles. *Environmental science & technology* **2012,** *46*, (13), 6934-6941.
51. Wilkinson, L. L. Visible and infrared emission from Er_2O_3 nanoparticles, and Ho^{+3}, Tm^{+3}, and Sm^{+3} doped in AlN for optical and biomedical applications. Ball State University, Muncie, Indiana, 2012.
52. Afrooz, A. N.; Das, D.; Murphy, C. J.; Vikesland, P.; Saleh, N. B., Co-transport of gold nanospheres with single-walled carbon nanotubes in saturated porous media. *Water Research* **2016,** *99*, 7-15.
53. Aich, N.; Boateng, L. K.; Sabaraya, I. V.; Das, D.; Flora, J. R.; Saleh, N. B., Aggregation kinetics of higher order fullerene clusters in aquatic systems. *Environmental science & technology* **2016,** *50*, (7), 3562-3571.
54. Afrooz, A. N.; Khan, I. A.; Hussain, S. M.; Saleh, N. B., Mechanistic heteroaggregation of gold nanoparticles in a wide range of solution chemistry. *Environmental science & technology* **2013,** *47*, (4), 1853-1860.
55. Khan, I. A.; Afrooz, A. R. M. N.; Flora, J. R. V.; Schierz, P. A.; Ferguson, P. L.; Sabo-Attwood, T.; Saleh, N. B., Chirality affects aggregation kinetics of single-walled carbon nanotubes. *Environmental science & technology* **2013,** *47*, (4), 1844-1852.
56. Khan, I. A.; Aich, N.; Afrooz, A. R. M. N.; Flora, J. R. V.; ferguson, L.; sabo-Attwood, T.; Saleh, N. B., Fractal structures of single-walled carbon nanotubes in biologically relevant conditions: role of chirality vs. media conditions. *Chemosphere* **2013** *93*, (9), 1997-2003.

57. Khan, I. A.; Flora, J. R. V.; Afrooz, A. R. M. N.; Aich, N.; Schierz, P. A.; Ferguson, P. L.; Sabo-Attwood, T.; Saleh, N. B., Change in chirality of semiconducting single-walled carbon nanotubes can overcome anionic surfactant stabilisation: a systematic study of aggregation kinetics. *Environmental Chemistry* **2015,** *12*, (6), 652-661.
58. Saleh, N. B.; Pfefferle, L. D.; Elimelech, M., Aggregation kinetics of multiwalled carbon nanotubes in aquatic systems: measurements and environmental implications. *Environmental Science & Technology* **2008,** *42*, (21), 7963-7969.
59. Mansfield, E.; Kar, A.; Hooker, S. A., Applications of TGA in quality control of SWCNTs. *Analytical and Bioanalytical Chemistry* **2010,** *396*, (3), 1071-1077.
60. Afrooz, A. R. M. N.; Khan, I. A.; Hussain, S. M.; Saleh, N. B., Mechanistic heteroaggregation of gold nanoparticles in a wide range of solution chemistry. *Environmental Science & Technology* **2013,** *47*, (4), 1853-1860.
61. Afrooz, A. R. M. N.; Sivalapalan, S. T.; Murphy, C. J.; Hussain, S. M.; Schlager, J. J.; Saleh, N. B., Spheres vs. rods: the shape of gold nanoparticles influences aggregation and deposition behavior. *Chemosphere* **2013,** *91*, (1), 93-98.
62. Rigdon, W. A.; Huang, X., Carbon monoxide tolerant platinum electrocatalysts on niobium doped titania and carbon nanotube composite supports. *Journal of Power Sources* **2014,** *272*, 845-859.
63. Miritello, M.; Savio, R. L.; Piro, A.; Franzo, G.; Priolo, F.; Iacona, F.; Bongiorno, C., Optical and structural properties of Er2O3 films grown by magnetron sputtering. *Journal of applied physics* **2006,** *100*, (1), 013502.
64. Hassan, M. S.; Akhtar, M. S.; Shim, K.-B.; Yang, O.-B., Morphological and electrochemical properties of crystalline praseodymium oxide nanorods. *Nanoscale research letters* **2010,** *5*, (4), 735.
65. Wepasnick, K. A.; Smith, B. A.; Bitter, J. L.; Fairbrother, D. H., Chemical and structural characterization of carbon nanotube surfaces. *Analytical and bioanalytical chemistry* **2010,** *396*, (3), 1003-1014.
66. Naumkin, A. V.; Kraut-Vass, A.; Gaarenstroom, S. W.; Powell, C. J., NIST X-ray Photoelectron Spectroscopy Database *NIST Standard Reference Database 20, Version 4.1* **2012**.
67. Naumkin, A. V.; Kraut-Vass, A.; Gaarenstroom, S. W.; Powell, C. J., NIST X-ray Photoelectron Spectroscopy Database In 2012.
68. Aksel, S.; Eder, D., Catalytic effect of metal oxides on the oxidation resistance in carbon nanotube–inorganic hybrids. *J. Mater. Chem.* **2010,** *20*, (41), 9149-9154.
69. Eder, D.; Windle, A. H., Morphology control of CNT-TiO 2 hybrid materials and rutile nanotubes. *Journal of Materials Chemistry* **2008,** *18*, (17), 2036-2043.
70. Aich, N.; Boateng, L. K.; Flora, J. R.; Saleh, N. B., Preparation of non-aggregating aqueous fullerenes in highly saline solutions with a biocompatible non-ionic polymer. *Nanotechnology* **2013,** *24*, (39), 395602.
71. Khan, I. A.; Flora, J. R.; Afrooz, A. N.; Aich, N.; Schierz, P. A.; Ferguson, P. L.; Sabo-Attwood, T.; Saleh, N. B., Change in chirality of semiconducting single-walled carbon nanotubes can overcome anionic surfactant stabilisation: a systematic study of aggregation kinetics. *Environmental Chemistry* **2015,** *12*, (6), 652-661.

72. Yi, P.; Chen, K. L., Influence of surface oxidation on the aggregation and deposition kinetics of multiwalled carbon nanotubes in monovalent and divalent electrolytes. *Langmuir* **2011,** *27*, (7), 3588-3599.
73. Smith, B.; Wepasnick, K.; Schrote, K. E.; Cho, H.-H.; Ball, W. P.; Fairbrother, D. H., Influence of surface oxides on the colloidal stability of multi-walled carbon nanotubes: a structure-property relationship. *Langmuir* **2009,** *25*, (17), 9767-9776.
74. Smith, B.; Wepasnick, K.; Schrote, K. E.; Bertele, A. R.; Ball, W. P.; O'Melia, C.; Fairbrother, D. H., Colloidal Properties of Aqueous Suspensions of Acid-Treated, Multi-Walled Carbon Nanotubes. *Environmental Science & Technology* **2009,** *43*, (3), 819-825.
75. Saleh, N. B.; Pfefferle, L. D.; Elimelech, M., Influence of biomacromolecules and humic acid on the aggregation kinetics of single-walled carbon nanotubes. *Environmental Science & Technology* **2010,** *44*, (7), 2412-2418.
76. Sano, M.; Okamura, J.; Shinkai, S., Colloidal nature of single-walled carbon nanotubes in electrolyte solution: the Schulze-Hardy rule. *Langmuir* **2001,** *17*, (22), 7172-7173.
77. Chowdhury, I.; Duch, M. C.; Mansukhani, N. D.; Hersam, M. C.; Bouchard, D., Colloidal properties and stability of graphene oxide nanomaterials in the aquatic environment. *Environmental Science & Technology* **2013,** *47*, (12), 6288-6296.
78. Lanphere, J. D.; Luth, C. J.; Walker, S. L., Effects of solution chemistry on the transport of graphene oxide in saturated porous media. *Environmental Science & Technology* **2013,** *47*, (9), 4255-4261.

Chapter 3: Insights into Metal Oxide and Metal Nanocrystal Formation During the Sol-gel Hybridization Process

3.1 INTRODUCTION

The aim of this chapter is to gain insight into the metal oxide crystal formation (i.e., process and degree of crystallinity) and also to assess applicability of the sol-gel technique (developed in Chapter 2) for hybridizing multiwalled carbon nanotubes (MWNTs) with oxides and zero-valent crystals of a wide range of metal species. The insights gained herein will allow for achieving better control over crystal growth and will facilitate the use of the developed sol-gel method to synthesize nanohybrids (NHs) with metal or metal oxide of choice.

When preparing metallic NMs, achieving crystalline order (of the synthesized materials) is essential to extract the desired optical, electronic, and chemical properties[1]. Synthesis methods and operating conditions (e.g., temperature[2], reducing agent[3]) are adjusted to prepare metal nanocrystals with ordered crystallinity[2] and desired redox state of the metal species[4]. Calcination of MO nanoparticles at elevated temperature can facilitate preparing ordered structures; however, the feasibility of applying such high temperature can be limited when carbon nanotubes are involved in the mix. MWNTs are known to oxidize completely in air when heated up to 500 °C or higher[5, 6]. Hybridization with metallic nanocrystals can facilitate MWNT oxidation and lower the MWNT oxidation temperature via chemical modification of the MWNT surface[6]. Hence, required temperature for desired crystallinity in specific metallic nanocrystals might not be achieved for the *in situ* sol-gel synthesis process.

Applicability of the sol-gel synthesis process for hybridizing zero-valent metals with MWNTs will depend on the synthesis conditions as the metal ions would need to be reduced to form zero-valent metals. Formation of zero-valent nanocrystals can be achieved by addition of strong reducing agents (e.g., sodium borohydride) [3, 7]. Addition of such a reducing agent can be utilized in a sol-gel synthesis technique while hybridizing zero-valent metal nanoparticles with MWNTs. However, it may impose a significant limitation on the quality of the materials produced. In the presence of a strong reducing agent, a large amount of individual zero-valent nanocrystals can form that are not chemically bound to the MWNTs, which will require rigorous post-treatment of the materials to separate the NHs from the unattached nanocrystals. Thus, further modification of the sol-gel technique may be necessary to better control the degree of crystallinity and to prepare metal vs. metal oxides under comparable sets of synthesis conditions.

Standard electron potential (SEP) of a metal species can dictate reaction pathway, and hence can control the composition (i.e., metal vs. metal oxide) of the crystal grown on MWNT surfaces. SEP values considered here represent electron transfer capabilities between the oxidized and the zero-valent metallic forms of a metal species (i.e., $M^{n+} + ne^- \leftrightarrow M$, where M is the metal species and n is the number of electrons involved in the reaction). Literature evidence show that metals with negative SEP preferentially form MOs while those with positive values tend to form zero-valent metallic form of the same. Following are the MOs that are reported in the literature to form on carbon nanotube (CNT) surfaces: Al_2O_3[8-10], CeO_2[11, 12], CoO_3[13, 14], Eu_2O_3[15, 16], Fe_xO_y[17-20], HfO_2[21, 22], MgO[23], MoO_2[24], NiO[25], SiO_2[26-28], SnO_2[29], TiO_2[30, 31], V_xO_y[32], ZnO[33], and ZrO_2[34]. On the other hand, Ag[35],

Au[36], Pt[37], and Pd[38] with positive SEP are reported to form zero-valent metals on CNT surfaces. Cu and W (with positive SEP) and Fe (with negative SEP) demonstrate exceptions; i.e., despite positive values of SEP, Cu[39] and W[40] are shown to form oxides, whereas Fe with negative SEP can form zero-valent metal nanocrystals[41]. Table B2 (appendix B) shows the SEPs of different metal species. The abovementioned discussion clearly indicates that SEP can determine formation of metal vs MO on the MWNT surface. The challenge, however, is to comment on the role of SEP on forming metal vs MO while utilizing the sol-gel method developed in chapter 2 to synthesize MWNT based NHs. This chapter aims to provide insight into the crystal formation and assesses the degree of crystallinity of the metal oxides grown onto MWNT surfaces. X-ray diffraction (XRD) has been used to characterize the materials before and after calcination. Applicability of sol-gel method to prepare MWNT-zero-valent metal NHs without the use of a reducing agent has been assessed. The choice of the metal species is guided by the SEP values (i.e., Cu and Ag with +0.345 and +0.799 V SEP values, respectively). These are two metal species with some of the lowest magnitude of SEP values (among the positive SEP species), and hence are most relevant to determine the threshold SEP for zero-valent metal crystal formation. XRD has been used to characterize the crystalline features of these NHs as well.

3.2 MATERIALS AND METHODS

3.2.1 Chemicals and Reagents

Pristine MWNTs (O.D. 8-15 nm) were procured from Cheap Tubes Inc. (Brattleboro, VT). Concentrated nitric acid, sulfuric acid, titanium (IV) isopropoxide (TTIP), erbium (III) nitrate pentahydrate, praseodymium (III) nitrate hexahydrate, and copper (II) nitrate monohydrate were purchased from Sigma Aldrich (St. Louis, MO). Trace metal grade silver nitrate was purchased from Alfa Aesar (Haverhill, MA). Isopropanol and dimethylformamide (DMF) was obtained from Fisher Scientific (Pittsburgh, PA) while zinc (II) nitrate hexahydrate was purchased from J.T Baker (Center Valley, PA). For preparing all aqueous suspensions and solutions, 18.2 mΩ (Milli-Q) water was used unless otherwise stated.

3.2.2 Material Synthesis

All materials were synthesized using the sol-gel technique developed in Chapter 2. In brief, MWNTs (1 g) were acid-etched by ultrasonication (Qsonica LLC, Newtown, CT) in 300 mL of concentrated nitric and sulfuric acid mixture (1:1 volume basis). Upon sonication, the mixture was refluxed at 100 °C for 3 h under continuous stirring. The oxidized MWNTs were subsequently filtered until the pH of the filtrate reached >5.5 and then were dried for 48 h in a desiccator. Once dried, the oxidized MWNTs were re-suspended in isopropanol with an ultrasonic dismembrator (Qsonica, Newtown, CT) and transferred into a round bottom flask. Appropriate amounts of precursors were added to 10 mL of isopropanol and introduced drop wise to the MWNT-isopropanol suspension at

0.301 mL/min with a peristaltic pump (Ismatec, Wertheim, Germany). The slow rate of precursor addition was maintained to provide sufficient mixing time. The entire suspension was refluxed at 80 °C for 3 h in a nitrogen environment. For MWNT-TiO_2 NH, 5 mL of water was added drop wise into the reaction vessel to promote TiO_2 crystal formation on the MWNT backbone via a hydrolysis process over 1 h. Similar hydrolysis step was performed for $AgNO_3$ precursor as well since the $AgNO_3$ was anhydrous. Afterwards, the refluxed mixture was washed 4 times with isopropanol (as a purification step), which removed any unreacted reagent. Finally, isopropanol was evaporated, the dry materials were powdered using a mortar and pestle, and the resultant materials were calcined at 400 °C for 3 h under nitrogen to facilitate crystal formation.

3.2.3 Analysis of Crystallinity

The crystallinity of all the materials was evaluated with XRD. A 600 W Rigaku MiniFlex 600 (Rigaku, Japan) with a Cu-Kα irradiator (0.154 nm wavelength) and a graphite monochromator was used at a step width of 0.04° (between 2θ values of 15° to 70°) and a scanning rate of 2°/min.

3.3 Results and Discussion

3.3.1. Mechanism of Metal Oxide Crystal Formation

The MWNTs utilized in synthesis were etched with oxygen functional moieties via acid etching[42, 43]. These functional sites enhanced dispersibility of these MWNTs in isopropanol and also served as binding and nucleation sites for the metal oxide nanocrystals[44]. The preferential localization of metal cations is likely electrostatic in

origin[44], which is facilitated by an increased number of anionic binding sites on the functionalized MWNTs.

TiO_2 and ZnO nanocrystals growth on the MWNT surfaces was promoted by the negatively charged oxygen moieties on MWNT surfaces. Literature discusses such mechanism for TiO_2 nanocrystal formation on oxidized MWNTs[30]. In brief, upon addition of TIP in oxidized MWNT suspension, the TTIP interacts with the oxygen-containing groups on the MWNT surfaces, giving rise to a C-O-Ti bond formation[30]. The C-O-Ti bond acts as a nucleation cite and, upon hydrolysis, the TiO_2 nanocrystals are formed around the nucleation site[30]. These TiO_2 nanocrystals are primarily amorphous and these undergo phase-transformation to form cyrstalline (anatase) nano-TiO_2 upon calcination. A likely pathway for MWNT-TiO_2 NH formation is shown below.

$$MWNT \xrightarrow{[acid\ etch]} O-MWNT^- \xrightarrow{Ti(O-C_2H_6)_4} MWNT-O-Ti(O-C_2H_6)_3 + C_2H_6OH$$

$$MWNT-O-Ti(O-C_2H_6)_3 \xrightarrow{Hydrolysis} MWNT-TiO_2 \xrightarrow{Calcination} MWNT-TiO_2\ (Anatase)$$

Nanocrystal formation mechanism for MWNT-ZnO has been evaluated in this study with XRD characterization on the materials, before and after calcination (Figure 3.1). Reactions are likely initiated in a similar way, where electrostatic attraction between zinc cations and anionic surface groups on MWNTs associate the Zn^{2+} with the MWNT surfaces. These ions then react with water molecules (generated from the hydrated zinc nitrate salt) to form $Zn(OH)_2$ on the MWNT surface, which serve as nucleation sites for further growth of amorphous and mixed-phased $Zn(OH)_2$ and ZnO. XRD spectra before calcination shows evidence of both the crystal phases (Figure 3.1). During calcination at elevated temeperature (at 400 °C in this case), the $Zn(OH)_2$ likely loses the excess water

and forms ZnO crystal phases onto MWNTs. XRD spectrum on the NH after calcinaton shows no evidence of $Zn(OH)_2$ phase (Figure 3.1) and confirms this likely crystal formation pathway. Literature reports on XRD patterns for amorphous $Zn(OH)_2$ and ZnO has been used to relate peak positions with specific crystalline planes[45]. The reaction pathway for MWNT-ZnO NH formation is shown below.

$$O-MWNT^{-} \xrightarrow{Zn(NO_3)_2} O-MWNT^{-}Zn^{2+} \xrightarrow{H_2O} MWNT-ZnO/Zn(OH)_2(amorphous)$$

$$\xrightarrow{Heat} MWNT-ZnO\ (crystalline)$$

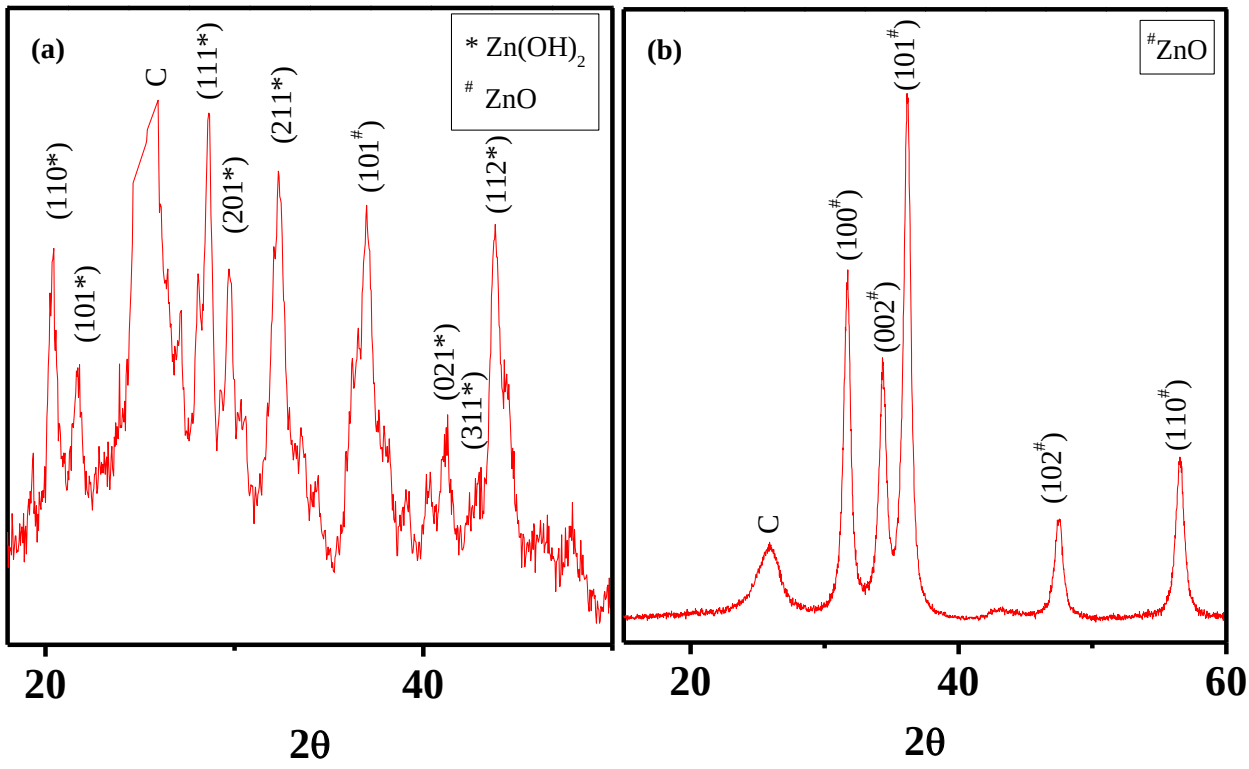

Figure 3.1: Representative XRD spectra of MWNT-ZnO NH before (a) and after (b) calcination at 400 °C for 3 hours. The peak positions are labeled to indicate the respective crystal planes.

3.3.2 Assessing the Crystallinity of the Lanthanide Series Metal Oxides

It is hypothesized that the MO growth mechanism for the MWNT-MO NHs with lanthanide series metals (i.e., MWNT-Er_2O_3 and MWNT-Pr_6O_{11}) is similar to that of MWNT-ZnO NH, since the oxides of all these three metals use nitrate precursors of the respective metals. Prior to calcination, MWNT-Er_2O_3 NHs show significant widening of XRD peaks (Figure 3.2), indicating amorphous behavior of the nanofeatures grown. The uncalcined MWNT-Pr_6O_{11} demonstrates random crystalline peaks similar to that of uncalcined MWNT-ZnO. The crystalline peaks, however, did not match Er hydroxide or Pr hydroxide crystalline peaks[46]. The lack of a true match between literature reported $Er(OH)_3$ peaks and those reported here indicates likely presence of amorphous Er_2O_3 and/or $Er(OH)_3$. On the other hand, some of the crystalline peaks of uncalcined MWNT-Pr_6O_{11} overlap with the $Pr(OH)_3$ crystalline peaks at 2θ values of ~16°, ~28°, ~40°, and ~50°[46]; however, lack of a true match with the literature reported spectrum limits drawing any conclusion on the crystalline composition of this material. The existing crystalline phases may be a mixture of $Pr(OH)_3$ and/or $Pr(NO_3)_3$. Thus, crystal formation pathway for the MWNT-Er_2O_3 and MWNT-Pr_6O_{11} NHs cannot be conclusively discerned in this work.

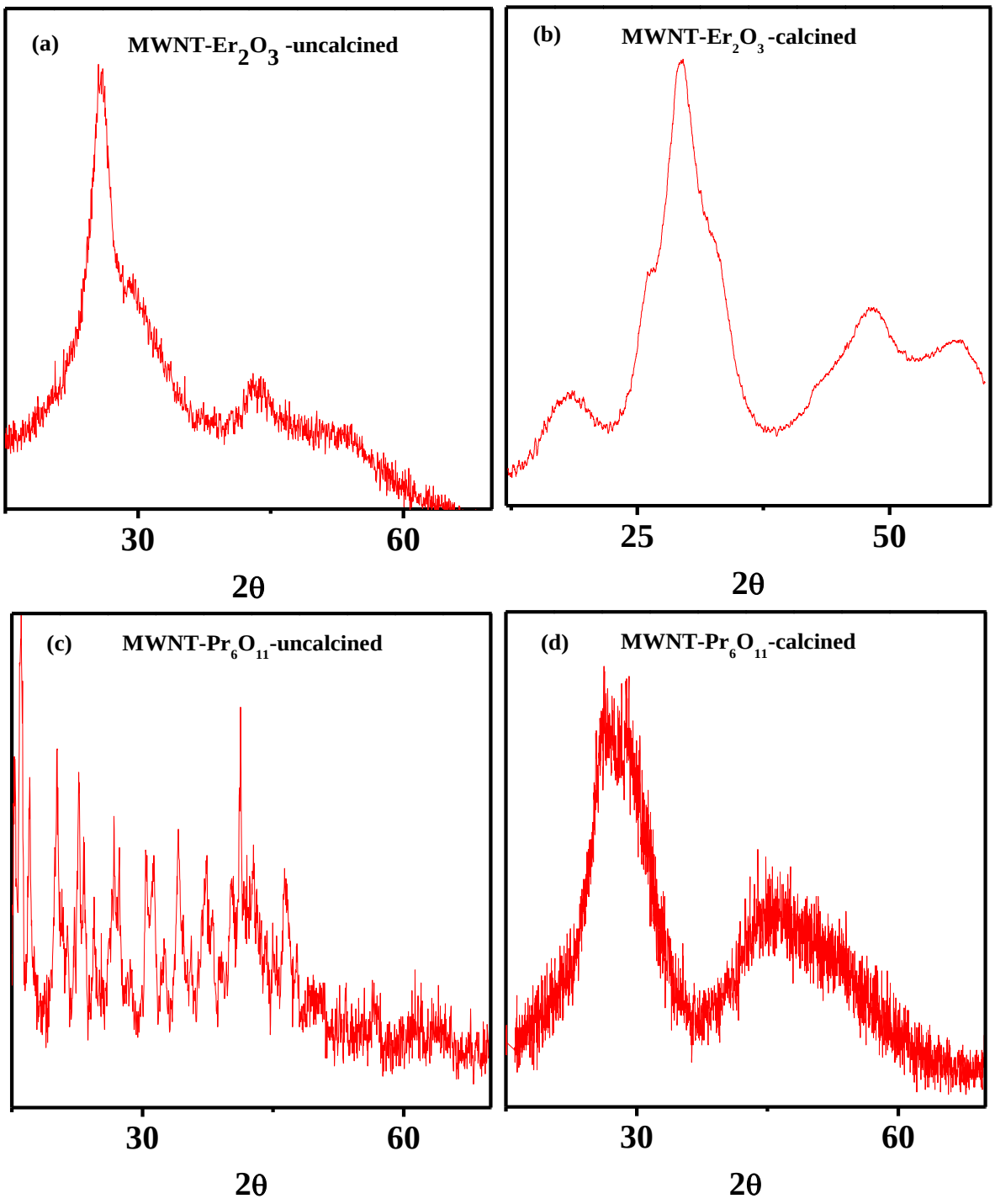

Figure 3.2: XRD spectra of NH with lanthanide series MOs before and after calcination at 400 °C for 3 hours in air: MWNT-Er_2O_3 NH (a) before and (b) after calcination and MWNT-Pr_6O_{11} NH (c) before and (d) after calcination. Both NHs were synthesized using the same sol-gel technique.

In chapter 2, the HRTEM micrographs of the MWNT-Er_2O_3 and MWNT-Pr_6O_{11} demonstrated lattice fringes of their MO contents (Figure 2.1). Hence, in order to assess the physical morphology and crystallinity of the Er_2O_3, and Pr_6O_{11} MOs in the NHs, the MWNT component of these NHs were completely oxidized at 600 °C in air for 3 hours. The residual MO nanocrystals were collected and characterized by TEM for size and by XRD for crystallinity. The TEM micrographs (Figure 3.3 a and b) on these materials show similar sized nanocrystals with individual particle diameters ranging from 5-15 nm. These nanocrystals also show distinct lattice fringes, which confirm that the metal oxides are ordered.

XRD spectra of the Er_2O_3 and Pr_6O_{11} show sharp and defined peaks, which indicates high degree of crystallinity as opposed to their respective NHs (Figure 3.3 c and d). The Er_2O_3 MOs show XRD peaks corresponding to (211), (222), (400), (411), (332), (431), (400), and (622)[47] while the crystalline planes of Pr_6O_{11} MOs have been found to be (111), (200), (220), (311), (222), and (400)[48]. These results are significant and suggest that increased calcination temperature in air can enhance the degree of crystallinity on the lanthanide series MO nanocrystals. However, if the NHs are calcined at this elevated temperature in an oxic environment, carbon nanotubes will undergo complete oxidation and the NHs will not be obtained. Hence, further modification to the sol-gel process is necessary while applying this technique in an air-free environment in order to increase the degree of MO crystallinity in these NHs. Another possibility is that the hybridization process is somehow masking the crystallinity of Er_2O_3 and Pr_6O_{11} and because of that

reason, the XRD spectra of MWNT-Er_2O_3 and MWNT-Pr_6O_{11} NHs are not showing ordered MO crystallinity despite the MO lattice fringes observed in their HRTEM.

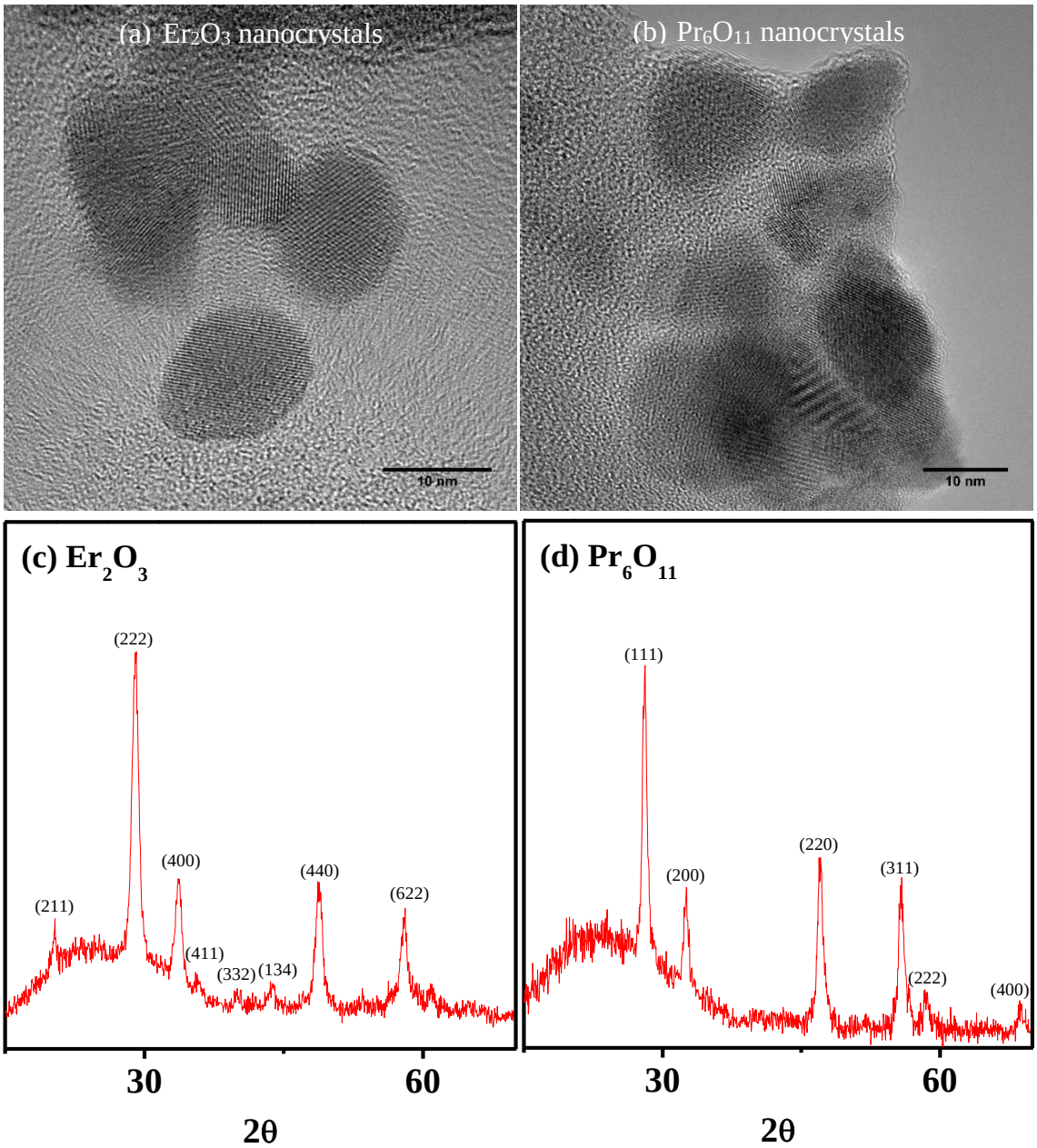

Figure 3.3: Representative HRTEM micrographs (a,b) and XRD spectra (c,d) of lanthanide series MO nanocrystals obtained after complete oxidation of the NHs. (a,c) Er_2O_3, and (b,d) Pr_6O_{11}. MO nanocrystals were obtained by complete oxidation of MWNT content from their respective NHs at 600 °C for 3 hours in air. The peak positions in the XRD spectra are labeled as their respective crystal planes.

In an effort to grow lanthanide series metal oxides with a high degree of crystallinity, synthesis of NHs at elevated temperature (600 °C for 3 h) in a nitrogen environment were performed. XRD analysis (Figure 3.4) continues to show peak broadening, i.e., presence of amorphous materials on the MWNT surfaces. However, XRD spectra of both materials display appearance of additional crystalline peaks (Figure 3.4), which were not observed in the NHs calcined at 400 °C (Figure 3.2). These results demonstrate that temperature needs to be further elevated to achieve a higher degree of crystallinity.

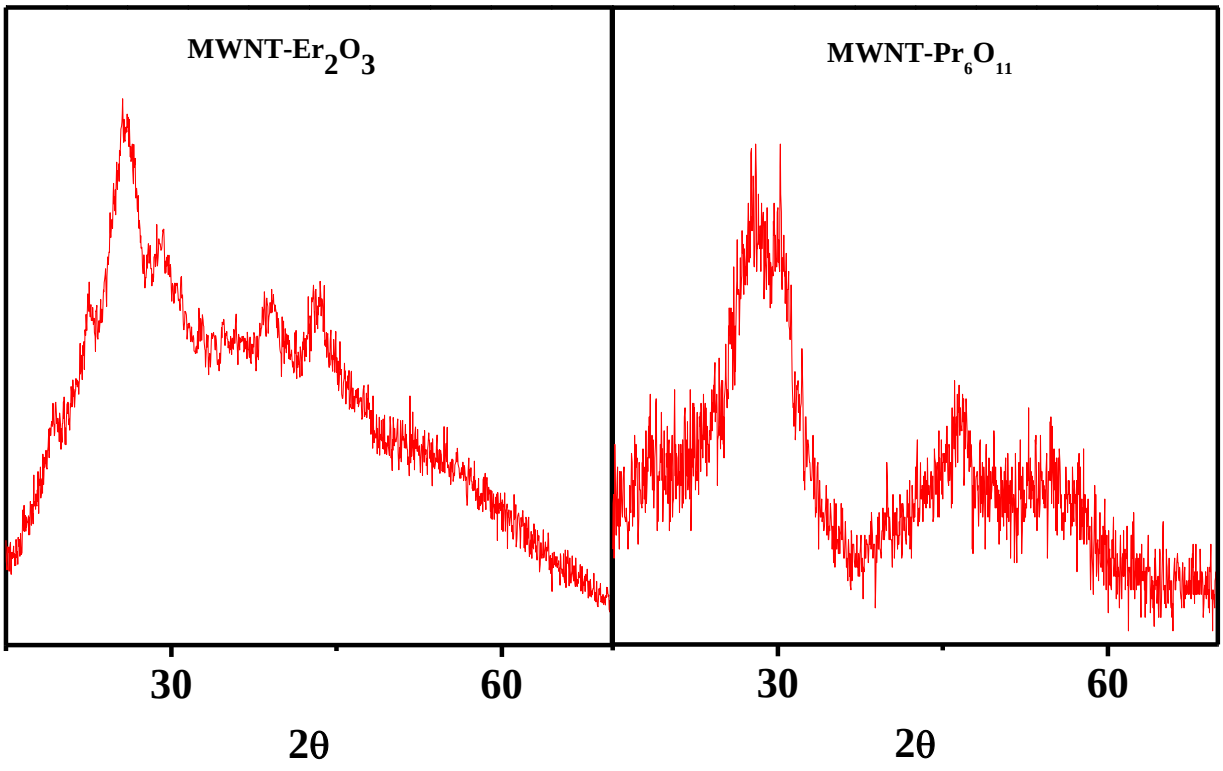

Figure 3.4: XRD pattern of MWNT-Er_2O_3 and MWNT-Pr_6O_{11} NH synthesized using the sol-gel technique and calcined at 600 °C in a nitrogen environment for 3 hours.

Since oxidation of the MWNTs initiates around 350 °C in oxic condition, calcination was performed at a lower temperature (i.e., 320 °C) to assess if calcination in an oxic environment can increase the degree of crystallinity. Figure 3.5 shows the XRD spectra of the two NHs, where the amorphous nature of the materials continues to be evident. These results suggest that further elevation of the synthesis as well as calcination temperature is necessary to enhance the degree of crystallinity of the lanthanide series oxides. Thus, careful experimental design modifications are desired to perform such synthesis in an anoxic environment.

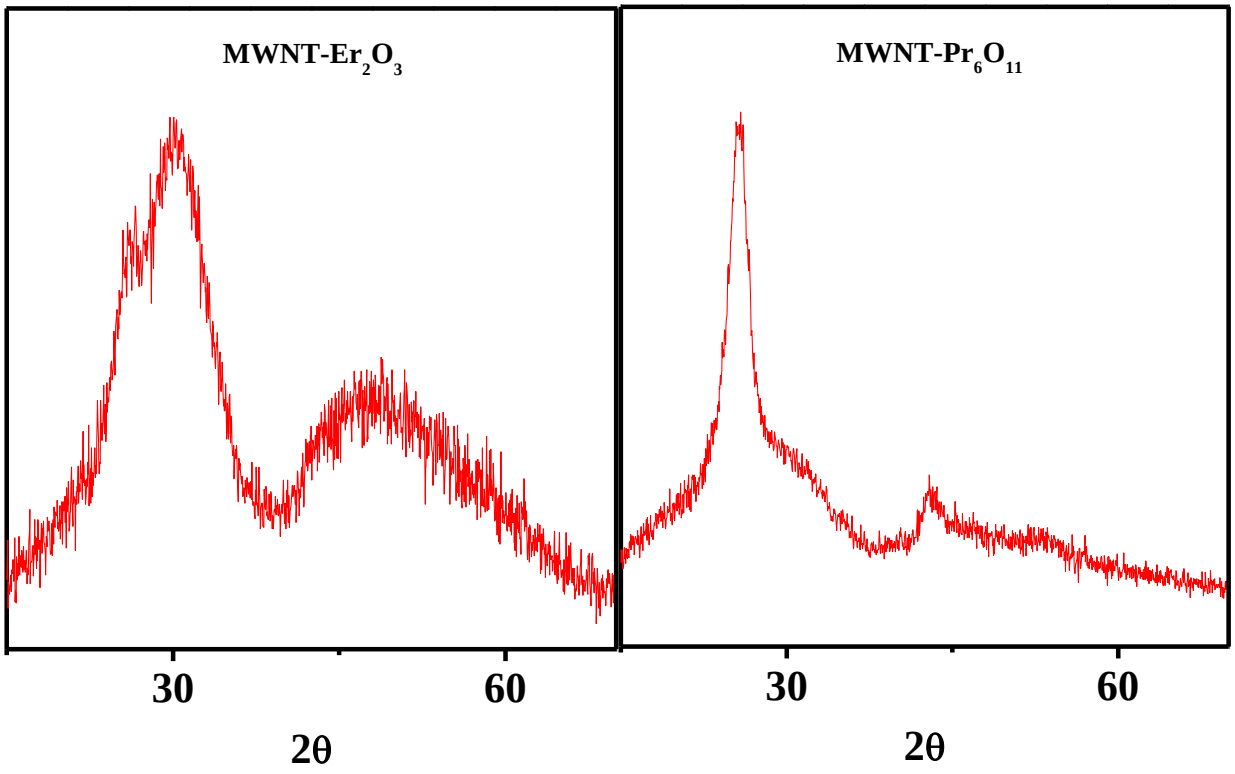

Figure 3.5: XRD spectra of MWNT-Er_2O_3 and MWNT-Pr_6O_{11} NH calcined at 320 °C in air using the sol-gel method. All other synthesis parameters were unchanged.

3.3.3 Applicability of the Sol-gel Method for MWNT-Zero-Valent Metal Synthesis

MWNT has been successfully hybridized with zero-valent Ag (with SEP of +0.799) following the developed sol-gel method. The TEM micrograph (Figure 3.6 a) show nano-sized spherical features that are not very well distributed on the MWNT surfaces. The XRD spectrum of the MWNT-Ag NH (Figure 3.6 c) shows peaks corresponding to (111), (200), (220), and (311) crystal planes, which correspond to zero-valent Ag nanoparticles[49].

Hybridization of MWNTs with Cu was performed following similar experimental conditions. TEM micrograph (Figure 3.6 b) shows similar nano-sized features on the MWNT surfaces. However, the XRD spectrum (Figure 3.6 d) shows presence of both zero-valent and oxidized forms of Cu by displaying defined peaks at (111), (200), and (220) and (111) and (220) for Cu and Cu_2O crystal planes, respectively[50]. Literature reports on zero-valent Cu nanoparticle suggest that such behavior can stem from unavoidable oxidation of zero-valent Cu while performing XRD[50, 51]. Some literature evidences also suggest that such XRD patterns are typical for Cu/Cu_2O core/shell nanocrystals[50].

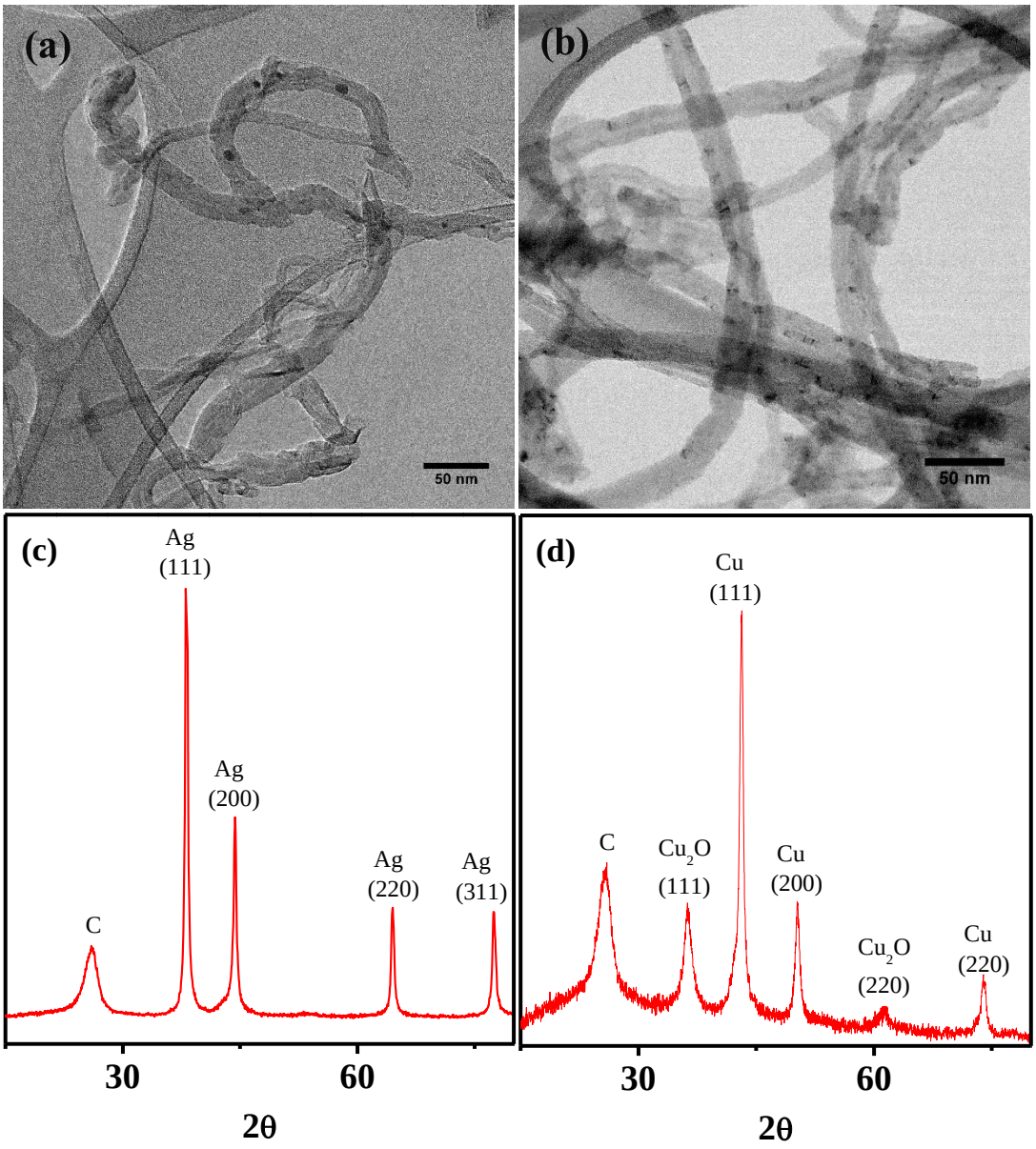

Figure 3.6: Representative HRTEM micrographs of (a) of CNT-Ag NH and (b) CNT-Cu/Cu_2O NH and representative XRD spectra of (c) CNT-Ag NH and (d) of CNT-Cu/Cu_2O NH.

To investigate whether the Cu_2O in the MWNT-Cu/Cu_2O NH stemmed from the oxidation of zero-valent Cu during XRD, synthesis of the NHs has also been attempted in oxygen-free environment. In order to do so, the developed sol-gel process was further

modified, where the MWNT-isopropanol suspension was purged with nitrogen for an hour and $Cu(NO_3)_2.H_2O$ reagent was added in the MWNT suspension. Upon completion of the reaction process, the reaction vessel was transferred to a glove box, which was purged with nitrogen. In this anaerobic synthesis process, the purification step to remove any unreacted reagent could not performed due to a lack in vacuum pressure inside the glove box. The final synthesis steps including evaporation of isopropanol and calcination were also performed under nitrogen environment. The synthesized NHs were then transferred into an airtight XRD sample holder and analysis was performed.

Figure 3.7 shows the XRD spectrum of the MWNT-Cu/Cu_2O NH, synthesized under anaerobic conditions. The spectrum shows evolution of two additional Cu_2O crystal planes (110) and (200), and also indicates a relative increase in intensity of the peaks corresponding to (111) and (220) planes that are relevant to Cu_2O, when compared to the peaks corresponding to the same Cu_2O peaks found in the NH synthesized under aerobic (Figure 3.6 d). Thus, formation of zero-valent Cu on MWNT surfaces was unsuccessful despite all necessary precautions to perform synthesis and characterization of the materials in an oxygen-free environment. The results indicate that the Cu_2O peaks in the NH, synthesized under aerobic condition, did not originate from oxidation of zero-valent Cu during XRD experiment. The possible sources of oxygen, which might have facilitated the formation of excess Cu_2O under anaerobic condition is the H_2O or NO_3^-, which could not be removed at the end of the initial reaction step due to the skipped filtration step. After analyzing the results, it is recommended that the MWNT-Cu/Cu_2O NH can be converted

to MWNT-Cu_2O NH by adding HNO_3 in the MWNT-isopropanol-$Cu(NO_3)_2$ reaction mixture and creating an oxidizing environment. Inversely, the MWNT-Cu/Cu_2O NH can possibly be converted to MWNT-Cu NH by adding a reducing agent in the reaction mixture. These experimental results for MWNT-Ag and MWNT-Cu/Cu_2O NHs suggest that, when using the sol-gel technique developed in chapter 2, the minimum threshold SEP value of a metal species needs to be greater than +0.345 to be able to form nanoparticles of its zero-valent state on MWNT surface.

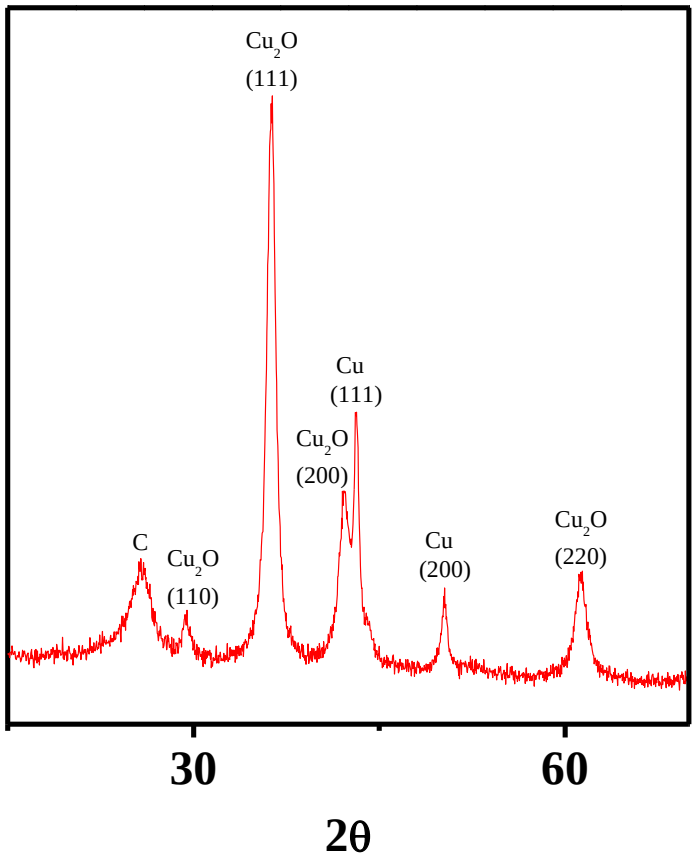

Figure 3.7: XRD spectrum of MWNT-Cu/Cu_2O NH synthesized using the sol-gel process under oxygen-free conditions. Special air-tight XRD sample holder was used for XRD analysis of this material.

3.3.4 Effect of slow reducer on Cu_2O formation in the MWNT-Cu/Cu_2O NH

In order to investigate the effect of using a solvent with a relatively higher reduction potential than that of isopropanol, MWNT-Cu/Cu_2O NH was synthesized using a similar sol-gel process, however with dimethyl formamide (DMF) as the solvent. DMF has been successfully used as a weak reducing agent for synthesizing Ag nanoparticles[51]. This synthesis was performed in presence of oxygen and hence the excess reagents could be removed upon completion of the reaction.

Figure 3.8 shows the XRD spectrum of MWNT-Cu/Cu_2O synthesized with DMF, which demonstrates lowering of the peak intensity corresponding to Cu_2O (111) plane. The Cu_2O (220) peak, that was found in the MWNT-Cu/Cu_2O NH synthesized using isopropanol as a solvent (Figure 3.6), is not found in this XRD spectrum. The results suggest that DMF's reducing ability can be utilized to hybridize zero-valent Cu NHs, with a presence of a small amount of Cu_2O. Although DMF has been used as a reducing agent[51], no literature evidence could be found that support the claim of DMF being a better reducer than isopropanol. In order to investigate whether DMF created an enhanced reducing environment compared to isopropanol, oxidation reduction potentials (ORPs) for both these systems were measured by a portable ultrameter (Myron L Company, Carlsbad, CA). It is to be noted that the ultrameter is designed to measure ORP in an aqueous environment. However, since only a relative ORP comparison between the two synthesis processes was desired and both isopropanol and DMF are miscible in water, the ORP measurements were performed despite the solvent-related limitations. Two reaction mixtures, i.e., MWNT+isopropanol+$Cu(NO_3)_2.H_2O$ and MWNT+DMF+$Cu(NO_3)_2.H_2O$ were heated at

70 °C for 1 h. After calibrating the ultrameter, 1 mL of both samples were placed in the ORP measurement chamber separately. The isopropanol system showed ORP value of +597 mV, while the DMF system showed a value of +504 mV. The lower ORP value of the DMF system indicates that the DMF system creates a better reducing environment than the isopropanol system[52]. These observations also explain the reduction of Cu_2O content in the MWNT-Cu/Cu_2O NH, synthesized using DMF.

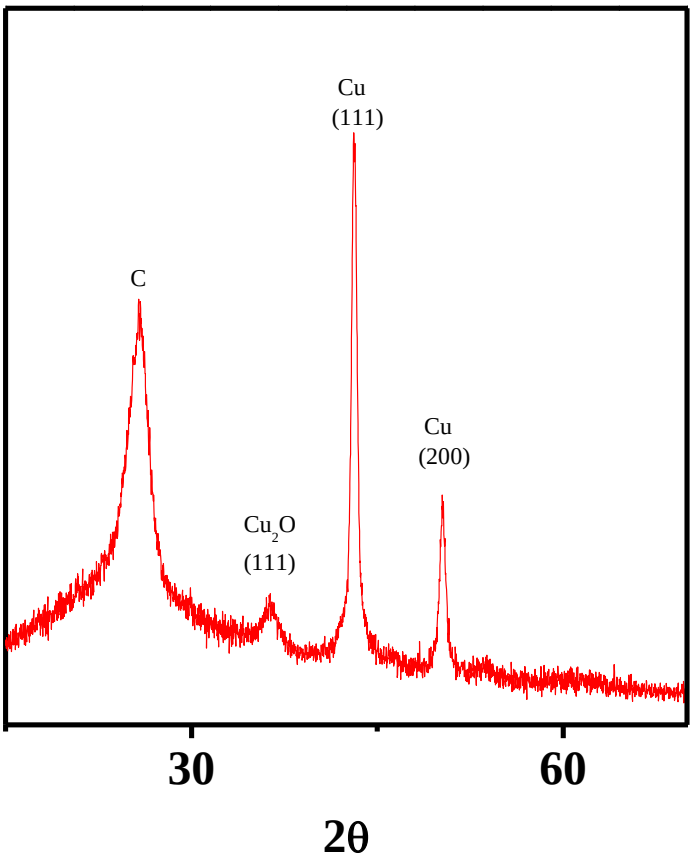

Figure 3.8: XRD spectrum of MWNT-Cu/Cu_2O NH synthesized in aerobic conditions, using DMF as a solvent in place of isopropanol and keeping all other parameters used in the sol-gel process unchanged. XRD was also performed under atmospheric conditions.

3.4 SUMMARY

The crystal formation pathway of the four different MWNT-NHs (MWNT-TiO_2, MWNT-ZnO, MWNT-Er_2O_3, and MWNT-Pr_6O_{11}), synthesized by the sol-gel process has been discussed. Based on literature and experimental observations, hybridization schemes for the MWNT-TiO_2 and MWNT-ZnO NHs have been proposed. For the MWNT-Er_2O_3 and MWNT-Pr_6O_{11} NHs, the synthesis scheme could not be proposed due to lack of literature evidence. Based on the experimental results, it is suggested that the sol-gel synthesis process for the MWNT-Er_2O_3, and MWNT-Pr_6O_{11} needs further engineering or alternative synthesis approaches needs to be executed in order to ensure ordered crystallinity in their MO components. One of such alternative approaches can be *ex-situ* hybridization of the Er_2O_3 and Pr_6O_{11} MOs with the MWNTs with the aid of a linker. The role of SEP (while considering electron transfer from oxidized metal ion to its zero-valent form) on formation of metal/metal oxide (exclusively for the sol-gel process described in this study) from the metal precursors was also evaluated. It was found that, using the sol-gel technique described in Chapter 2, the metal species with a negative standard electrode potential can be hybridized in their oxide form. The results also suggested that the minimum SEP value of a metal species needs to be greater than +0.345 V to be able to form nanoparticles of its zero-valent state on MWNT surface. Furthermore, the study also recommended that for metal species like Cu, which have a positive standard electrode potential and can easily be oxidized in presence of air, a better oxidizing environment than that in the sol-gel technique used here needs to be created in the reaction mixture in order

to form pure MO nanoparticles. Inversely, solvents with higher reducing capabilities should be used in order to form pure zero-valent metallic nanoparticles.

3.5 LITERATURE CITED

1. Rao, C. N. R.; Müller, A.; Cheetham, A. K., *The chemistry of nanomaterials: synthesis, properties and applications*. John Wiley & Sons: 2006.
2. Vorkapic, D.; Matsoukas, T., Effect of temperature and alcohols in the preparation of titania nanoparticles from alkoxides. *Journal of the American Ceramic Society* 1998, *81*, (11), 2815-2820.
3. Raveendran, P.; Fu, J.; Wallen, S. L., Completely "green" synthesis and stabilization of metal nanoparticles. *Journal of the American Chemical Society* 2003, *125*, (46), 13940-13941.
4. He, F.; Zhao, D., Manipulating the size and dispersibility of zerovalent iron nanoparticles by use of carboxymethyl cellulose stabilizers. *Environmental science & technology* 2007, *41*, (17), 6216-6221.
5. Bom, D.; Andrews, R.; Jacques, D.; Anthony, J.; Chen, B.; Meier, M. S.; Selegue, J. P., Thermogravimetric analysis of the oxidation of multiwalled carbon nanotubes: evidence for the role of defect sites in carbon nanotube chemistry. *Nano Letters* 2002, *2*, (6), 615-619.
6. Das, D.; Plazas-Tuttle, J.; Sabaraya, I. V.; Jain, S. S.; Sabo-Attwood, T.; Saleh, N. B., An elegant method for large scale synthesis of metal oxide-carbon nanotube nanohybrids for nano-environmental application and implication studies. *Environmental Science: Nano* 2017, *4*, (1), 60-68.
7. Mulfinger, L.; Solomon, S. D.; Bahadory, M.; Jeyarajasingam, A. V.; Rutkowsky, S. A.; Boritz, C., Synthesis and study of silver nanoparticles. *J. Chem. Educ* 2007, *84*, (2), 322.
8. Mo, C. B.; Cha, S. I.; Kim, K. T.; Lee, K. H.; Hong, S. H., Fabrication of carbon nanotube reinforced alumina matrix nanocomposite by sol–gel process. *Materials Science and Engineering: A* 2005, *395*, (1), 124-128.
9. Sun, J.; Gao, L.; Li, W., Colloidal processing of carbon nanotube/alumina composites. *Chemistry of Materials* 2002, *14*, (12), 5169-5172.
10. Kumari, L.; Zhang, T.; Du, G.; Li, W.; Wang, Q.; Datye, A.; Wu, K., Synthesis, microstructure and electrical conductivity of carbon nanotube–alumina nanocomposites. *Ceramics International* 2009, *35*, (5), 1775-1781.
11. Zhang, D.; Shi, L.; Fu, H.; Fang, J., Ultrasonic-assisted preparation of carbon nanotube/cerium oxide composites. *Carbon* 2006, *44*, (13), 2853-2855.
12. Kalubarme, R. S.; Kim, Y.-H.; Park, C.-J., One step hydrothermal synthesis of a carbon nanotube/cerium oxide nanocomposite and its electrochemical properties. *Nanotechnology* 2013, *24*, (36), 365401.
13. Lang, J.; Yan, X.; Xue, Q., Facile preparation and electrochemical characterization of cobalt oxide/multi-walled carbon nanotube composites for supercapacitors. *Journal of Power Sources* 2011, *196*, (18), 7841-7846.
14. Wang, G.; Shen, X.; Yao, J.; Wexler, D.; Ahn, J.-h., Hydrothermal synthesis of carbon nanotube/cobalt oxide core-shell one-dimensional nanocomposite and application

as an anode material for lithium-ion batteries. *Electrochemistry Communications* 2009, *11*, (3), 546-549.
15. Yang, H.; Zhang, D.; Shi, L.; Fang, J., Synthesis and strong red photoluminescence of europium oxide nanotubes and nanowires using carbon nanotubes as templates. *Acta materialia* 2008, *56*, (5), 955-967.
16. Chuansheng, C.; Tiangui, L.; Xiaohua, C.; Bin, Y.; Zhenwu, N.; Zhenwu, N.; Can, Z.; Chenchong, H., Preparation of Multi-Walled Carbon Nanotubes/Europium Oxide Composite. *RARE METAL MATERIALS AND ENGINEERING* 2009, *38*, 477-480.
17. Chen, C.; Hu, J.; Shao, D.; Li, J.; Wang, X., Adsorption behavior of multiwall carbon nanotube/iron oxide magnetic composites for Ni (II) and Sr (II). *Journal of hazardous materials* 2009, *164*, (2), 923-928.
18. Hu, J.; Shao, D.; Chen, C.; Sheng, G.; Li, J.; Wang, X.; Nagatsu, M., Plasma-induced grafting of cyclodextrin onto multiwall carbon nanotube/iron oxides for adsorbent application. *The Journal of Physical Chemistry B* 2010, *114*, (20), 6779-6785.
19. Chen, C.; Wang, X.; Nagatsu, M., Europium adsorption on multiwall carbon nanotube/iron oxide magnetic composite in the presence of polyacrylic acid. *Environmental science & technology* 2009, *43*, (7), 2362-2367.
20. Wang, Q.; Li, J.; Chen, C.; Ren, X.; Hu, J.; Wang, X., Removal of cobalt from aqueous solution by magnetic multiwalled carbon nanotube/iron oxide composites. *Chemical Engineering Journal* 2011, *174*, (1), 126-133.
21. Ikuno, T.; Yasuda, T.; Honda, S.-i.; Oura, K.; Katayama, M.; Lee, J.-G.; Mori, H., Coating carbon nanotubes with inorganic materials by pulsed laser deposition. *Journal of applied physics* 2005, *98*, (11), 114305.
22. Ikuno, T.; Katayama, M.; Kamada, K.; Honda, S.-i.; Lee, J.-G.; Mori, H.; Oura, K., Insulator-coated carbon nanotubes synthesized by pulsed laser deposition. *Japanese journal of applied physics* 2003, *42*, (11B), L1356.
23. Pan, L.; Konishi, Y.; Tanaka, H.; Chakrabarti, S.; Hokushin, S.; Akita, S.; Nakayama, Y., Effect of MgO coating on field emission of a stand-alone carbon nanotube. *Journal of Vacuum Science & Technology B* 2007, *25*, (5), 1581-1583.
24. Wang, M. Y.; Li, J. H.; Cui, K. Z., Preparation of Pt-MoOx/CNT Electrode and Its Electrocatalytic Property for Ethanol Electrooxidation. *Chinese Journal of Chemistry* 2006, *24*, (7), 881-886.
25. Roro, K. T.; Tile, N.; Mwakikunga, B.; Yalisi, B.; Forbes, A., Solar absorption and thermal emission properties of multiwall carbon nanotube/nickel oxide nanocomposite thin films synthesized by sol–gel process. *Materials Science and Engineering: B* 2012, *177*, (8), 581-587.
26. Wen, B.; Cao, M.-S.; Hou, Z.-L.; Song, W.-L.; Zhang, L.; Lu, M.-M.; Jin, H.-B.; Fang, X.-Y.; Wang, W.-Z.; Yuan, J., Temperature dependent microwave attenuation behavior for carbon-nanotube/silica composites. *Carbon* 2013, *65*, 124-139.
27. Sivakumar, R.; Guo, S.; Nishimura, T.; Kagawa, Y., Thermal conductivity in multi-wall carbon nanotube/silica-based nanocomposites. *Scripta Materialia* 2007, *56*, (4), 265-268.

28. Bottini, M.; Tautz, L.; Huynh, H.; Monosov, E.; Bottini, N.; Dawson, M. I.; Bellucci, S.; Mustelin, T., Covalent decoration of multi-walled carbon nanotubes with silica nanoparticles. *Chemical Communications* 2005, (6), 758-760.
29. Wongchoosuk, C.; Wisitsoraat, A.; Tuantranont, A.; Kerdcharoen, T., Portable electronic nose based on carbon nanotube-SnO 2 gas sensors and its application for detection of methanol contamination in whiskeys. *Sensors and Actuators B: Chemical* 2010, *147*, (2), 392-399.
30. Eder, D.; Windle, A. H., Carbon–inorganic hybrid materials: the carbon-nanotube/TiO2 interface. *Advanced Materials* 2008, *20*, (9), 1787-1793.
31. Ding, M.; Sorescu, D. C.; Star, A., Photoinduced Charge Transfer and Acetone Sensitivity of Single-Walled Carbon Nanotube–Titanium Dioxide Hybrids. *Journal of the American Chemical Society* 2013, *135*, (24), 9015-9022.
32. Wu, G.-M.; Wang, A.-R.; Zhang, M.-X.; Yang, H.-Y.; Zhou, B.; Shen, J., Investigation on properties of V2O5–MWCNTs composites as cathode materials. *Journal of Sol-Gel Science and Technology* 2008, *46*, (1), 79-85.
33. Green, J. M.; Dong, L.; Gutu, T.; Jiao, J.; Conley Jr, J. F.; Ono, Y., ZnO-nanoparticle-coated carbon nanotubes demonstrating enhanced electron field-emission properties. *Journal of applied physics* 2006, *99*, (9), 094308.
34. Sun, Z.; Zhang, X.; Na, N.; Liu, Z.; Han, B.; An, G., Synthesis of ZrO2− Carbon Nanotube Composites and Their Application as Chemiluminescent Sensor Material for Ethanol. *The Journal of Physical Chemistry B* 2006, *110*, (27), 13410-13414.
35. Gao, C.; Li, W.; Jin, Y. Z.; Kong, H., Facile and large-scale synthesis and characterization of carbon nanotube/silver nanocrystal nanohybrids. *Nanotechnology* 2006, *17*, (12), 2882.
36. Rahman, G.; Guldi, D. M.; Zambon, E.; Pasquato, L.; Tagmatarchis, N.; Prato, M., Dispersable carbon nanotube/gold nanohybrids: evidence for strong electronic interactions. *Small* 2005, *1*, (5), 527-530.
37. Wu, B.; Kuang, Y.; Zhang, X.; Chen, J., Noble metal nanoparticles/carbon nanotubes nanohybrids: synthesis and applications. *Nano Today* 2011, *6*, (1), 75-90.
38. Jawale, D. V.; Gravel, E.; Boudet, C.; Shah, N.; Geertsen, V.; Li, H.; Namboothiri, I. N.; Doris, E., Room temperature Suzuki coupling of aryl iodides, bromides, and chlorides using a heterogeneous carbon nanotube-palladium nanohybrid catalyst. *Catalysis Science & Technology* 2015, *5*, (4), 2388-2392.
39. Kecsenovity, E.; Endrődi, B.; Pápa, Z.; Hernádi, K.; Rajeshwar, K.; Janáky, C., Decoration of ultra-long carbon nanotubes with Cu 2 O nanocrystals: a hybrid platform for enhanced photoelectrochemical CO 2 reduction. *Journal of Materials Chemistry A* 2016, *4*, (8), 3139-3147.
40. Chen, L.; Tsang, S. C., Ag doped WO 3-based powder sensor for the detection of NO gas in air. *Sensors and Actuators B: Chemical* 2003, *89*, (1), 68-75.
41. Sohrabi, M. R.; Mansouriieh, N.; Khosravi, M.; Zolghadr, M., Removal of diazo dye Direct Red 23 from aqueous solution using zero-valent iron nanoparticles immobilized on multi-walled carbon nanotubes. *Water Science and Technology* 2015, *71*, (9), 1367-1374.

42. Khan, I. A.; Aich, N.; Afrooz, A. R. M. N.; Flora, J. R. V.; ferguson, L.; sabo-Attwood, T.; Saleh, N. B., Fractal structures of single-walled carbon nanotubes in biologically relevant conditions: role of chirality vs. media conditions. *Chemosphere* 2013 *93*, (9), 1997-2003.
43. Wepasnick, K. A.; Smith, B. A.; Bitter, J. L.; Fairbrother, D. H., Chemical and structural characterization of carbon nanotube surfaces. *Analytical and bioanalytical chemistry* 2010, *396*, (3), 1003-1014.
44. Jia, B.; Gao, L.; Sun, J., Self-assembly of magnetite beads along multiwalled carbon nanotubes via a simple hydrothermal process. *Carbon* 2007, *45*, (7), 1476-1481.
45. Li, P.; Xu, Z. P.; Hampton, M. A.; Vu, D. T.; Huang, L.; Rudolph, V.; Nguyen, A. V., Control preparation of zinc hydroxide nitrate nanocrystals and examination of the chemical and structural stability. *The Journal of Physical Chemistry C* 2012, *116*, (18), 10325-10332.
46. Li, C.; Liu, H.; Yang, J., A facile hydrothermal approach to the synthesis of nanoscale rare earth hydroxides. *Nanoscale research letters* 2015, *10*, (1), 1-6.
47. Losurdo, M.; Giangregorio, M. M.; Capezzuto, P.; Bruno, G.; Toro, R. G.; Malandrino, G.; Fragalà, I. L.; Armelao, L.; Barreca, D.; Tondello, E., Multifunctional nanocrystalline thin films of Er2O3: Interplay between nucleation kinetics and film characteristics. *Advanced Functional Materials* 2007, *17*, (17), 3607-3612.
48. Hassan, M. S.; Akhtar, M. S.; Shim, K.-B.; Yang, O.-B., Morphological and electrochemical properties of crystalline praseodymium oxide nanorods. *Nanoscale research letters* 2010, *5*, (4), 735.
49. Sun, Y.; Xia, Y., Shape-controlled synthesis of gold and silver nanoparticles. *Science* 2002, *298*, (5601), 2176-2179.
50. Ghodselahi, T.; Vesaghi, M.; Shafiekhani, A.; Baghizadeh, A.; Lameii, M., XPS study of the Cu@ Cu 2 O core-shell nanoparticles. *Appl. Surf. Sci.* 2008, *255*, (5), 2730-2734.
51. Pastoriza-Santos, I.; Liz-Marzán, L. M., Formation and stabilization of silver nanoparticles through reduction by N, N-dimethylformamide. *Langmuir* 1999, *15*, (4), 948-951.
52. Lowry, R. W.; Dickman, D., The ABC's of ORP—Clearing up some of the mystery of Oxidation-Reduction Potential. *Service Industry News* 2010.

Chapter 4: Aggregation Behavior of Multiwalled Carbon Nanotube-Titanium Dioxide Nanohybrids: Role of Titanium Dioxide Loading

4.1 INTRODUCTION

With recent advances in material science and engineering, passive nanostructures have advanced to complex hierarchical heterostructures, known as nanohybrids (NHs). These complex NMs aim to meet the increasing demand for multifunctionality in various applications including biomedicine[1], biomedical imaging[2], supercapacitors[3], optoelectronics[4], solar cell technology[5], electrochemical fuel cells[6], electrocatalysis[7], chemical sensing[8], among many others. Such widespread applications of NHs will likely be associated with environmental release and exposure. Hence, a systematic assessment of environmental health and safety (EHS) of these heterostructures is necessary. These complex multifunctional NHs with emergent properties will likely manifest environmental behavior, exceeding that of the sum of their component parts[9-12].

Carbon nanotube-metal oxide NHs are one of the most used heterostructures, particularly as catalyst supports in electrochemical fuel cells[13]. Nano-scale TiO_2 particles are grown on multiwalled carbon nanotube (MWNT-TiO_2) surfaces to serve as anodic materials in microbial fuel cells for performance improvement[14] as well as support for Pt, a widely used catalyst in proton exchange membrane fuel cells[15]. The MWNT backbone of the MWNT-TiO_2 NHs provides corrosion resistance and enhanced electrical conductivity[16], while TiO_2 increases the stability and durability of Pt against diffusion, detachment, and dissolution[17-19]. Though Pt use per unit fuel cell has decreased significantly over the past decades, by 2050, at least 300,000 kg of Pt is projected to be

used each year[20, 21]. The global decrease in the Pt reserve requires extraction and recovery of this metal (employing harsh acid-digestion techniques) at the end of the lifecycle of the fuel cells[22]. MWNT-TiO_2 NHs that are used to support Pt catalysts in fuel cell industry thus have a high likelihood to be released, most likely during the end of life metal recovery process and necessitate systematic assessment of their EHS.

The aggregation behavior of MWNT and TiO_2 components has been studied extensively[23]. Carbon nanotubes (CNTs)[24, 25] and TiO_2[26] have been reported to follow the classical Derjaguin-Landau-Verwey-Overbeek (DLVO) type aggregation behavior. The dominant factors in CNT aggregation are found to be surface oxidation[27, 28], solution chemistry[24, 25, 29], and chirality[30, 31]; while nano-scale TiO_2 aggregation has been shown to be influenced by size,[26] surface area,[26] composition,[26] shape,[26] and surface functionality[32]. However, when hybridized, the physicochemical properties of the MWNT-TiO_2 NHs will likely differ from those of both MWNTs and TiO_2, hence will present significant uncertainty in predicting NH behavior from its components.

Composite materials bring in complexity and heterogeneity to the surface by virtue of the combination of multiple materials with unique chemical origin. Hybridization can alter the surface potential as well as modulate the van der Waals attraction forces of the component materials.[33] Furthermore, when TiO_2 nanocrystals are grown on MWNT surfaces, these nano features will likely enhance the surface roughness of the nanotube and may also induce heterogeneous charge distribution, both of which increase uncertainty in aggregation behavior of these complex materials. A recent study[33] on aggregation of a carbonaceous-metal oxide NH, i.e., reduced graphene oxide-TiO_2 (rGO-TiO_2) presented

observational aggregation data and claims to estimate the Hamaker constant value for the NH. However, this study does not elucidate any underlying aggregation mechanisms of the NH and also does not compare the aggregation behavior with that of the component materials. Following are the pertinent questions on NH aggregation. Can the NH aggregation be captured by the aggregation of the components? Is the aggregation behavior of the NH controlled by the van der Waals or electrostatic contribution of the component materials? Does the carbon:metal ratio, i.e., the NH composition, play a significant role in modulating the aggregation behavior?

The objective of this study is to answer these pertinent questions by systematically assessing the aggregation behavior of MWNT-TiO_2 NHs with a wide range of C:Ti loading (C:Ti molar ratios of 1:0.1, 1:0.05, and 1:0.033), synthesized employing the sol-gel method reported in Chapter 2. The C:Ti molar ratio of 1:0.1 was chosen since it is one of the most used and commercialized MWNT-TiO_2 composition [34]. The 1:0.1 loading has shown complete coverage of MWNT surfaces (Chapter 2) leaving a TiO_2 external surface for interaction. To better assess the role of surface complexity on interfacial interaction, NHs with lower TiO_2 loadings are desired, which will introduce TiO_2 properties on MWNT while preserving both MWNT and TiO_2 properties at the NH-water interface. Transmission electron microscopy (TEM) has been used to perform morphological analysis and estimate surface roughness of the composites, while X-ray diffraction (XRD) was employed to assess the crystallinity of the grown TiO_2. Energy dispersive spectroscopy (EDS) with scanning transmission electron microscopy (STEM) was used for elemental mapping. Chemical composition of the NHs was also assessed with X-ray photoelectron

spectroscopy (XPS). Aggregation kinetics of these NHs has been studied using time-resolved dynamic light scattering (TRDLS) under a wide range of mono-valent (NaCl) salt concentrations. Relative contributions from van der Waals and electrostatic interactions have been enumerated with electrophoretic mobility (EPM) measurements. Effects of the type of cation and natural organic matter were evaluated by determining aggregation rate at 10 mM ionic strength (i.e., 1 mM $CaCl_2$ + 7 mM NaCl) with and without the presence of Suwanee River humic acid (SRHA). For clarity, the oxidized MWNTs will be denoted as MWNTs, and the three NHs with different loadings will be denoted as NH-High (C:Ti 1:0.1), NH-Mid (C:Ti 1:0.05), and NH-Low (C:Ti 1:0.033), while MWNTs that are heat-treated (without any titanium precursor) will be denoted as MWNT-ISP from hereon.

4.2 MATERIALS AND METHODS

4.2.1 Synthesis of NHs

The MWNT-TiO_2 NHs were synthesized using a previously published protocol[35]. In brief, MWNTs (O.D. 8-15 nm), procured from Cheap Tubes Inc. (Brattleboro, VT), were refluxed with concentrated nitric and sulfuric acid. The oxidized MWNTs were subsequently filtered and dried for 48 h in a desiccator and re-suspended in isopropanol with an ultrasonic dismembrator (Qsonica LLC, Newtown, CT). Titanium isopropoxide, TTIP (Sigma Aldrich, St. Louise, MO) was introduced as a precursor to grow TiO_2 on the MWNT surfaces *in situ*. NHs with three different TiO_2 nanocrystal loading (C:Ti molar ratio of 1:0.1, 1:0.05, and 1:0.033) were synthesized by varying the amount of TTIP used in the reaction. The TTIP and MWNT mixture in isopropanol was then stirred for 3 h at 70

°C under nitrogen environment. After 3 h, water was added dropwise into the reaction vessel to promote TiO_2 crystal formation on the MWNT backbone via a hydrolysis process. This mixture was kept under the same stirring conditions for an additional 2 h and afterwards washed 4 times with isopropanol to remove any unreacted reagent. Finally, isopropanol was evaporated and the resultant materials were calcined at 400 °C for 3 h in a Lindberg/Blue M Mini mite tube furnace (Thermo Scientific) to facilitate ordered crystallinity and phase transformation of the TiO_2 nanocrystals.

4.2.2 Preparation of TiO_2 Nanocrystals and Isopropanol and Heat Treated MWNT (MWNT-ISP)

TiO_2 nanocrystals were obtained by complete oxidation of MWNTs from the MWNT-TiO_2 NHs. The MWNT-TiO_2 NHs were calcined in air in a Lindberg/Blue M Mini mite tube furnace (Thermo Scientific) at 650 °C for 2 h. The MWNTs were burnt off at this temperature leaving a white TiO_2 nanocrystal residue.

To understand the effect of heat treatment on MWNT surface functionality and therefore its contribution to aggregation, oxidized MWNTs were exposed to the identical experimental conditions used for synthesizing the MWNT-TiO_2 NHs (i.e., refluxed in isopropanol and calcined for 3 h at 400 °C with 2 additional h of refluxing in water) to obtain MWNT-ISP.

4.2.3 Preparation of Aqueous Suspensions

Aqueous stock suspensions of all materials (i.e., MWNTs, NHs with three different TiO_2 loadings, TiO_2 nanocrystals, and MWNT-ISP) were prepared by ultrasonicating each

material in 50 mL of ultrapure water for 30 min. These suspensions were kept quiescently in the dark at 4 °C overnight to settle out larger clusters. Finally, the supernatant was decanted and the stock suspensions were appropriately diluted for further studies.

4.2.4 Solution Chemistry

To assess the effects of monovalent cation on aggregation kinetics, 55-400 mM NaCl was used. Effect of divalent cation and natural organic matter (NOM) was evaluated by determining particle aggregation rate at 10 mM ionic strength (1 mM $CaCl_2$ + 7 mM NaCl) with and without 2.5 mg TOC/L standard II SRHA (International Humic Substances Society, Denver, CO). All experiments were performed at 25 °C with pH adjusted to 6.9±0.2 with 0.5 M NaOH or 0.5 M HCl.

4.2.5 Physicochemical Characterization

The physical morphology of the NMs was characterized using a JEOL 2010F HRTEM equipped with EDS. Electron micrographs were obtained at an acceleration voltage of 200 kV. High annular angle dark field STEM images were obtained using the same equipment while EDS was employed to obtain elemental mapping for the NHs. The details of the HRTEM and EDS have been described elsewhere[24, 30, 31, 36-39]. For determining the elemental composition of the dry NMs, a Kratos XPS-Axis Ultra DLD, equipped with a monochromated Al K_α X-ray source was employed. The XPS data analysis was performed by fitting the high-resolution element specific peaks using CasaXPS (Casa Software Ltd., Japan). The crystallinity of the NMs was evaluated with XRD. A 600 W Rigaku MiniFlex 600I XRD with a Cu-Kα irradiator (wavelength of 0.154 nm) and a

graphite monochromator was used. Details of the experimental protocol for XPS and XRD analyses is described in earlier studies[30, 35].

4.2.6 Electrokinetic Properties

The electrophoretic mobility (EPM) of the aqueous suspensions of all NMs was measured using a Malvern Zetasizer (Malvern Instruments Ltd., Worcestershire, UK) at 20 °C. For each measurement, 900 µL of the NM suspension was introduced into a disposable capillary cell (DTS 1070). Six different cells were used for EPM measurement of the 6 NMs in this study. Measurements were performed in triplicate for a wide range of NaCl concentrations (0.1 to 400 mM) using a well-established protocol[24, 30, 31, 36-39]. The cells were washed with DI water and ethanol between measurements.

4.2.7 Aggregation Kinetics

The aggregation kinetics of the NMs were measured using an ALV/CGS-3 compact goniometer system (ALV-Laser GmbH, Langen/Hessen, Germany), equipped with a 22 mW HeNe 632.8 nm laser and a high QE APD detector with photomultipliers of 1:25 sensitivity. The experimental details of the aggregation kinetics experiments and data analysis have been described elsewhere[24, 30, 31, 37, 40, 41]. In brief, an aliquot of the diluted stock suspensions was mixed with an appropriate amount of NaCl or the NaCl and $CaCl_2$ mixture, and in presence or absence of SRHA. 2 mL of the sample was injected into a pre-cleaned borosilicate glass vial[24, 30, 31, 37, 40, 41] and vortexed for 2 s prior to insertion into the toluene-filled goniometer sample housing. The scattered laser was collected every 15 s for at least 25 min at 90°. A cumulant fit was used to analyze the collected data and the average

hydrodynamic radii (HDR) were obtained for every 15s segment during the entire duration of the experiment.

The average HDR over time was plotted and slopes at the initial stages of the aggregation history were estimated (equation 4.1) by regressing up to 1.26 times the initial HDR[37, 42] (measured by the instrument at t=0). In some cases, the final cluster size (after t=25 min) did not increase by 26% of the initial cluster size. The aggregation rates, for such cases, were obtained by calculating slopes over the entire size range. The attachment efficiency parameter (α) for each condition was calculated (equation 4.2) by normalizing the rate of initial change of the HDR at any condition by that at the most favorable condition[24, 30, 31, 37, 40, 41].

$$k \propto \frac{1}{N_0}\left[\frac{dR_h(t)}{dt}\right]_{t\to 0} \quad \ldots\ldots\ldots\ldots\ldots\ldots\ldots\ldots\ldots\ldots\ldots (4.1)$$

$$\alpha = \frac{\frac{1}{N_0}\left[\frac{dR_h(t)}{dt}\right]_{t\to 0}}{\frac{1}{N_{0,fav}}\left[\frac{dR_h(t)}{dt}\right]_{t\to 0,fav}} \quad \ldots\ldots\ldots\ldots\ldots\ldots\ldots\ldots (4.2)$$

Here, *k* is the aggregation rate, $\frac{dR_h(t)}{dt}$ is rate of change in particle radius with time and N_0 is the particle concentration in suspension. Aggregation rate reported in this paper was calculated as $\frac{dR_h(t)}{dt}$, consistent with earlier studies[30, 37, 40, 43]. Finally, the attachment efficiencies were plotted against NaCl concentration in a logarithmic plot to produce stability plots.

4.2.8 DLVO Modeling

The attachment efficiencies were modeled by estimating the stability ratios calculated with equation 4.3 to evaluate the efficacy of the DLVO theory to predict aggregation behavior of these complex NHs. Similar types of DLVO modeling have previously been used to analyze aggregation behavior of NMs[42].

$$W = \frac{\int_0^{\infty} \beta(h) \frac{\exp[V_T(h)/kT]}{(2a+h)^2}}{\int_0^{\infty} \beta(h) \frac{\exp[V_A(h)/kT]}{(2a+h)^2}} \dots\dots\dots (4.3)$$

In equation 4.3, h is the surface-to-surface separation distance between two particles, a is the particle radius, k is the Boltzmann constant, and T is the absolute temperature. The total interaction energy between two particles, $V_T(h)$, is the sum of the van der Waals attraction, $V_A(h)$, and electrical double layer interaction, $V_R(h)$. The dimensionless function $\beta(h)$ corrects for the hydrodynamic resistance (interaction) between the two approaching particles[42].

$$\beta(h) = \frac{6\left(\frac{h}{a}\right)^2 + 13\left(\frac{h}{a}\right) + 2}{6\left(\frac{h}{a}\right)^2 + 4\left(\frac{h}{a}\right)} \dots\dots\dots (4.4)$$

$$V_T(h) = V_R(h) + V_A(h) \dots\dots\dots (4.5)$$

$$V_R(h) = 64\pi \frac{n_b kT}{\kappa^2} \frac{a^2}{(h+2a)} [\tanh\left(\frac{z\widetilde{\psi_d}}{4}\right)]^2 \exp(-\kappa h) \dots\dots\dots (4.6)$$

$$V_A(h) = -\frac{A_H}{6}\left(\frac{2}{\bar{h}^2-4}+\frac{2}{\bar{h}^2}+ln\frac{\bar{h}^2-4}{\bar{h}^2}\right) \ldots\ldots\ldots (4.7)$$

Here, $V_R(h)$ is the repulsive energy between two particles originating from their electrostatic double layer, n_b is the number concentration of cations in bulk solution (no./m^3), k is Boltzmann constant, T is absolute temperature, κ is the Debye–Hückel parameter, z is charge number, and $\widetilde{\psi_d} = \frac{e\psi_d}{k_B T}$, where $\psi_d$is surface potential and e is elementary charge (1.6022×10^{-19} C). A_H is the Hamaker constant of material in aqueous suspension and $\bar{h} = \frac{h+2a}{a}$. Equation 4.6, used to model the stability plots with DLVO theory, is based on the Gouy-Chapman model. Hence, it can be applied for colloidal aggregation with no limits on the surface potential of the particle[44]. The Gouy-Chapman model works only for electrolyte solutions where the cations and anions have the same charge[44]. Since the DLVO model was applied to fit stability plots obtained using NaCl, use of equation 4.6 for DLVO modeling is appropriate.

4.3 Results and Discussion

4.3.1 Morphological Properties and Chemical Composition

A representative TEM (Figure C1a) micrograph of the MWNTs shows that the tubes are mostly debundled and are free from catalyst metals with an average outside diameter of 21.3±2.6 nm. TEM micrograph of the TiO_2 nanocrystals (Figure C1b) shows large aggregates or sintered particles. Such aggregated structure is expected for these TiO_2 nanocrystals, since these are produced by complete oxidation of the MWNT component of the NH-High at 650 °C.

The STEM assisted elemental mapping of the NHs (Figure 4.1) confirm the presence of Ti and O atoms in all the NHs. The TEM micrographs clearly show that the TiO_2 nanocrystal loading is the highest in NH-High and the lowest in NH-Low. Furthermore, TEM micrograph of the NH-Mid shows that the TiO_2 nanocrystals are evenly distributed on the MWNT surface, while that of NH-High show patchy TiO_2 nanocrystal accumulation on the surface of the already coated MWNTs (with TiO_2). Furthermore, a lowering of Ti intensity with decreasing TiO_2 loading is observed in the element-specific mapping series shown in Figure 4.1.

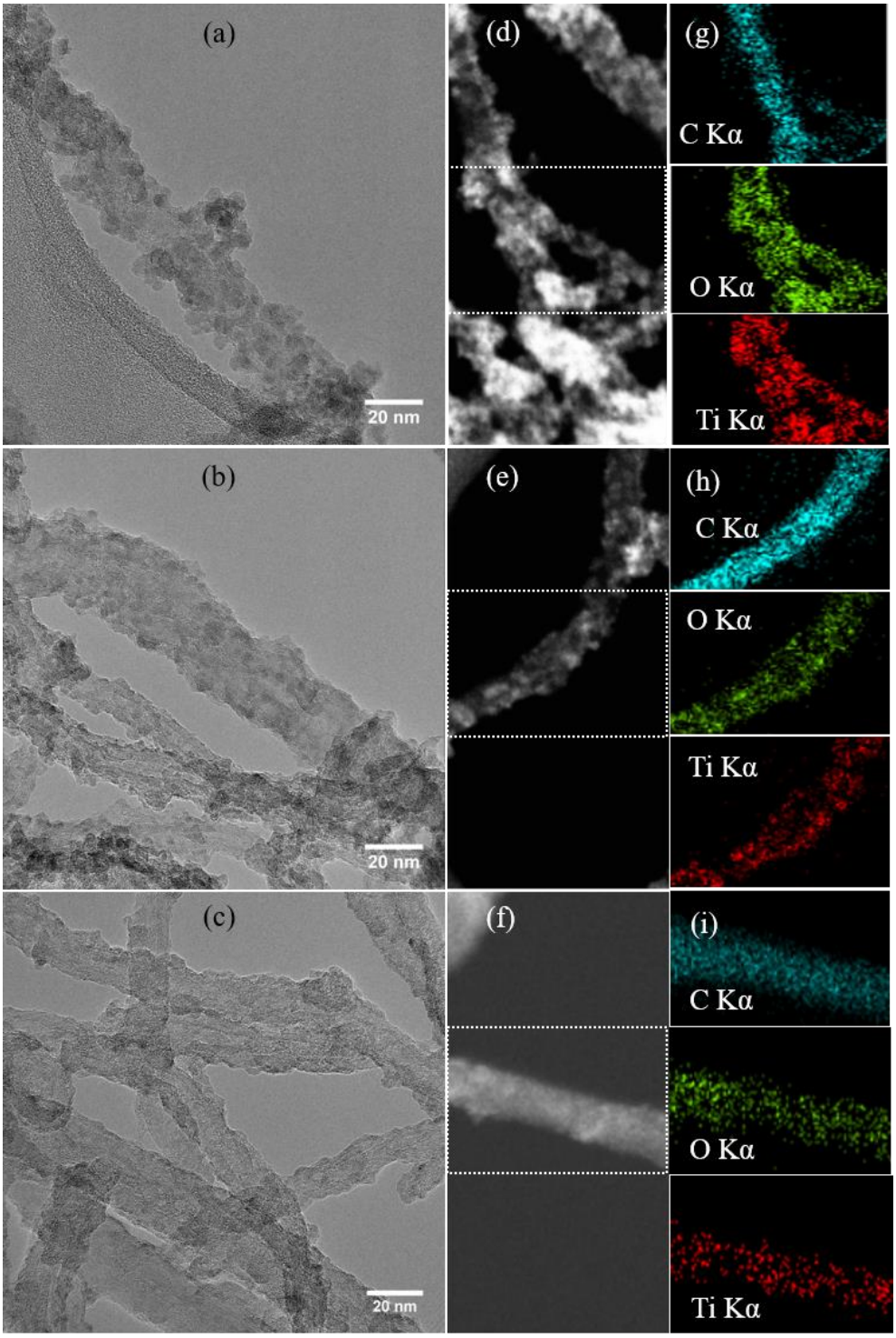

Figure 4.1: Representative HRTEM (a-c) and STEM (d-f) micrographs and elemental mapping (g-i); (a, d, g) NH-High, (b, e, h) NH-Mid, and (c, f, i) NH-Low. All images were taken at comparable magnification.

Further quantitation of the NH and component composition has been assessed with XPS. Figure C2a presents the XPS spectrum for C 1s in acid functionalized MWNTs. The peak positions of the de-convoluted plot indicate the presence of multiple oxygen containing moieties (i.e., carboxylates, hydroxyls, and carbonyls) on the MWNT surfaces, which is in agreement with previously reported XPS data on acid treated MWNTs[45]. For the NHs, representative XPS spectrum for Ti (Figure C2 b) shows peaks at 458.3 and 464.3 eV, which accurately match with the characteristic peaks for $Ti_{3/2}$ and $Ti_{1/2}$ of anatase phase TiO_2[46]. The Ti peaks for the NHs represent single fitting component, which indicate that TiO_2 nanocrystals have only one oxidation state.

Table 4.1 presents the elemental composition of the materials, obtained from XPS. The oxidized MWNTs' oxygen content is 10.9±0.2%, which decreases to 2.23% upon treatment with isopropanol and heat. Heating of the oxidized MWNTs in a nitrogen environment, which causes deoxygenation and fixes defects on nanotube surfaces, is primarily responsible for such reduction in oxygen content. Similar heat induced reduction in oxygen content has also been reported for graphene oxide[35]. Elemental composition also validates the decreasing presence of Ti in NH-High to NH-Low (Table 4.1). The excess oxygen content (oxygen, not associated with TiO_2 nanocrystals) also decreases as the C:Ti ratio increases (Table 4.1). The oxygen containing functional groups on the MWNT surface are the most likely source of the excess oxygen. Another possible source of the excess oxygen can be moisture; which is not likely in these cases since all samples are kept under a very high vacuum (~10^{-8} Torr) overnight, prior to the XPS measurements. These results indicate that, in the case of NH-High, heat treatment was not successful in reducing the

surface oxygen groups, which mostly were protected by the TiO_2 crystals that are overcoating the MWNT surfaces. As the TiO_2 content is lowered, excess %O is also lowered, indicating more effective heat-mediated deoxygenation of the MWNT surfaces. Such conclusion is further validated by the presence of lowest %O on MWNT-ISP, where heat-mediated deoxygenation is more profound as there is no TiO_2 to shield these groups from heat-mediated deoxygenation.

Table 4.1: XPS analyses of MWNTs and the NHs

Nanomaterials	**% O**	**% Ti**	**% O in TiO_2**	**Excess %O**
MWNT	10.9±0.2	N/A	N/A	N/A
NH-High (C:Ti molar ratio of 1:0.1)	27.3±1.1	8.6±0.3	17.2	10.1
NH-Mid (C:Ti molar ratio of 1:0.05)	17.6±0.4	4.5±0.1	9.0	8.6
NH-Low (C:Ti molar ratio of 1:0.033)	10.9±0.4	3.2±0.05	6.4	4.5
MWNT-ISP	2.23±0.1	N/A	N/A	N/A

The XRD patterns of the MWNTs, TiO_2 nanocrystals, and the MWNT-TiO_2 NHs are presented in Figure 4.2. The MWNT XRD spectrum show strong graphitic carbon peak at 25.7º and is in excellent agreement with previously reported XRD patterns of the oxidized MWNT[34]. TiO_2 nanocrystals show XRD peaks at 2θ values of 25º, 37.5º, 48º, 55.5º, 62.8º and 69.5º, corresponding to (101), (004), (200), (211), (204), and (116) crystal planes, respectively. All these crystal planes suggest that the TiO_2 nanocrystals are in pure anatase phase[47]. NHs with highest TiO_2 nanocrystal loading show strong occurrence of

peaks in the C and Ti scatter regions, and the peak intensities are stronger with the increase in TiO_2 loading.

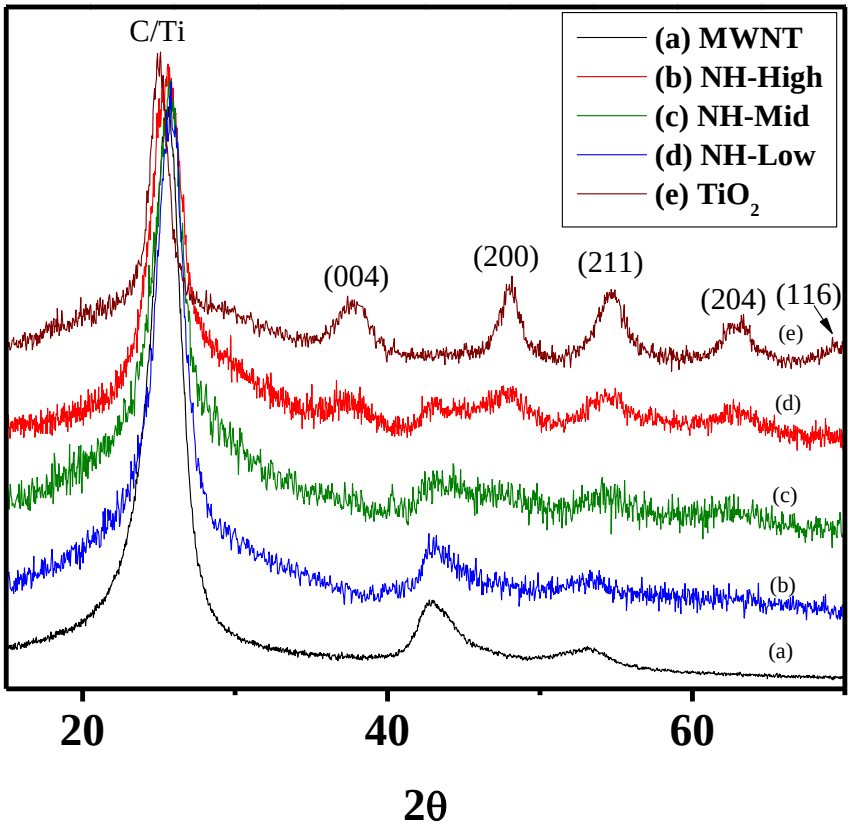

Figure 4.2: XRD spectra for (a) oxidized MWNTs and (b-d) MWNT-TiO_2 NHs, and (e) TiO_2 obtained from oxidizing the MWNTs in the NHs. C:Ti molar ratio is 1:0.1 (b), 1:0.05 (c), and 1:0.033 (d), corresponding to NH-High, NH-Mid, and NH-Low. The anatase crystal planes are labeled on top of the peaks. The overlapped crystal planes of C and Ti at 2θ of 25.5 degree is labeled as C/Ti

4.3.2 Electrokinetic Properties

All the materials exhibit negative electrophoretic mobility, which decrease with the increase in NaCl concentration (Figure 4.3). The electrokinetic behavior of these materials follow classical electrostatic compression in presence of increased amount of electrolytes [24, 30, 31, 37, 40, 41]. The MWNTs show the highest EPM values among all the materials (-

3.15±0.09 × 10^{-8} to -1.87±0.07 × 10^{-8} m^2 V^{-1} S^{-1} at 1 to 100 mM NaCl), and the values are within the range of previous literature reports (-3.5 × 10^{-8} to -2.4 × 10^{-8} m^2 V^{-1} S^{-1} with high and low oxygen content, respectively at low ionic strength)[27]. The highly negative EPM values of the MWNTs likely originates from the oxygen containing surface moieties that get etched into the MWNT exterior surfaces and at the open tube ends during the acid-treatment process[27-29]. Other carbon allotropes such as single-walled carbon nanotubes[25, 30, 48] and graphene[49, 50] have also shown similar electrokinetic properties upon oxidation. TiO_2 shows the least negative EPM values among all (ranging from -1.8±0.06 × 10^{-8} to -0.51±0.12 × 10^{-8} m^2 V^{-1} S^{-1} under 1 to 100 mM NaCl conditions). Similar EPM values have previously been reported for bare TiO_2 nanocrystals in aqueous suspensions[51]. The EPM trends for the NHs show a gradual decrease in EPM values with the decrease in TiO_2 loading (Figure 4.3). This trend is consistent with that of the excess oxygen content discussed earlier. Thus, the electrokinetic contribution to the NHs has mostly occurred from the oxygen functional moieties. Hence, among the NHs, NH-High will provide the strongest electrostatic contribution in colloidal stability, followed by the NHs with lower TiO_2 loadings, NH-Mid and NH-Low.

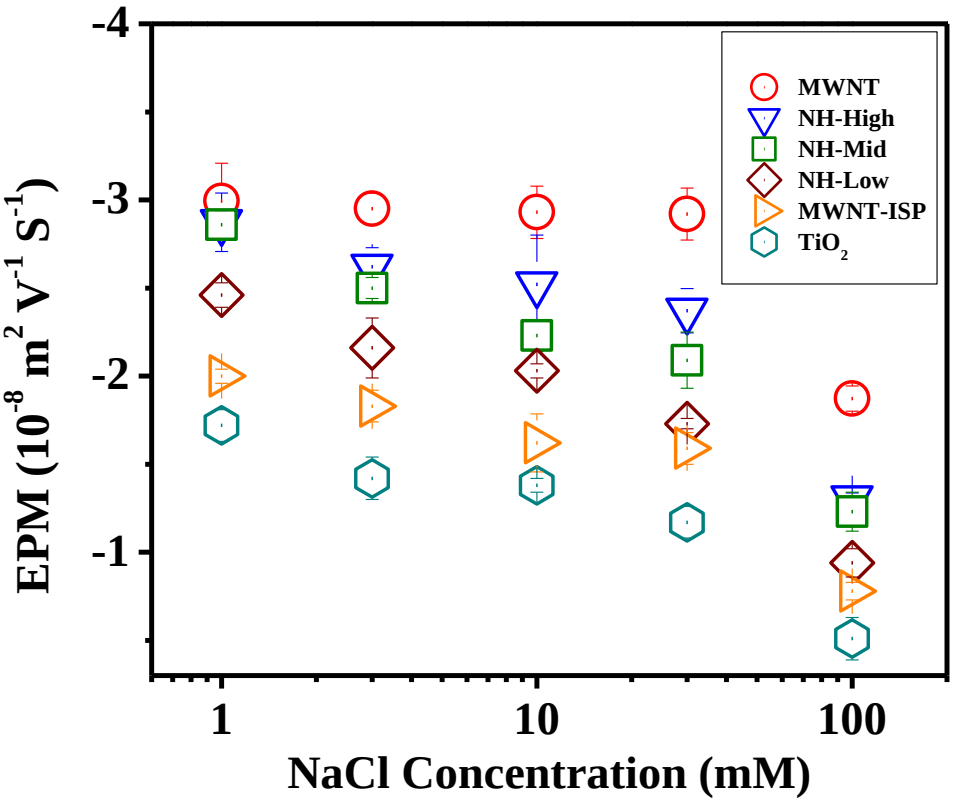

Figure 4.3: Electrophoretic mobility of NHs and the component materials at a range of NaCl (1 to 100 mM). Measurements were taken right after adding appropriate NaCl amounts in the aqueous NM suspensions. All experiments were performed at 25 °C at a pH of 6.9±0.2.

4.3.3 Aggregation Behavior and Underlying Mechanisms

The initial average hydrodynamic radii (HDR) of the MWNTs and the NHs lie between 75±2 nm to 101±2 nm (Figure C5). The MWNT-ISP show larger aggregate size (133±3), likely due to a high degree of deoxygenation during heat treatment, leading to a higher degree of clustering. The HDR of the TiO_2 nanocrystals is 87±2 nm, which is in a similar size range of that of the NH and MWNT clusters. The TiO_2 cluster size is higher than that shown via TEM, mostly due to high aggregation propensity of these materials,

which have no surface coatings and low EPM resulting in compromised stability in aqueous suspensions.

The stability plots (Figure 4.4) indicate interesting aggregation behavior of the NHs with respect to the component materials. Stability plots for all NMs show distinct unfavorable reaction limited colloid aggregation (RLCA) regime and favorable diffusion limited colloid aggregation (DLCA) regimes. The aggregation propensity of all the materials is bound (i.e., minimum and maximum) by that of the two components materials'; i.e., MWNTs shows to be the most stable material (RLCA regime ranging from 55 to 175 mM NaCl), while TiO_2 is the least (RLCA regime of 1 to 15 mM NaCl). Similar colloidal stability for MWNTs[27-29] and TiO_2[52] has previously been reported. The stability of these component materials follows the trend shown in the electrokinetic properties of these materials (Figure 4.3); i.e., the aggregation of these materials is primarily controlled by electrostatic interaction, which is a strong function of electrolyte concentration in the medium. NH aggregation reveals interesting interplay between van der Waals and electrostatic interactions.

The observed NH-High aggregation propensity (RLCA regime 5.5 to 48 mM NaCl) is closer to that of the TiO_2 than the MWNTs (Figure 4.4); though the electrostatic contribution for this NH is one of the strongest as observed from the EPM results and is comparable to those of the MWNTs (Figure 4.3). Attachment efficiencies of NH-Mid (with a lower TiO_2 loading than that of NH-High) on the other hand, shows a significant rightward shift (RLCA regime 5.5 to 70 mM NaCl), indicating a strong gain in stability. The EPM trend for this NH, however, indicates a weaker electrostatic contribution

(compared to that of the NH-High). Such experimental observation suggests that contribution of the TiO_2 on the surface (with higher van der Waals attraction) is much stronger for NH-High compared to NH-Mid (with lower TiO_2 loading), causing instability to the NH-High. The aggregation behavior of the NHs gets more complex when the TiO_2 loading lowers even further, as in the case of NH-Low. Lowering the contribution from the TiO_2 in this case is balanced out by the lower contribution from electrostatics (Figure 4.3), resulting in arresting the stabilization trend of the NHs with lower TiO_2 loading.

To assess the effect of deoxygenation (via heat treatment during NH synthesis) on stability, aggregation kinetics has also been studied for MWNTs treated in isopropanol and heat (MWNT-ISP), in identical synthesis conditions as the NHs except that no Ti precursor was present. The MWNT-ISP show destabilization (RLCA regime 3 to 30 mM NaCl) similar to TiO_2 (Figure 4.4), and the EPM values, when compared, agree with the observed aggregation behavior. Thus MWNT-ISP aggregation is likely controlled by electrokinetics.

The observed aggregation behavior of the NHs and component materials appears to be following the classical DLVO theory, which considers attractive van der Waals and repulsive electrostatic double layer interaction to describe particle-particle interaction. However, the fundamental assumptions of DLVO theory, i.e., spherical particle shape, uniform charge distribution, and smooth particle surfaces, are mostly violated by the complex NHs as suggested by the morphological characteristics described earlier. Such particle-water interfacial complexities have previously been reported to be influencing colloidal aggregation[53-56] and necessitates assessment of efficacy of the DLVO theory in predicting aggregation of these complex NHs.

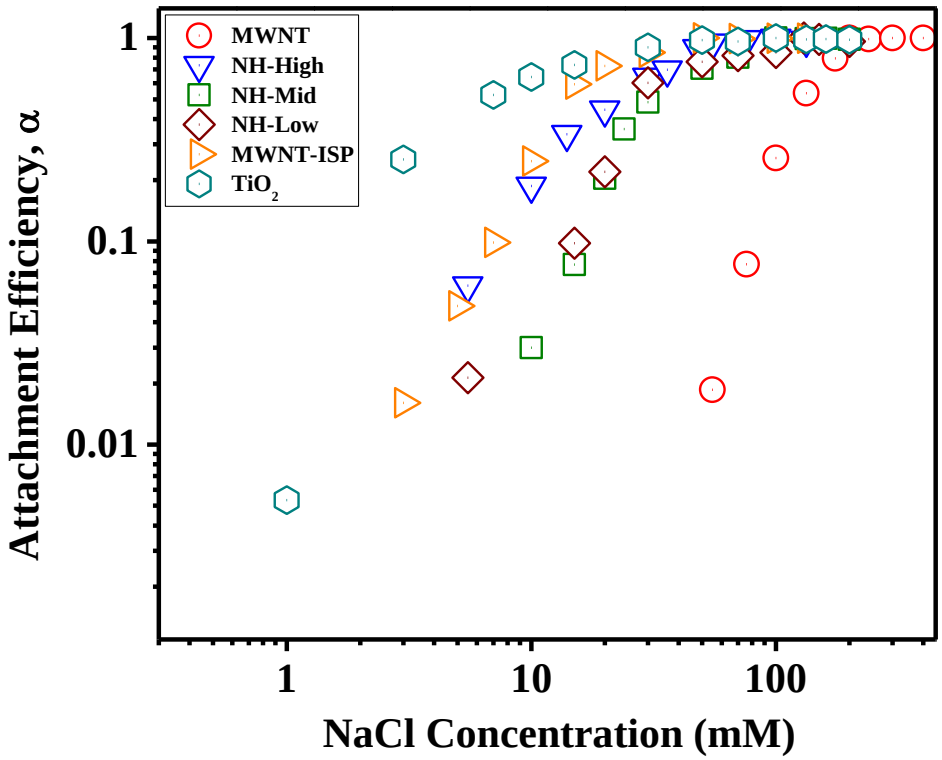

Figure 4.4: Stability plots of the NHs and the components. Each point on the stability plots represents attachment efficiency of the respective NMs at specific NaCl concentration. All experiments are performed at 25 °C at a pH of 6.9±0.2.

4.3.5 Efficacy of DLVO Theory

Figure 4.5 shows the DLVO fitting of the experimental stability plots (using the EPM values and material properties). The stability plots of the component materials (i.e., MWNTs, MWNT-ISP, and TiO_2) are best predicted with the DLVO model. Classical DLVO model shows deviation from stability behavior of the NHs, with an increasing error in prediction with an increase in TiO_2 loading. Monovariate regression coefficient (R^2) values have been compared to compare the experimental data with the theoretical predictions.

The deviation of the experimentally observed aggregation behavior from the DLVO theory can stem from a number of factors. The assumptions on the DLVO theory include

perfectly spherical shape of the particles considered and uniform distribution of charge on the particle surfaces. Hence, the experimental stability plots for the NMs tested, are not expected to exactly follow the DLVO prediction. Among the NMs, higher deviation is expected for the NHs because of their surface roughness upon hybridization. The TEM micrographs of the NHs show presence of a high degree of surface roughness, which increased with the increase in TiO_2 nanocrystal loading. Effect of surface roughness in colloidal interactions has previously been investigated[57], where interaction between rough latex particles and a flat surface was considered. Surface roughness on the latex particles was calculated as roughness indices by considering the rough surface of the latex particles as uniformly distributed small hemispherical asperities on the surface. Results from this study demonstrated that experimental deposition rate of the rough particles on the smooth surfaces at unfavorable conditions was higher than that predicted by the DLVO theory for deposition of smooth particles on a smooth flat plate. NH-High also shows higher aggregation propensity than DLVO prediction in the unfavorable aggregation regime (Figure 4.5). Other NHs, however, do not show such behavior for unfavorable conditions. DLVO over-predicts attachment efficiencies for all the NHs in the favorable aggregation regime. Thus, surface roughness generated from the TiO_2 loading on MWNTs needs to be quantified and its role on aggregation has to be assessed. Surface charge heterogeneity, although not considered in this discussion, can contribute towards deviation of experimental aggregation behavior to DLVO prediction and hence, also needs to be quantified.

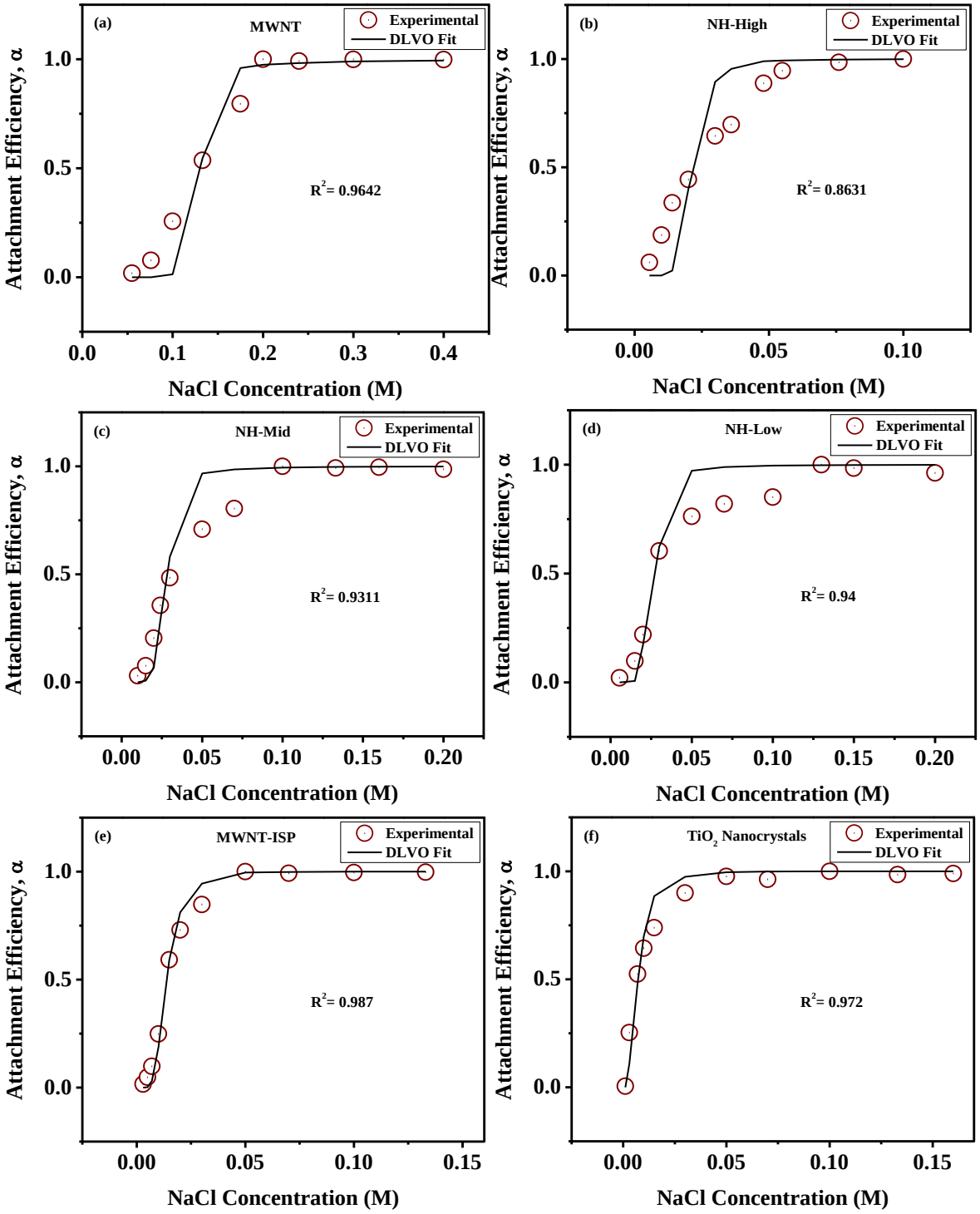

Figure 4.5: DLVO models for experimental stability plots (a) oxidized MWNTs, (b) NH-High (1:0.1), (c) NH-Mid (1:0.05), (d) NH-Low (1:0.033), (e) MWNT-ISP, and (f) TiO_2 nanocrystals. The experimental stability plots are fitted by DLVO estimated attachment efficiencies calculated from the stability ration equation using Matlab software.

4.3.6 Effect of Divalent Cation and SRHA on Aggregation

For electrostatically stable colloids, presence of divalent cations is expected to facilitate aggregation by effective compression of the electrical double layer and specific adsorption[37]. All NMs, except NH-High demonstrate a higher aggregation rate at 10 mM ionic strength with Ca^{2+} compared to the same ionic strength comprised of only monovalent cations (Figure 4.6). MWNTs show the strongest response to divalent cations (Figure 4.6) as observed earlier[27]. A likely mechanism is specific adsorption of Ca^{2+} onto oxygen moieties on the MWNT surfaces [27]. Colloidal bridging of particles with surface oxygen groups is also known to have occurred with divalent Ca^{2+} ions[58]. Similarly, MWNT-ISP shows fast aggregation rate (lower than MWNTs and higher than NHs and TiO_2) in presence of Ca^{2+} (Figure 4.6); which is likely a result of decreased specific ion adsorption and Ca^{2+} bridging, mediated by low oxygen containing moieties.

The aggregation rate of NH-High in 10 mM ionic strength is similar, with and without the presence of Ca^{2+} (i.e., 0.029±0.0021 nm/sec and 0.031±0.003 nm/sec, respectively). As previously discussed, TiO_2 on MWNT surfaces likely served as a shield to the oxygen containing groups and prevented specific adsorption of Ca^{2+} ions. TiO_2 nanocrystals also demonstrate similar aggregation rate in 10 mM ionic strength with and without the presence of Ca^{2+} ions (0.1949±0.016 nm/sec and 0.2±0.048 nm/sec, respectively). The aggregation rates of the NH-Mid and NH-Low increase significantly with the presence of divalent Ca^{2+}. As the TiO_2 content decreases in the NHs, a larger fraction of the oxygen moieties likely get exposed to the surface, and hence can allow enhanced interaction with Ca^{2+} ions.

Presence of only 2.5 mg TOC/L SRHA dominates the aggregation behavior of the NHs with and without the presence of divalent Ca^{2+} (Figure 4.6). Such SRHA mediated colloidal stabilization has previously been reported[24, 25, 37]. The MWNT aggregation rate decreases from 0.60±0.076 nm/sec to 0.05±0.016 nm/sec with Ca^{2+}. For the other materials, the aggregation rates reduce to a negligible level when SRHA is present. Lowering of aggregation rate indicates strong stabilization of all the materials by SRHA, resulting in electrosteric hindrance to aggregation[36]. The faster aggregation of the MWNTs than other NMs in presence of 2.5 mg/L TOC SRHA indicates likely bridging of MWNTs, mediated by Ca^{2+}.

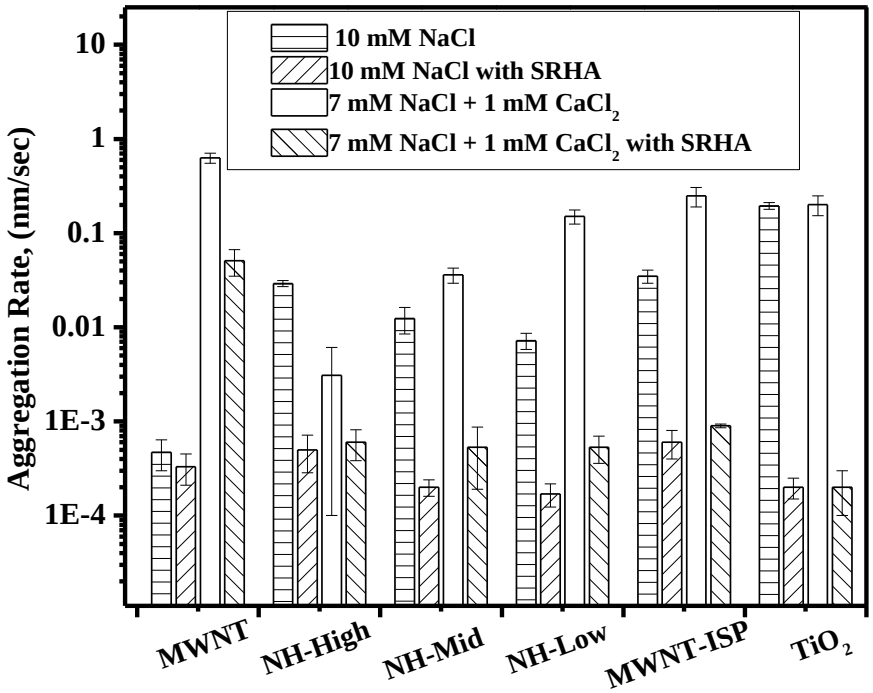

Figure 4.6: Aggregation rates of all materials at 10 mM ionic strength (10 mM NaCl only and 7 mM NaCl + 1 mM $CaCl_2$) with and without SRHA (2.5 mg/L TOC). All experiments were performed at 25 °C at a pH 6.9±0.2. The bar charts indicate mean aggregation rates and the error bars represent standard deviation.

4.4 SUMMARY

This study assessed the effects of TiO_2 loading on MWNT-TiO_2 NH aggregation behavior. TiO_2 loading was systematically varied from a C:Ti molar ratio of 1:0.1 to 1:0.033. Results indicate that NH-High with the highest TiO_2 loading behaves similarly to TiO_2 nanocrystals while interacting with both mono- and di-valent cations. As the TiO_2 loading is decreased, the presence of oxygen containing functional moieties on the NH surfaces also decreased (shown with XPS) due to deoxygenation during NH synthesis, which leads to increased stability of the NH-Mid and NH-Low. With divalent cations, NH-Low demonstrated the highest aggregation propensity among the NHs, likely due to specific adsorption of Ca^{2+} on likely exposed MWNT oxygen moieties. DLVO theory has shown to be unable to fit experimental results, particularly those of the NHs. Such deviation is likely caused by surface roughness and possibly by surface charge heterogeneity on the NHs, both of which violate the underlying assumptions of the DLVO theory. Presence of SRHA at 2.5 mg TOC/L concentration stabilized the NHs and the components (except MWNTs).

From the experimental results, it can be concluded that the sum of the aggregation behavior of the parts may not capture that of the whole (i.e., of the NHs). TiO_2 loading on the MWNT surfaces changes the chemical composition of the NHs, which leads to a strong variation in the interfacial interaction of these materials in an aqueous environment. In the presence of SRHA, NHs will exhibit increased stability and higher residence time in a water column.

4.5 LITERATURE CITED

1. Chen, W.; Xu, N. F.; Xu, L. G.; Wang, L. B.; Li, Z. K.; Ma, W.; Zhu, Y. Y.; Xu, C. L.; Kotov, N. A., Multifunctional Magnetoplasmonic Nanoparticle Assemblies for Cancer Therapy and Diagnostics (Theranostics). *Macromolecular Rapid Communications* **2010,** *31*, (2), 228-236.
2. Fan, Z.; Shelton, M.; Singh, A. K.; Senapati, D.; Khan, S. A.; Ray, P. C., Multifunctional plasmonic shell–magnetic core nanoparticles for targeted diagnostics, isolation, and photothermal destruction of tumor cells. *Acs Nano* **2012,** *6*, (2), 1065-1073.
3. Chen, J. H.; Mao, S.; Wen, Z. H. One-Pot Fabrication of Crumpled Graphene-Based Nanohybrids for Supercapacitors. 2013.
4. Alley, N. J.; Liao, K. S.; Andreoli, E.; Dias, S.; Dillon, E. P.; Orbaek, A. W.; Barron, A. R.; Byrne, H. J.; Curran, S. A., Effect of carbon nanotube-fullerene hybrid additive on P3HT:PCBM bulk-heterojunction organic photovoltaics. *Synth. Met.* **2012,** *162*, (1-2), 95-101.
5. Zhu, P.; Nair, A. S.; Yang, S.; Peng, S.; Elumalai, N. K.; Ramakrishna, S., Rice grain-shaped TiO2-CNT composite-A functional material with a novel morphology for dye-sensitized solar cells. *Journal of Photochemistry and Photobiology a-Chemistry* **2012,** *231*, (1), 9-18.
6. Park, D.-H.; Jeon, Y.; Ok, J.; Park, J.; Yoon, S.-H.; Choy, J.-H.; Shul, Y.-G., Pt Nanoparticle-Reduced Graphene Oxide Nanohybrid for Proton Exchange Membrane Fuel Cells. *Journal of Nanoscience and Nanotechnology* **2012,** *12*, (7), 5669-5672.
7. Muszynski, R.; Seger, B.; Kamat, P. V., Decorating graphene sheets with gold nanoparticles. *J. Phys. Chem. C* **2008,** *112*, (14), 5263-5266.
8. Liu, J. M.; Wang, X. X.; Cui, M. L.; Lin, L. P.; Jiang, S. L.; Jiao, L.; Zhang, L. H., A promising non-aggregation colorimetric sensor of AuNRs-Ag+ for determination of dopamine. *Sensors and Actuators B-Chemical* **2013,** *176*, 97-102.
9. Saleh, N. B.; Aich, N.; Lead, J.; Plazas-Tuttle, J.; Lowry, G. V., Research strategy to determine when novel nanohybrids pose unique environmental risks. *Environmental Science: Nano* **2015,** *2*, 11-18 (Cover Article).
10. Saleh, N. B.; Afrooz, A.; Bisesi Jr, J. H.; Aich, N.; Plazas-Tuttle, J.; Sabo-Attwood, T., Emergent properties and toxicological considerations for nanohybrid materials in aquatic systems. *Nanomaterials* **2014,** *4*, (2), 372-407.
11. Kim, S.; Shin, D. H.; Kim, C. O.; Hwang, S. W.; Choi, S. H.; Ji, S.; Koo, J. Y., Enhanced ultraviolet emission from hybrid structures of single-walled carbon nanotubes/ZnO films. *Applied Physics Letters* **2009,** *94*, (21).
12. Li, F. S.; Cho, S. H.; Son, D. I.; Kim, T. W.; Lee, S. K.; Cho, Y. H.; Jin, S. H., UV photovoltaic cells based on conjugated ZnO quantum dot/multiwalled carbon nanotube heterostructures. *Applied Physics Letters* **2009,** *94*, (11).
13. Gund, G. S.; Dubal, D. P.; Shinde, S. S.; Lokhande, C. D., Architectured Morphologies of Chemically Prepared NiO/MWCNTs Nanohybrid Thin Films for High Performance Supercapacitors. *Acs Applied Materials & Interfaces* **2014,** *6*, (5), 3176-3188.

14. Wen, Z. H.; Ci, S. Q.; Mao, S.; Cui, S. M.; Lu, G. H.; Yu, K. H.; Luo, S. L.; He, Z.; Chen, J. H., TiO2 nanoparticles-decorated carbon nanotubes for significantly improved bioelectricity generation in microbial fuel cells. *Journal of Power Sources* **2013,** *234*, 100-106.
15. Sealy, C., The problem with platinum. *Materials Today* **2008,** *11*, (12), 65-68.
16. Tang, Z.; Chua, D. H. C., Investigation of Pt/CNT-Based Electrodes in Proton Exchange Membrane Fuel Cells Using AC Impedance Spectroscopy. *Journal of The Electrochemical Society* **2010,** *157*, (6), B868.
17. Akalework, N. G.; Pan, C.-J.; Su, W.-N.; Rick, J.; Tsai, M.-C.; Lee, J.-F.; Lin, J.-M.; Tsai, L.-D.; Hwang, B.-J., Ultrathin TiO2-coated MWCNTs with excellent conductivity and SMSI nature as Pt catalyst support for oxygen reduction reaction in PEMFCs. *Journal of Materials Chemistry* **2012,** *22*, (39), 20977.
18. Jiang, Z.-Z.; Gu, D.-M.; Wang, Z.-B.; Qu, W.-L.; Yin, G.-P.; Qian, K.-J., Effects of anatase TiO2 with different particle sizes and contents on the stability of supported Pt catalysts. *Journal of Power Sources* **2011,** *196*, (20), 8207-8215.
19. Xia, B. Y.; Ding, S.; Wu, H. B.; Wang, X.; Wen, X., Hierarchically structured Pt/CNT@TiO2 nanocatalysts with ultrahigh stability for low-temperature fuel cells. *Rsc Advances* **2012,** *2*, (3), 792.
20. Usui, T. *World budget of platinum*; Stanford University: 2010.
21. Wilburn, D. R.; Bleiwas, D. I. *Platinum-group metals-world supply and demand* U.S. Geological Survey: 2004.
22. Pehnt, M., Life-cycle analysis of fuel cell system components. *Handbook of Fuel Cells* **2003**.
23. Brunelli, A.; Zabeo, A.; Semenzin, E.; Hristozov, D.; Marcomini, A., Extrapolated long-term stability of titanium dioxide nanoparticles and multi-walled carbon nanotubes in artificial freshwater. *Journal of Nanoparticle Research* **2016,** *18*, (5), 1-13.
24. Saleh, N. B.; Pfefferle, L. D.; Elimelech, M., Aggregation kinetics of multiwalled carbon nanotubes in aquatic systems: measurements and environmental implications. *Environmental Science & Technology* **2008,** *42*, (21), 7963-7969.
25. Saleh, N. B.; Pfefferle, L. D.; Elimelech, M., Influence of biomacromolecules and humic acid on the aggregation kinetics of single-walled carbon nanotubes. *Environmental Science & Technology* **2010,** *44*, (7), 2412-2418.
26. Liu, X.; Chen, G.; Su, C., Effects of material properties on sedimentation and aggregation of titanium dioxide nanoparticles of anatase and rutile in the aqueous phase. *Journal of Colloid and Interface Science* **2011,** *363*, (1), 84-91.
27. Yi, P.; Chen, K. L., Influence of surface oxidation on the aggregation and deposition kinetics of multiwalled carbon nanotubes in monovalent and divalent electrolytes. *Langmuir* **2011,** *27*, (7), 3588-3599.
28. Smith, B.; Wepasnick, K.; Schrote, K. E.; Cho, H.-H.; Ball, W. P.; Fairbrother, D. H., Influence of surface oxides on the colloidal stability of multi-walled carbon nanotubes: a structure-property relationship. *Langmuir* **2009,** *25*, (17), 9767-9776.

29. Smith, B.; Wepasnick, K.; Schrote, K. E.; Bertele, A. R.; Ball, W. P.; O'Melia, C.; Fairbrother, D. H., Colloidal Properties of Aqueous Suspensions of Acid-Treated, Multi-Walled Carbon Nanotubes. *Environmental Science & Technology* **2009,** *43*, (3), 819-825.
30. Khan, I. A.; Afrooz, A. R. M. N.; Flora, J. R. V.; Schierz, P. A.; Ferguson, P. L.; Sabo-Attwood, T.; Saleh, N. B., Chirality affects aggregation kinetics of single-walled carbon nanotubes. *Environmental science & technology* **2013,** *47*, (4), 1844-1852.
31. Khan, I. A.; Flora, J. R. V.; Afrooz, A. R. M. N.; Aich, N.; Schierz, P. A.; Ferguson, P. L.; Sabo-Attwood, T.; Saleh, N. B., Change in chirality of semiconducting single-walled carbon nanotubes can overcome anionic surfactant stabilisation: a systematic study of aggregation kinetics. *Environmental Chemistry* **2015,** *12*, (6), 652-661.
32. Shih, Y. H.; Liu, W. S.; Su, Y. F., Aggregation of stabilized TiO2 nanoparticle suspensions in the presence of inorganic ions. *Environmental Toxicology and Chemistry* **2012,** *31*, (8), 1693-1698.
33. Hua, Z.; Zhang, J.; Bai, X.; Ye, Z.; Tang, Z.; Liang, L.; Liu, Y., Aggregation of TiO2–graphene nanocomposites in aqueous environment: Influence of environmental factors and UV irradiation. *Science of The Total Environment* **2016,** *539*, 196-205.°°C
34. Rigdon, W. A.; Huang, X., °arbon monoxide tolerant platinum electrocatalysts on niobium doped titania and carbon nanotube composite supports. *Journal of Power Sources* **2014,** *272*, 845-859.
35. Yang, D.; Velamakanni, A.; Bozoklu, G.; Park, S.; Stoller, M.; Piner, R. D.; Stankovich, S.; Jung, I.; Field, D. A.; Ventrice, C. A., Chemical analysis of graphene oxide films after heat and chemical treatments by X-ray photoelectron and Micro-Raman spectroscopy. *Carbon* **2009,** *47*, (1), 145-152.
36. Afrooz, A. N.; Das, D.; Murphy, C. J.; Vikesland, P.; Saleh, N. B., Co-transport of gold nanospheres with single-walled carbon nanotubes in saturated porous media. *Water Research* **2016,** *99*, 7-15.
37. Aich, N.; Boateng, L. K.; Sabaraya, I. V.; Das, D.; Flora, J. R.; Saleh, N. B., Aggregation kinetics of higher order fullerene clusters in aquatic systems. *Environmental science & technology* **2016,** *50*, (7), 3562-3571.
38. Afrooz, A. N.; Khan, I. A.; Hussain, S. M.; Saleh, N. B., Mechanistic heteroaggregation of gold nanoparticles in a wide range of solution chemistry. *Environmental science & technology* **2013,** *47*, (4), 1853-1860.
39. Khan, I. A.; Aich, N.; Afrooz, A. R. M. N.; Flora, J. R. V.; ferguson, L.; sabo-Attwood, T.; Saleh, N. B., Fractal structures of single-walled carbon nanotubes in biologically relevant conditions: role of chirality vs. media conditions. *Chemosphere* **2013** *93*, (9), 1997-2003.
40. Afrooz, A. R. M. N.; Khan, I. A.; Hussain, S. M.; Saleh, N. B., Mechanistic Heteroaggregation of Gold Nanoparticles in a Wide Range of Solution Chemistry. *Environ. Sci. Technol.* **2013,** *47*, (4), 1853-1860.
41. Afrooz, A. R. M. N.; Sivalapalan, S. T.; Murphy, C. J.; Hussain, S. M.; Schlager, J. J.; Saleh, N. B., Spheres vs. rods: the shape of gold nanoparticles influences aggregation and deposition behavior. *Chemosphere* **2013,** *91*, (1), 93-98.

42. Chen, K. L.; Elimelech, M., Aggregation and deposition kinetics of fullerene (C60) nanoparticles. *Langmuir* **2006,** *22*, (26), 10994-11001.
43. Huynh, K. A.; McCaffery, J. M.; Chen, K. L., Heteroaggregation of multiwalled carbon nanotubes and hematite nanoparticles: Rates and mechanisms. *Environmental Science & Technology* **2012,** *46*, (11), 5912-5920.
44. Benjamin, M. M.; Lawler, D. F., *Water quality engineering: physical/chemical treatment processes*. John Wiley & Sons: 2013.
45. Wepasnick, K. A.; Smith, B. A.; Bitter, J. L.; Fairbrother, D. H., Chemical and structural characterization of carbon nanotube surfaces. *Analytical and bioanalytical chemistry* **2010,** *396*, (3), 1003-1014.
46. Naumkin, A. V.; Kraut-Vass, A.; Gaarenstroom, S. W.; Powell, C. J., NIST X-ray Photoelectron Spectroscopy Database In 2012.
47. Yang, H. G.; Sun, C. H.; Qiao, S. Z.; Zou, J.; Liu, G.; Smith, S. C.; Cheng, H. M.; Lu, G. Q., Anatase TiO2 single crystals with a large percentage of reactive facets. *Nature* **2008,** *453*, (7195), 638-641.
48. Sano, M.; Okamura, J.; Shinkai, S., Colloidal nature of single-walled carbon nanotubes in electrolyte solution: the Schulze-Hardy rule. *Langmuir* **2001,** *17*, (22), 7172-7173.
49. Chowdhury, I.; Duch, M. C.; Mansukhani, N. D.; Hersam, M. C.; Bouchard, D., Colloidal properties and stability of graphene oxide nanomaterials in the aquatic environment. *Environmental Science & Technology* **2013,** *47*, (12), 6288-6296.
50. Lanphere, J. D.; Luth, C. J.; Walker, S. L., Effects of solution chemistry on the transport of graphene oxide in saturated porous media. *Environmental Science & Technology* **2013,** *47*, (9), 4255-4261.
51. Liao, D. L.; Wu, G. S.; Liao, B. Q., Zeta potential of shape-controlled TiO2 nanoparticles with surfactants. *Colloids and Surfaces A: Physicochemical and Engineering Aspects* **2009,** *348*, (1–3), 270-275.
52. Long, T. C.; Saleh, N.; Tilton, R. D.; Lowry, G. V.; Veronesi, B., Titanium dioxide (P25) produces reactive oxygen species in immortalized brain microglia (BV2): implications for nanoparticle neurotoxicity. *Environmental Science & Technology* **2006,** *40*, (14), 4346-4352.
53. Suresh, L.; Walz, J. Y., Direct measurement of the effect of surface roughness on the colloidal forces between a particle and flat plate. *Journal of Colloid and Interface Science* **1997,** *196*, (2), 177-190.
54. Bouyer, F.; Robben, A.; Yu, W. L.; Borkovec, M., Aggregation of colloidal particles in the presence of oppositely charged polyelectrolytes: effect of surface charge heterogeneities. *Langmuir* **2001,** *17*, (17), 5225-5231.
55. Behrens, S. H.; Christl, D. I.; Emmerzael, R.; Schurtenberger, P.; Borkovec, M., Charging and aggregation properties of carboxyl latex particles: Experiments versus DLVO theory. *Langmuir* **2000,** *16*, (6), 2566-2575.
56. Kihira, H.; Ryde, N.; Matijević, E., Kinetics of heterocoagulation. Part. 2—The effect of the discreteness of surface charge. *Journal of the Chemical Society, Faraday Transactions* **1992,** *88*, (16), 2379-2386.

57. Suresh, L.; Walz, J. Y., Effect of Surface Roughness on the Interaction Energy between a Colloidal Sphere and a Flat Plate. *Journal of Colloid and Interface Science* **1996,** *183,* (1), 199-213.

Chapter 5: Summary and Conclusions

5.1 SUMMARY

This dissertation is based on novel research on the environmental aspects of complex, multicomponent multiwalled carbon nanotube-metal oxide (MWNT-MO) NHs. The research focuses on three important data gaps: 1) developing a facile synthesis platform for MWNT-MO NH preparation under comparable operational conditions, 2) understanding the crystal formation process during hybridization of MOs on the MWNT surfaces, and 3) evaluation of aggregation behavior of MWNT-MO NH and the component materials.

These data gaps were addressed by performing three tasks. In task 1, a wet-chemistry based sol-gel technique was modified. The modified technique was utilized as a platform for synthesizing a wide range of MWNT-MO NHs by merely changing the metal precursor. Four different MWNT-MO NHs (MWNT-TiO_2, MWNT-ZnO, MWNT-Er_2O_3, and MWNT-Pr_6O_{11}) were synthesized and a suite of characterization techniques was employed to characterize these NHs; electron microscopy (HRTEM and STEM with elemental mapping) for physical morphology, X-ray techniques (XRD and XPS) to assess crystallinity and chemical composition, thermal gravimetric analysis (TGA) to assess effective hybridization, and light scattering to evaluate cluster size in aqueous suspension.

Task 2 provided insights into the metal oxide crystal growth mechanism and degree of crystallinity (of the lanthanide series metal oxides). XRD was used to assess crystal structure of the metal oxides before and after calcination to gain such insights. Applicability of the sol-gel technique was tested by evaluating the role of standard

electrode potential (SEP) on zero-valent metal vs. metal oxide formation on the MWNT surface. Ag and Cu metal species were chosen to hybridize MWNTs with zero-valent nanocrystals of these species and assess applicability of the sol-gel method to synthesize these NHs.

In task 3, MWNT-TiO_2 NHs with a range of TiO_2 loading (C:Ti molar ratio of 1:0.1, 1:0.05, and 1:0.033) on MWNT surfaces were chosen for the evaluation of aggregation behavior in aqueous environment. The aggregation behavior of the NHs was compared with those of the component materials (i.e., MWNT and TiO_2). The modified sol-gel method was used to synthesize these NHs, which were characterized with HRTEM, STEM with elemental mapping for physical morphology, with XRD for their crystallinity, and with XPS for chemical composition. Aggregation behavior was assessed in a wide range of mono-valent NaCl concentration (1-100 mM) and in presence of 10 mM mixed electrolyte condition (7 mM NaCl and 1 mM $CaCl_2$) with and without Suwannee river humic acid (SRHA). The experimental aggregation data (stability plots) were also compared with theoretical DLVO predictions to assess the efficiency of this classical electrostatic theory to capture the aggregation behavior of the complex NHs.

5.2 CONCLUSIONS

The major conclusions of this research are summarized below:

5.2.1 An Elegant Method for Large Scale Synthesis of Metal Oxide-Carbon Nanotube Nanohybrids for Nano-environmental Application and Implication Studies

- A simple sol-gel synthesis process was modified for producing a wide range of MWNT-MO NHs (MWNT-TiO_2, MWNT-ZnO, MWNT-Er_2O_3, and MWNT-Pr_6O_{11} in this case), where the MO content on the MWNT surface can be varied just by changing the precursors
- The synthesis process was able to produce a relatively large quantity of NHs (100s of mg), typically necessary to perform a comprehensive environmental implication study.
- TEM, STEM and elemental mapping of these NHs demonstrated attachment of MOs on the MWNT surfaces.
- XRD patterns showed excellent crystallinity for MWNT-TiO_2 and MWNT-ZnO NHs. However, a significant amount of amorphous content was identified in the MWNT-Er_2O_3 and MWNT-Pr_6O_{11} NHs.
- TGA on these NHs demonstrated that the MOs are chemically bonded with the MWNT surfaces.
- XPS and TGA analyses on the NHs demonstrated material reproducibility between synthesized batches.
- Stable aqueous suspensions were prepared with the NHs with fairly uniform cluster sizes (standard deviation within 10% of the average cluster size).

- All NHs demonstrated negative surface potential which is the primary reason for particle stability

5.2.2 Insights into Metal Oxide and Metal Nanocrystal Formation During the Sol-gel Hybridization Process

- Calcination of the NHs was determined to be one the most important steps in crystal formation on the MWNT surfaces.
- The pathway for ZnO crystal formation includes $Zn(OH)_2$/ZnO mixed phase crystal formation, which converts to ZnO crystals during calcination.
- A low degree of crystallinity is observed on the metal oxides of MWNT-Er_2O_3 and MWNT-Pr_6O_{11} NHs. Calcination of the NHs at an elevated temperature decreased the amorphous content, but not entirely.
- The MO nanocrystals retrieved by complete oxidation of the MWNTs at high temperature showed comparable TEM sizes among themselves and demonstrated excellent crystallinity.
- It is suggested that the modified sol-gel technique can grow both metal and metal oxide nano-features onto MWNTs, and the crystal composition depends on the SEP of the metal species; i.e., metal vs. metal oxides are grown with metal species having positive and negative SEP values, respectively.
- Ag with a positive SEP value of 0.799 V formed zero-valent metal crystals on MWNT surfaces. However, Cu (with a positive SEP of 0.345 V) showed strong tendency to oxidize and form mixed phase Cu/Cu_2O (core/shell) nanostructures.

Synthesis under oxygen-free environment could not eliminate the oxide form of the Cu.

- It is suggested that metal species with positive SEP values, equal or higher than 0.799 V will form zero valent metal nanocrystals when synthesized with the modified sol-gel technique described in chapter 2.
- Using an alternative solvent, i.e., DMF, which is a stronger reducing agent compared to isopropanol (previously used solvent), the Cu_2O content were reduced significantly, even when the synthesis is performed in presence of oxygen.

5.2.3. Aggregation Behavior of Multiwalled Carbon Nanotube-Titanium Dioxide Nanohybrids: Role of Titanium Dioxide Loading

- The MWNT-TiO_2 NHs with all TiO_2 loadings demonstrated higher colloidal stability than TiO_2 and lower stability when compared to that of the oxidized MWNTs in presence of monovalent cations.
- NHs with C:Ti molar ratio of 1:0.1 (NH-High) showed the highest aggregation propensity among the NHs in presence of only NaCl. The NHs with C:Ti molar ratio of 1:0.05 (NH-Mid) and 1:0.033 (NH-Low) demonstrated similar aggregation behavior with NaCl.
- With an increased amount of TiO_2 loading, the MWNT surfaces get overcoated with the metal oxide, which controls the interfacial interaction of these NMs. Lowering the TiO_2 loading also allows for deoxygenation of the MWNT surface moieties (during synthesis), leading to a relative decrease in aggregation propensity (for the NH-Low).

- Presence of divalent Ca^{2+} ions showed increased aggregation rate for the NHs with lower TiO_2 loading (i.e., for NH-Med and NH-Low). However, NH with the highest TiO_2 loading showed minor increase in aggregation rate. These results indicate that overcoating of MWNT surfaces with TiO_2 (for NH-High) most likely shielded the charged surface moieties, resulting in a likely reduction of specific ion adsorption and thereby reduced the effect on aggregation rate.
- Fitting of the experimental data with the classical DLVO theory demonstrated that this classical electrostatic model is unable to fully capture the aggregation behavior of the NHs.
- NH-High showed the most deviation of the DLVO theory from the experimental data. Surface roughness of these NHs, contributed by overcoated TiO_2 has likely contributed to such deviation.
- Presence of SRHA decreased aggregation propensity for all materials indicating a strong binding of the natural organic matter to the NH and the component material surfaces, which results in enhanced stabilization.

5.3 Environmental Implication of the Research

With increasing use of multicomponent MWNT-MO nanohybrids in various biomedical and energy sectors, the risk associated with the environmental release is unavoidable, which necessitates systematic evaluation of their environmental implications. One of the major challenges for such studies is the availability of materials with tightly controlled physicochemical properties. This research presents a facile MWNT-MO NH

synthesis technique, where simple variation in reagent composition and ratio allows for controlling the metal oxide type and loading on nanotube surfaces. To the best of the author's knowledge, this is the only synthesis technique reported in the literature that can be used as a common platform to hybridize a wide range of MOs with MWNTs under a comparable set of synthesis conditions. Large material yield makes this method particularly useful for nano-environmental studies. Insights gained on crystal formation can guide better adjustment of the synthesis conditions to grow highly crystalline metal and metal oxides on MWNT surfaces.

The synthesis technique developed in the dissertation allowed controlled synthesis of MWNT-TiO_2 NH (with a range of TiO_2 loading), one of the most used and commercialized MWNT-MO NH. Results indicate that NHs with increasing MO loading will exhibit decreasing colloidal stability in the presence of monovalent cation only. The presence of divalent cation does not change the NH-High aggregation behavior observed for monovalent cations. However, NH-Mid and MH-Low demonstrated higher aggregation propensity with decreased MO loading in presence of a divalent cation. Thus, NH-Mid and NH-Low will likely be unstable in the presence of mono- and di-valent electrolytes. NH-High will likely exhibit higher stability in such conditions. The presence of SRHA will stabilize all the NHs and thus can facilitate environmental transport of these complex NMs.

5.4 RECOMMENDATIONS FOR FUTURE RESEARCH

The research presented in this study is one of the first of its kind and can be used as a platform to address key data gaps associated with environmental implications of MWNT-MO NHs.

5.4.1 Recommendations on NH Synthesis

The sol-gel synthesis process successfully synthesized four different MWNT-MO NHs. The synthesis process was proven to be reproducible for the MO loading used in the research. However, whether other MO loadings can be reproducibly attached on the MWNT surface remains unresolved. Additional experiments need to be performed to capture the highest MO loading that can be successfully attached to the MWNT surface using the sol-gel technique. The HRTEM micrographs of the NHs except for MWNT-TiO_2 indicated encapsulation of MO nanocrystals inside the MWNT core. Experiments need to be performed to quantify the encapsulation percentage as such encapsulation can alter the NH properties. Furthermore, aqueous suspensions of MWNT-ZnO, MWNT-Er_2O_3, and MWNT-Pr_6O_{11} NHs showed limited stability (~48 hours). Better aqueous stability of these NHs needs to be pursued for EHS studies requiring suspension stability for more than 48 hours (e.g., toxicity, porous media transport).

Since, the synthesis was performed with an inorganic solvent, the effect of pH was not considered on the synthesis process since the pH structure is completely different for the organic solvents. The pH structure for such organic solvents needs to considered to

better understand the effect of pH on synthesis which might facilitate improvement of the developed synthesis technique.

Although MWNT-TiO_2 and MWNT-ZnO showed excellent crystallinity, MWNT-Er_2O_3, and MWNT-Pr_6O_{11} NHs demonstrated amorphous MO content. The reported synthesis technique should be reengineered to enhance the crystallinity of the MO content in these NHs since, different ordered crystal planes can be responsible for different types of catalytic activities. Moreover, this research could not identify the hybridization scheme for MWNT-Er_2O_3, and MWNT-Pr_6O_{11} NHs. Experiments need to be performed to decipher the hybridization mechanism of these NHs.

Inorganic content in the synthesized MWNT-Cu/Cu_2O NH was addressed as core/shell nanoparticles as per literature suggestion. Some of the articles performed depth profiling of these nanocrystals based on XRD spectra, however, did not present evidence of the actual core/shell structure of these nanoparticles. Hence, additional characterization needs to be performed to validate their core/shell structure.

5.4.2 Recommendations on the Environmental Implication of the NHs

In this research, aggregation experiments were performed with MWNT-TiO_2 NHs with three different TiO_2 loadings. Although the research demonstrated the effect of TiO_2 loading and synthesis technique on the NH aggregation behavior, it did not investigate the role of surface roughness and surface charge heterogeneity on the aggregation behavior of the NHs. Additional research should be conducted to capture the aspect of surface roughness and charge heterogeneity since both these material properties are known to

influence particle aggregation. Novel techniques should also be developed to experimentally measure the van der Waals attraction forces of the NHs. These results will be able to set up correlations among MO loading, NH surface roughness, charge heterogeneity, surface potential, and the van der Waals attraction forces, which will enable researchers to better predict the aggregation behavior of the MWNT-TiO_2 NHs with different TiO_2 loadings other than the ones used for this research. Furthermore, this research only focused on the self-aggregation behavior of the MWNT-TiO_2 NHs. Other environmental implication studies (e.g., hetero-aggregation in presence of other colloidal particles, porous media transport, environmental transformation, and nanotoxicity) need to be performed. The aggregation study can complement these recommended studies to assess the environmental risks of these NHs.

Residence time of a nanomaterial in the water column dictates the fate of these particulates in surface water environments. Aggregation results reported in this dissertation indicate that residence time of the NHs will depend on the NH composition as well as the water quality (e.g., ionic strength, concentration of natural organic matter). If the water quality is favorable for particle aggregation, the residence time of the NHs would be shorter and the NHs will deposit faster. Self-aggregation associated with hetero-aggregation (NH aggregation with other engineered or naturally occurring colloids) studies can be used to estimate the NH residence time in the water column. Furthermore, in this study, only SRHA was used to investigate the effect of natural organic matter on particle aggregation. Depending on the waterbody, the nature of the bio and geo macromolecules can be different (e.g., presence of less humified substances than SRHA). NH interaction with such organics

also needs to be assessed because such interaction can completely change the NH environmental behavior.

One of the key factors controlling environmental implications of NHs is the material integrity under environmental exposure. Environmental transformation processes may compromise the integrity of these materials, hence may make implications studies on these composite materials irrelevant. Thus, assessment of NH integrity is essential to determine in order to evaluate behavior of a NH that may be persistent in the environment.

This research focused only on the MWNT-TiO_2 NHs. Hence, environmental behavior of other MWNT-MO NHs remains a major datagap. Such environmental implication studies need to be performed with other MWNT-MO NHs. The synthesis technique described in this research can be used to synthesize these NHs and the results from such studies can be used to understand the effect of different MO content on environmental behavior of different MWNT-MO NHs.

Appendices

APPENDIX A

Supplementary Information for Chapter 2

An Elegant Method for Large Scale Synthesis of Metal Oxide-Carbon Nanotube Nanohybrids for Nano-environmental Application and Implication Studies

Table A1: Residual Mass percentages and peak oxidation temperature of oxidized MWNTs and the NHs, obtained from TGA

Sample	Residual Mass (%)	Oxidation Temperature (°C)
MWNT	1.4±0.2	635.4±0.6
MWNT-TiO_2	40.3±2.3	560.5±1.1
MWNT-ZnO	46.1±1.9	587.1±8.3
MWNT-Er_2O_3	47.3±2.8	474.0±4.4
MWNT-Pr_6O_{11}	51.8±0.7	437.5±1.5

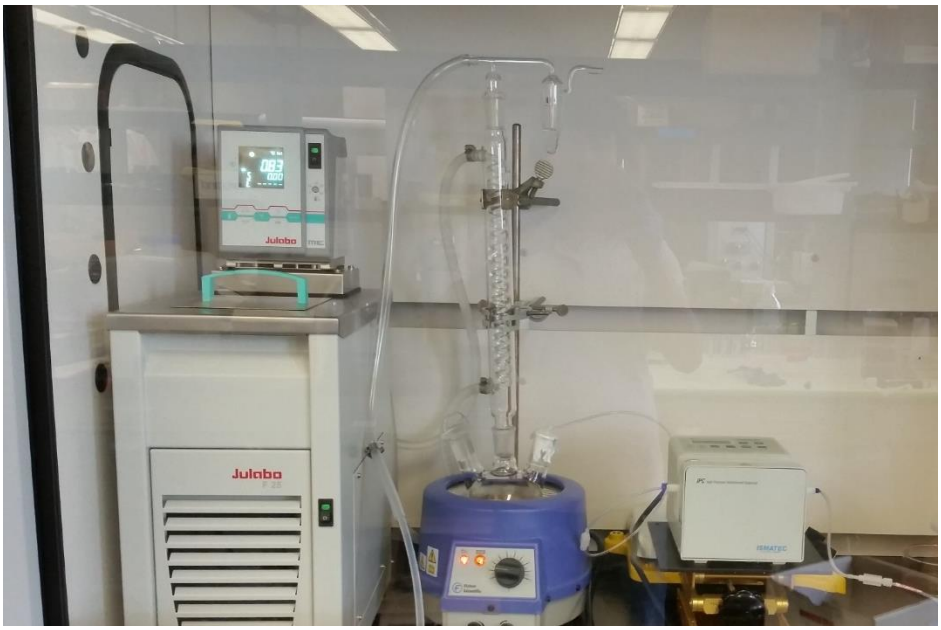

Figure A1: Experimental setup for NH synthesis.

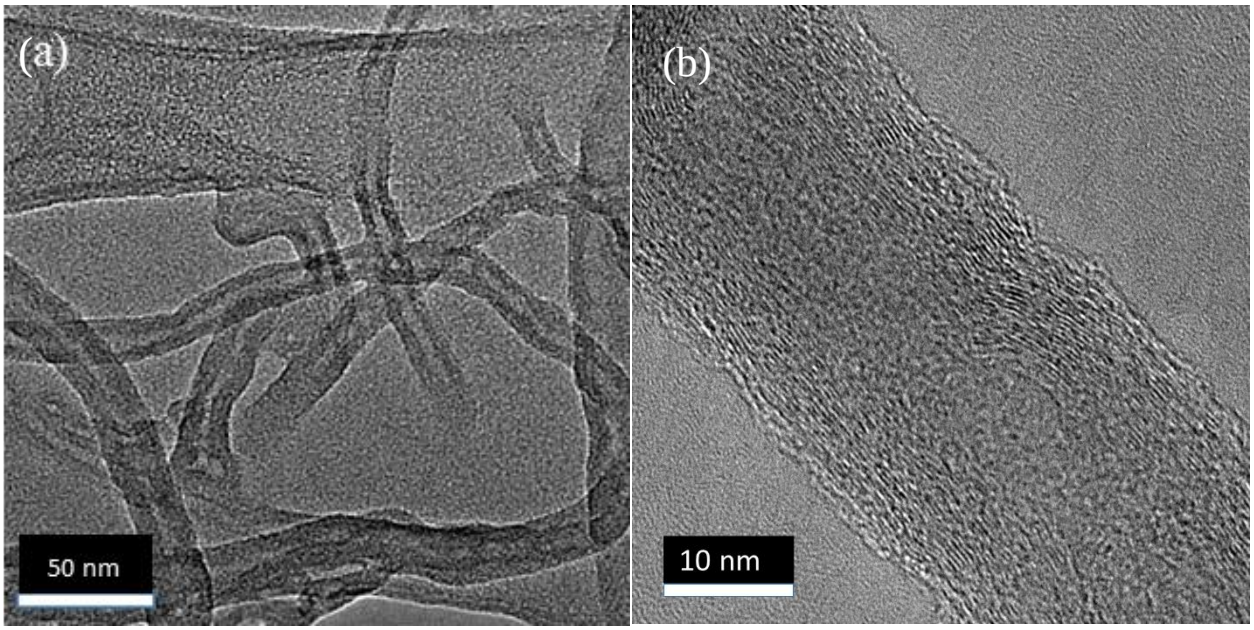

Figure A2: Representative (a) TEM and (b) HRTEM micrographs of oxidized MWNTs.

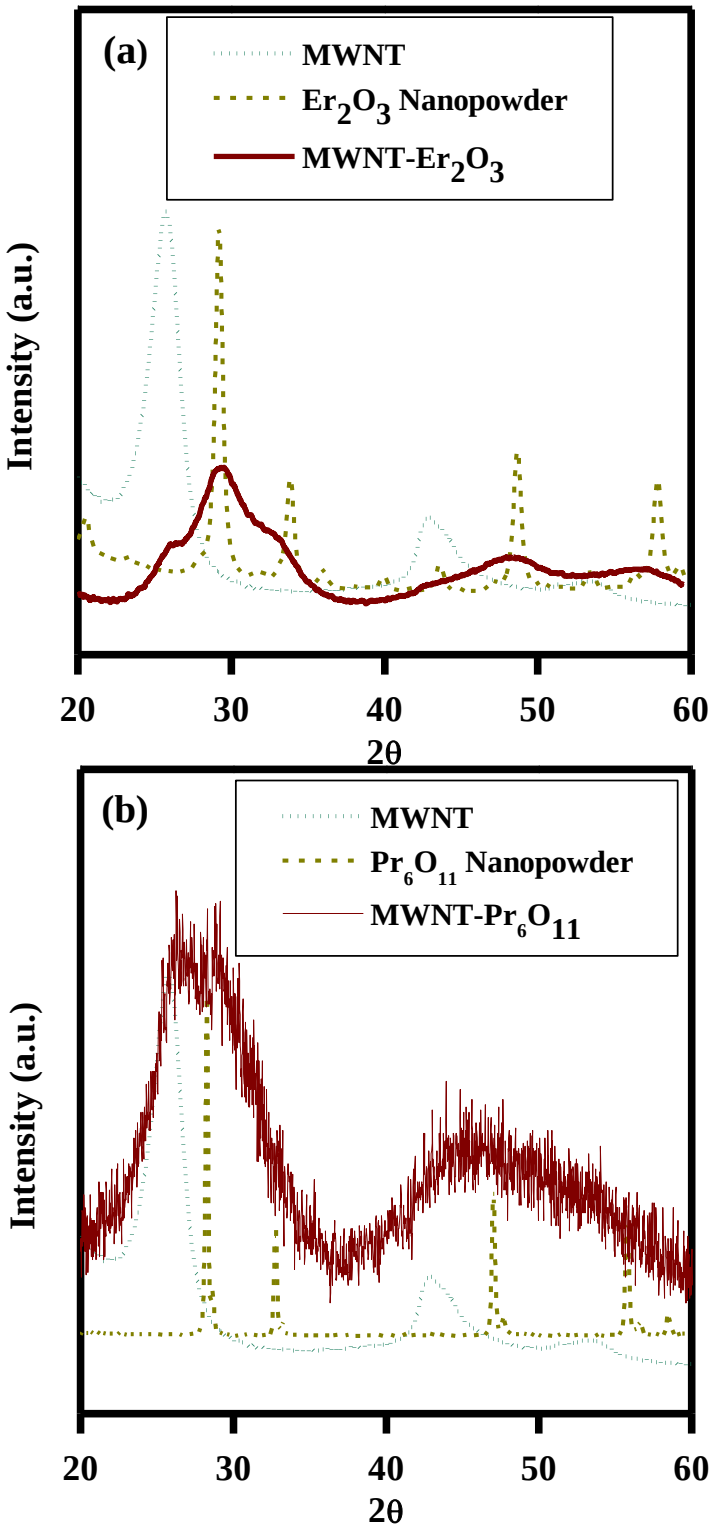

Figure A3: Representative XRD patterns comparing oxidized MWNTs with (a) Er_2O_3 nanopowder and MWNT-Er_2O_3; (b) Pr_6O_{11} nanopowder and MWNT-Pr_6O_{11}.

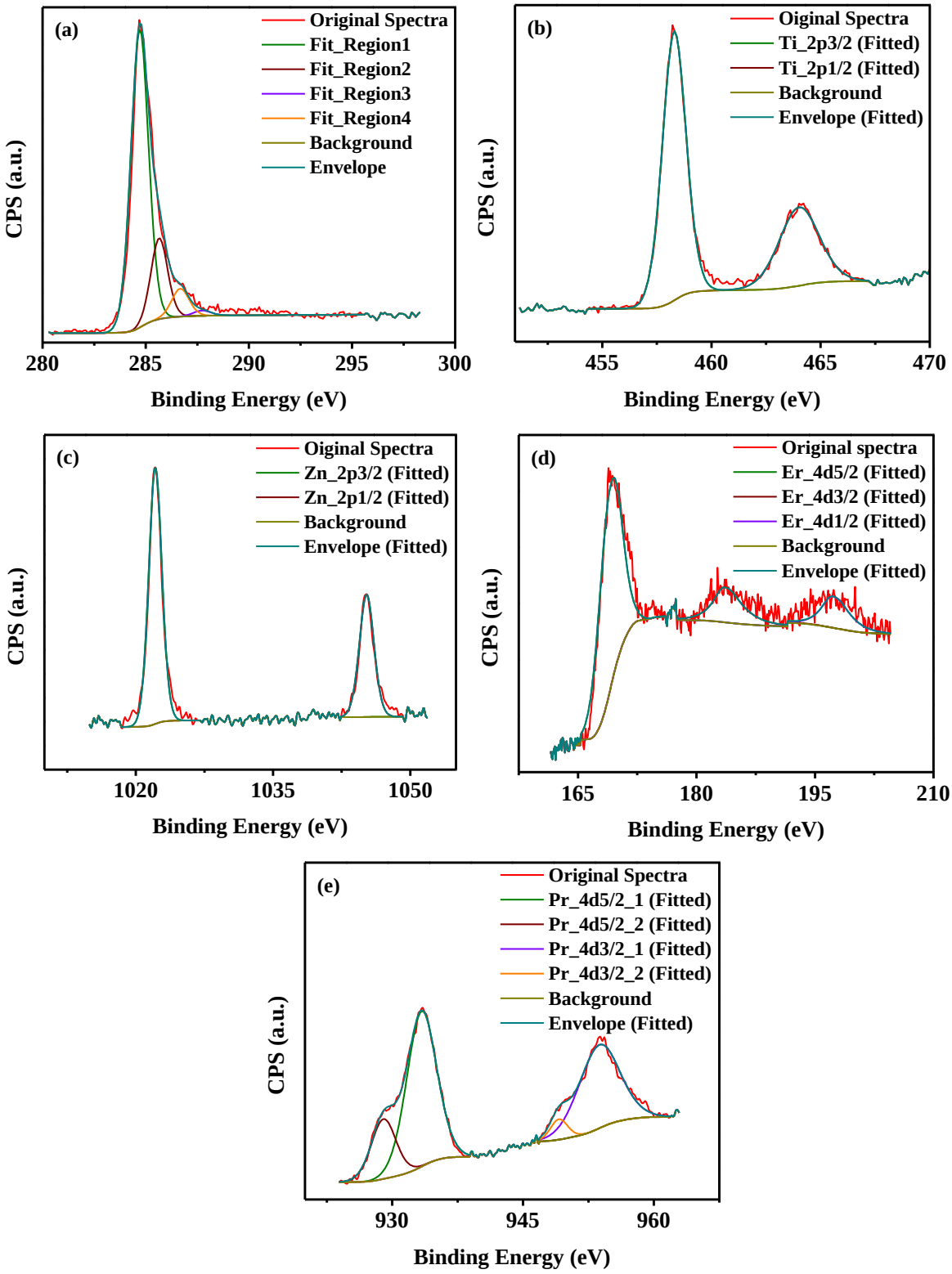

Figure A4: Characteristic XPS spectra for (a) C 1s in oxidized MWNT, (b) Ti 2p in MWNT-TiO_2 (c) Zn 2p in MWNT-ZnO**,** (d) Er 4d in MWNT-Er_2O_3, and (e) Pr 4d in MWNT-Pr_6O_{11} NHs.

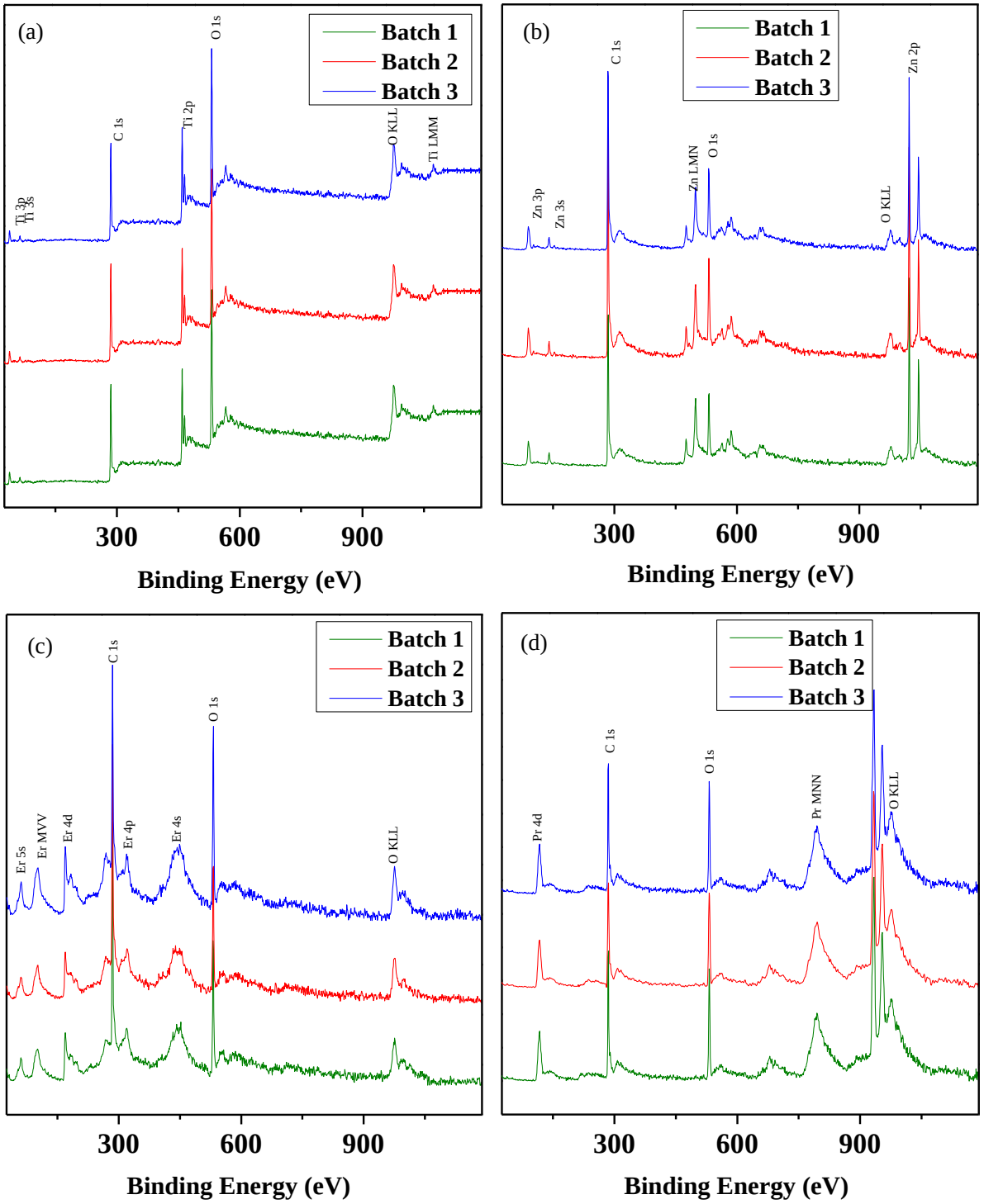

Figure A5: Comparative XPS survey spectra of the three different batches of each of the four NHs: (a) MWNT-TiO_2, (b) MWNT-ZnO, (c) MWNT-Er_2O_3, and (d) MWNT-Pr_6O_{11}. The peak labels perfectly align between all batches and are only labeled for the top spectrum to maintain clarity.

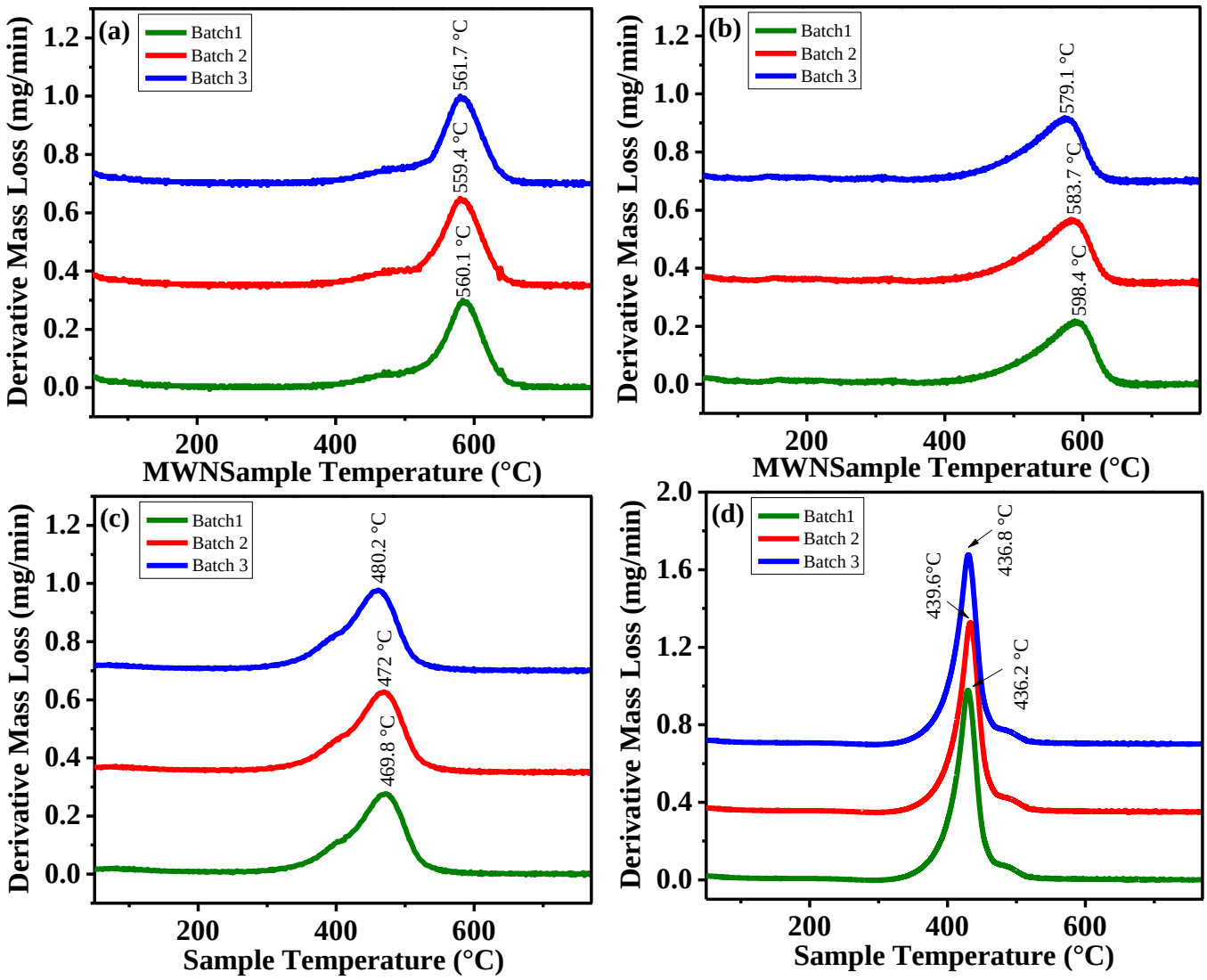

Figure A6: Comparative derivative mass loss profiles of the three different batches of each of the four NHs: (a) MWNT-TiO_2, (b) MWNT-ZnO, (c) MWNT-Er_2O_3, and (d) MWNT-Pr_6O_{11}. Oxidation temperatures are labeled as the peak positions of the derivative mass loss plots.

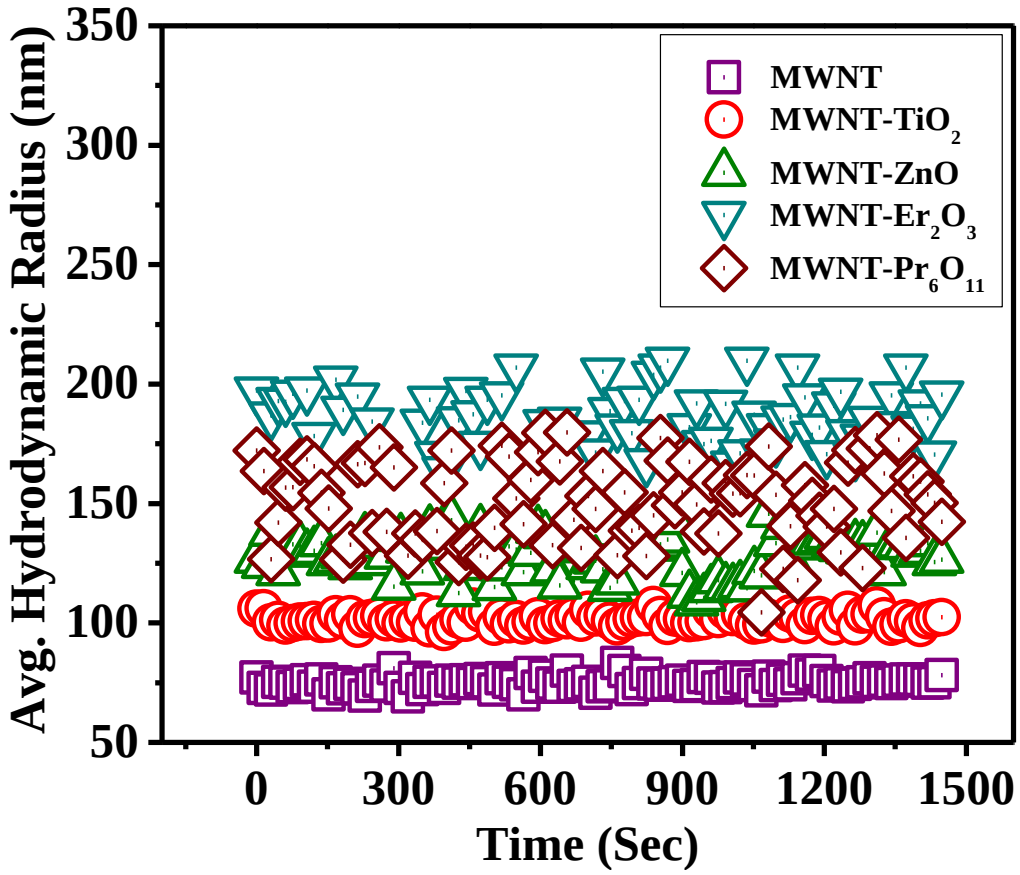

Figure A7: Average hydrodynamic radius of oxidized MWNTs and the NHs over time. All experiments were performed at pH of 6.9 and at 25 °C.

APPENDIX B

Supplementary Information for Chapter 3

Insights into Metal Oxide and Metal Nanocrystal Formation During the Sol-gel Hybridization Process

Table B1: Standard Electrode potential of different metal species: Reactions and values[1]

NH	Reaction	Standard Electrode Potential (V)
MWNT-Al_2O_3	$Al^{3+} + 3e^- \leftrightarrow Al$ (s)	-1.662
MWNT-CeO_2	$Ce^{3+} + 3e^- \leftrightarrow Ce$ (s)	-2.336
MWNT-CoO_3	$Co^{2+} + 2e^- \leftrightarrow Co$ (s)	-0.28
MWNT-Cu_2O	$Cu^{2+} + 2e^- \leftrightarrow Cu$ (s)	+0.345
MWNT-Er_2O_3	$Er^{3+} + 3e^- \leftrightarrow Er$ (s)	-2.331
MWNT-Eu_2O_3	$Eu^{3+} + 3e^- \leftrightarrow Eu$ (s)	-1.991
MWNT-Fe_xO_y	$Fe^{2+} + 2e^- \leftrightarrow Fe$ (s)	-0.44
MWNT-HfO_2	$Hf^{4+} + 4e^- \leftrightarrow Hf$ (s)	-1.55
MWNT-MgO	$Mg^{2+} + 2e^- \leftrightarrow Mg$ (s)	-2.372
MWNT-MnO	$Mn^{2+} + 2e^- \leftrightarrow Mn$ (s)	-1.185
MWNT-MoO_2	$Mo^{3+} + 3e^- \leftrightarrow Mo$ (s)	-0.200
MWNT-NiO	$Ni^{2+} + 2e^- \leftrightarrow Ni$ (s)	-0.25
MWNT-Pr_6O_{11}	$Pr^{3+} + 3e^- \leftrightarrow Pr$ (s)	-2.353
MWNT-SnO_2	$Sn^{2+} + 2e^- \leftrightarrow Sn$ (s)	-0.1375
MWNT-TiO_2	$Ti^{2+} + 2e^- \leftrightarrow Ti$ (s)	-1.63
MWNT-V_xO_y	$V^{2+} + 2e^- \leftrightarrow Pr$ (s)	-1.13
MWNT-WO_3	$W^{3+} + 3e^- \leftrightarrow W$ (s)	+0.1
MWNT-ZnO	$Zn^{2+} + 2e^- \leftrightarrow Zn$ (s)	-0.7628
MWNT-ZrO_2	$Zr^{4+} + 4e^- \leftrightarrow Zr$ (s)	-1.45
MWNT-Ag	$Ag^+ + e^- \leftrightarrow Ag$ (s)	+0.7996
MWNT-Au	$Au^{3+} + 3e^- \leftrightarrow Au$ (s)	+1.498
MWNT-Pd	$Pd^{2+} + 2e^- \leftrightarrow Pd$ (s)	+0.951
MWNT-Pt	$Pt^{2+} + 3e^- \leftrightarrow Pt$ (s)	+1.18

Literature Cited

1. Vanysek, P., Electrochemical series. *CRC handbook of chemistry and physics* **1998,** *87*.

APPENDIX C

Supplementary Information for Chapter 3

Aggregation Behavior of Multiwalled Carbon Nanotube-Titanium Dioxide Nanohybrid: Effects of Synthesis Process and Loading of Titanium Dioxide

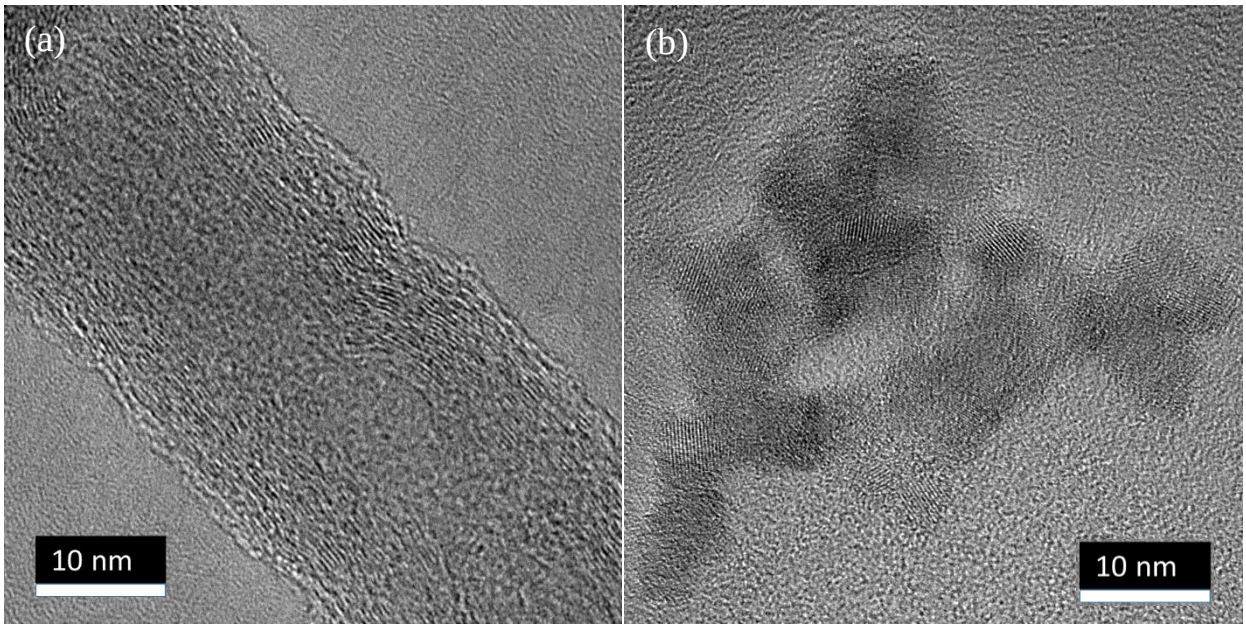

Figure C1: Representative HRTEM micrographs of (a) MWNT and (b) TiO_2 nanocrystals.

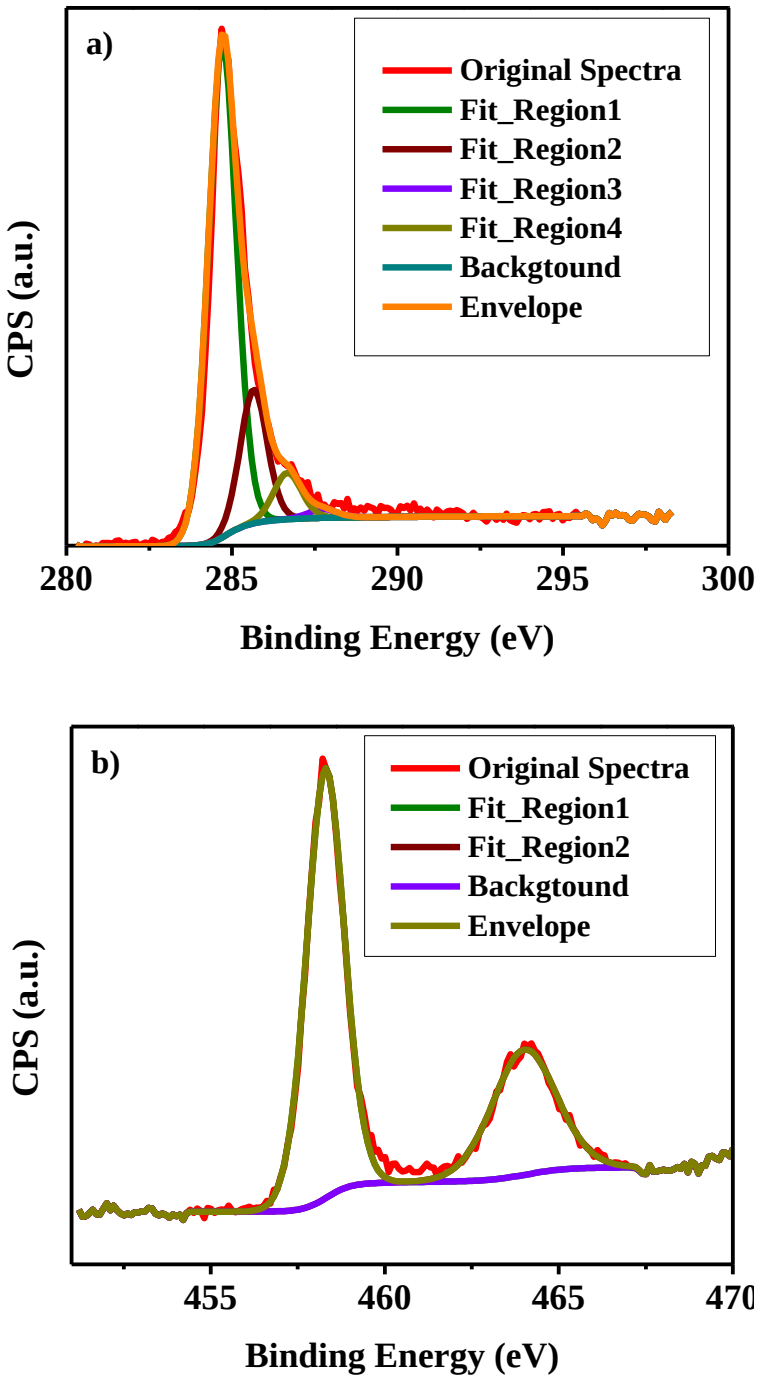

Figure C2: Characteristic XPS spectra for (a) C 1s in oxidized MWNT and (b) Ti 2p in MWNT-TiO_2 NH.

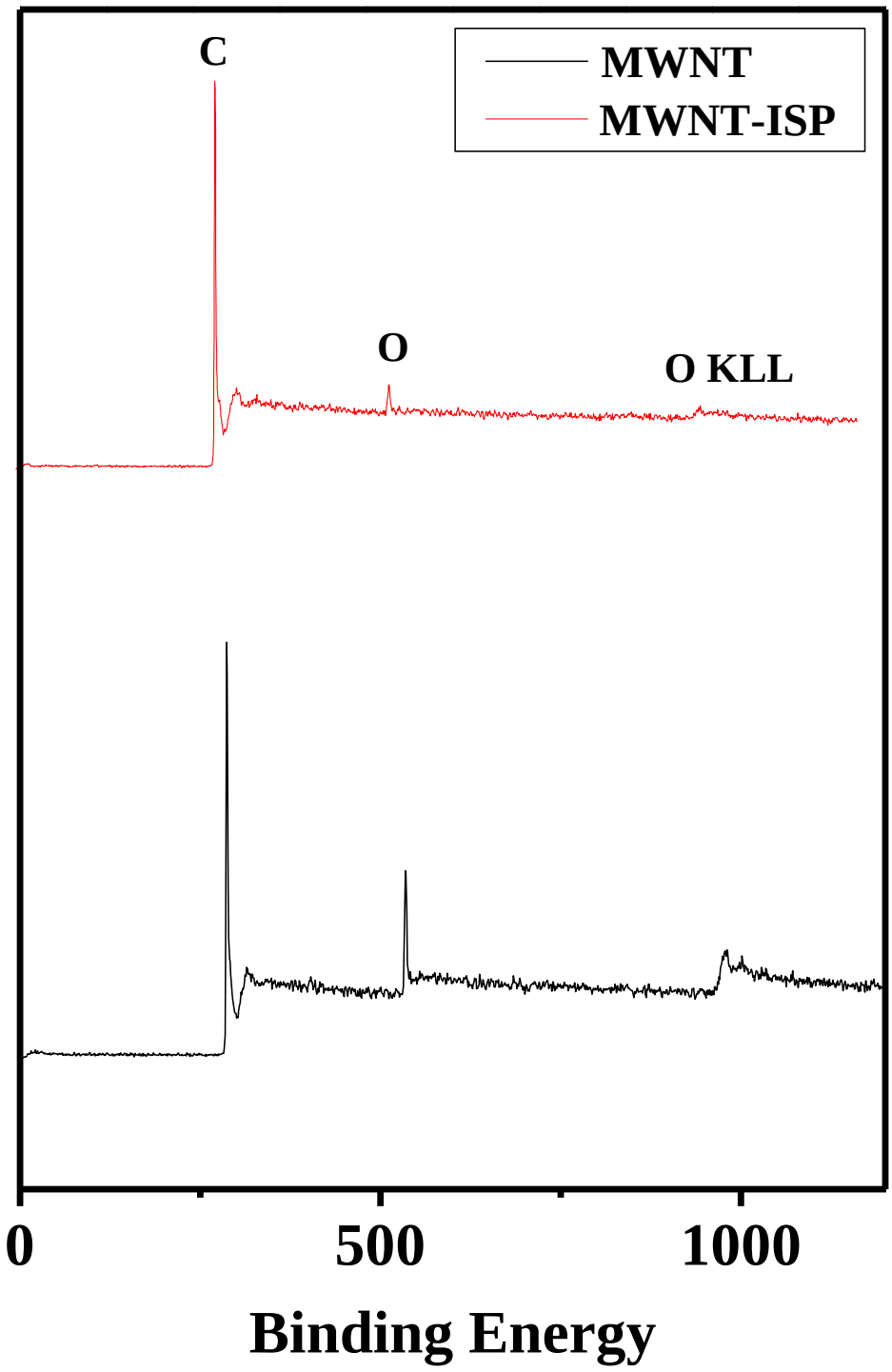

Figure C3: Characteristic XPS survey spectra for MWNT and MWNT-ISP

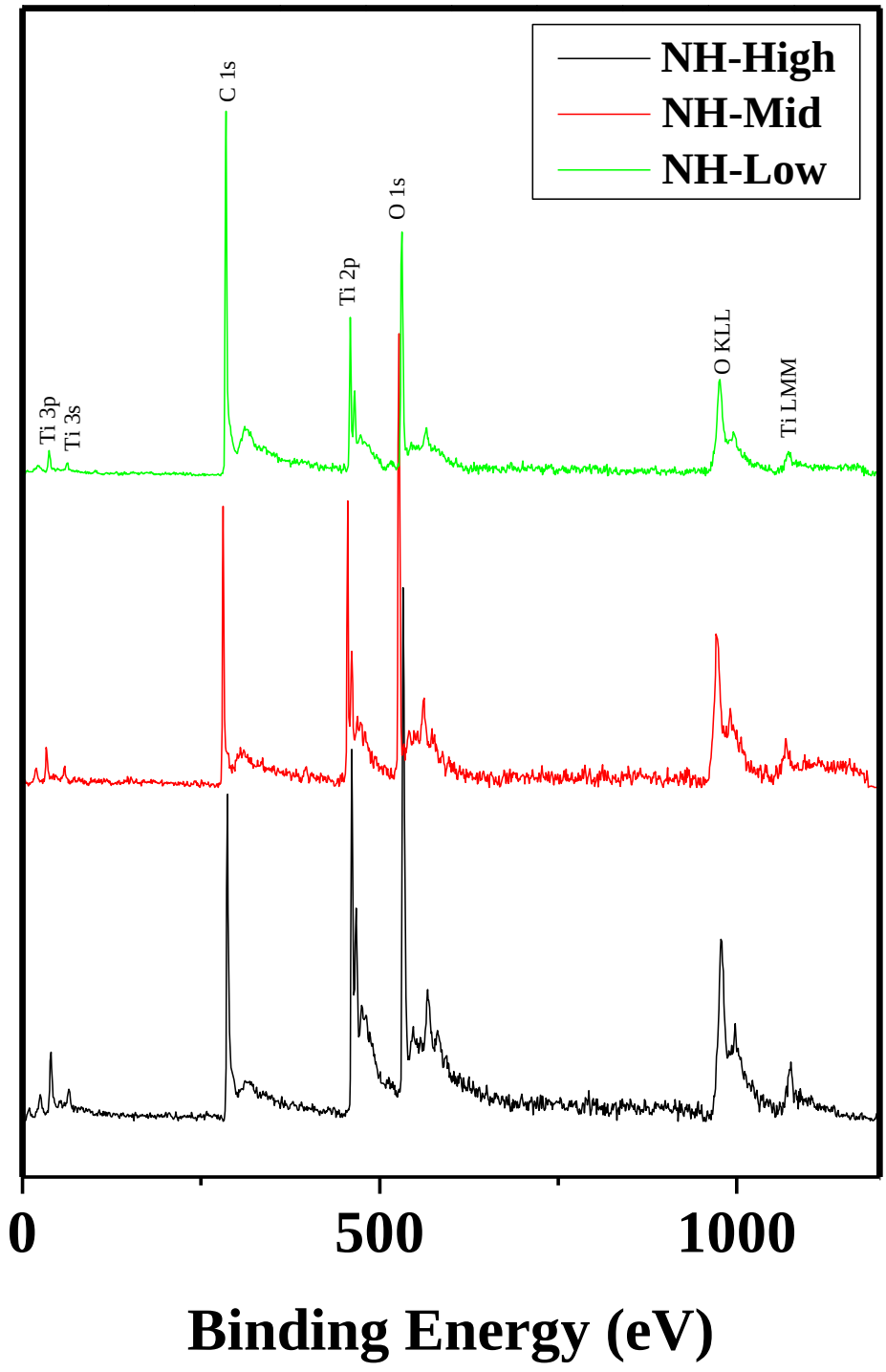

Figure C4: Characteristic XPS survey spectra for NH-High, NH-Mid, and NH-Low

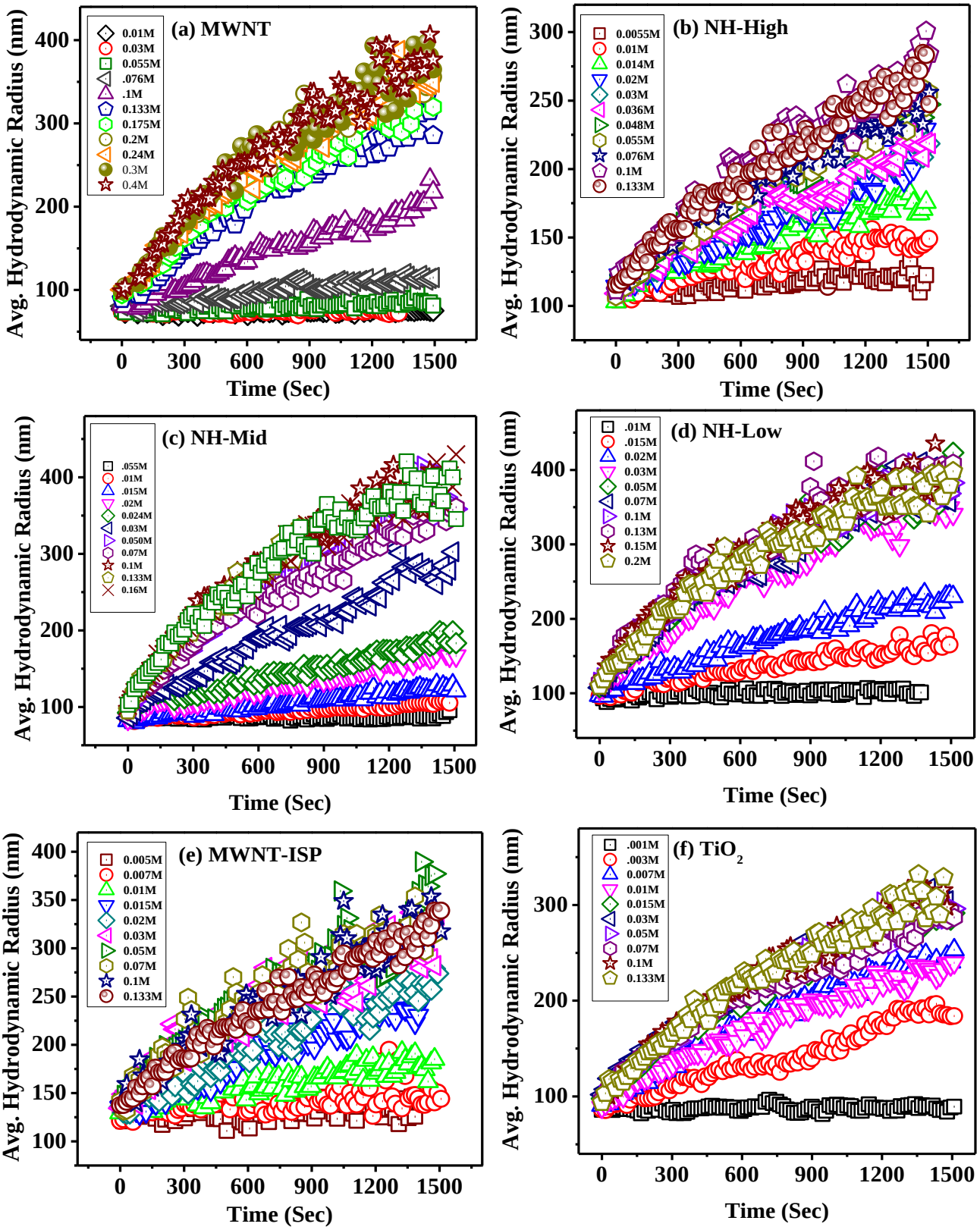

Figure C5: Aggregation history profile of (a) MWNTs, (b) NH-High, (c) NH-Mid, (d) NH-Low, (e) MWNT-ISP, and (f) TiO_2 at different electrolyte concentrations. All experiments were performed at 6.9±0.2 pH and at 25 °C.

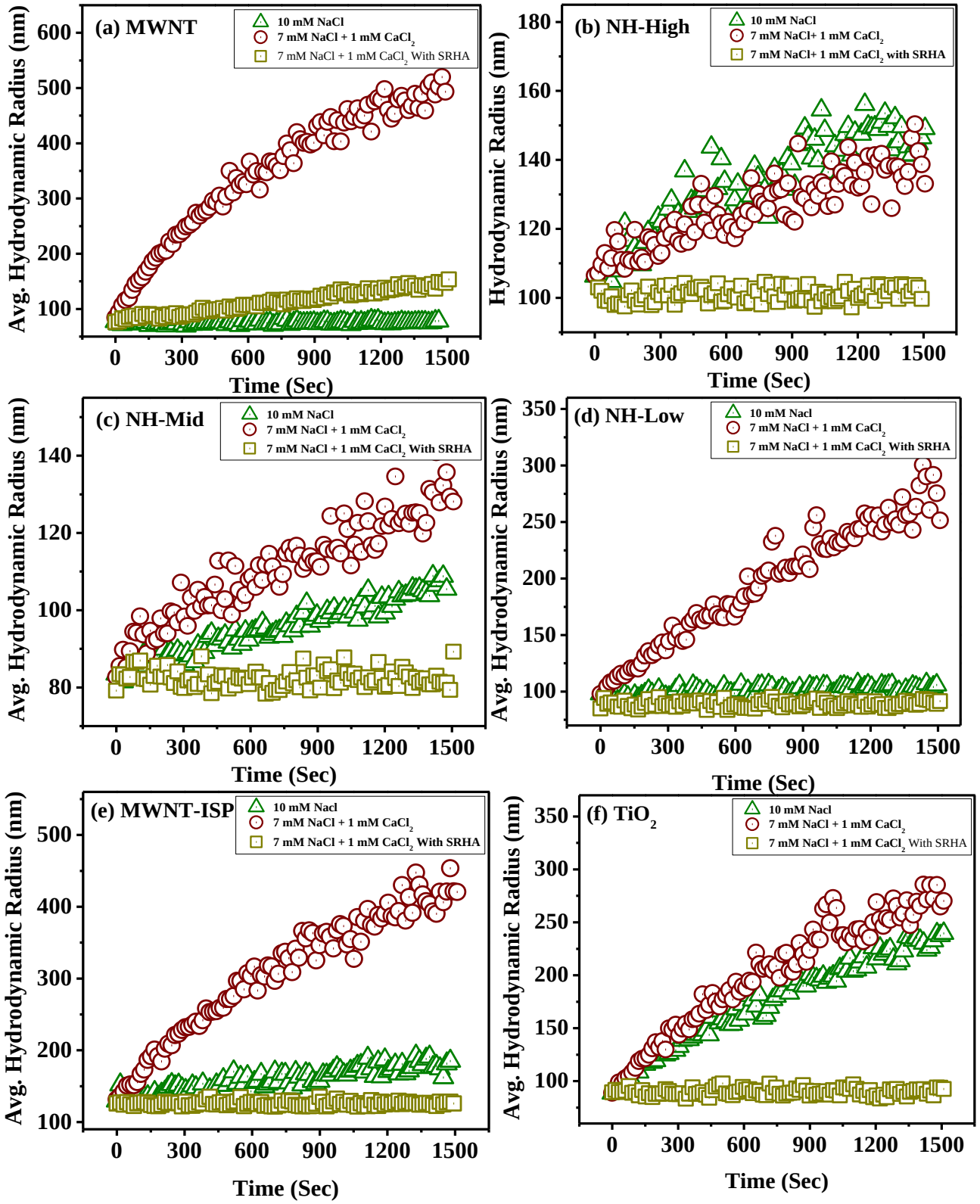

Figure C6: Aggregation history profile of (a) MWNTs, (b) NH-High, (c) NH-Mid, (d) NH-Low, (e) MWNT-ISP, and (f) TiO_2 at 10 mM NaCl concentration, 7 mM NaCl + 1 mM $CaCl_2$, and 7 mM NaCl + 1 mM $CaCl_2$ with SRHA. All experiments were performed at 6.9±0.2 pH and at 25 °C.

References

Chapter 1:

1. Smalley, R. E., Discovering the fullerenes. *Reviews of Modern Physics* **1997,** *69*, (3), 723.
2. Keller, A. A.; Vosti, W.; Wang, H.; Lazareva, A., Release of engineered nanomaterials from personal care products throughout their life cycle. *Journal of nanoparticle research* **2014,** *16*, (7), 2489.
3. Jariwala, D.; Sangwan, V. K.; Lauhon, L. J.; Marks, T. J.; Hersam, M. C., Carbon nanomaterials for electronics, optoelectronics, photovoltaics, and sensing. *Chemical Society Reviews* **2013,** *42*, (7), 2824-2860.
4. Chambers, B. A.; Afrooz, A. R. M. N.; Bae, S.; Aich, N.; Katz, L.; Saleh, N. B.; Kirisits, M. J., Effects of Chloride and Ionic Strength on Physical Morphology, Dissolution, and Bacterial Toxicity of Silver Nanoparticles. *Environmental science & technology* **2014,** *48*, (1), 761-769.
5. Serp, P.; Philippot, K., *Nanomaterials in catalysis*. Wiley: 2012.
6. Zohhadi, N. Functionalized graphitic nanoreinforcement for cement cmposites. University of South Carolina, Columbia, SC, 2014.
7. Khattak, M. J.; Khattab, A.; Rizvi, H. R.; Zhang, P., The impact of carbon nano-fiber modification on asphalt binder rheology. *Construction and Building Materials* **2012,** *30*, 257-264.
8. Arora, A.; Padua, G., Review: nanocomposites in food packaging. *Journal of Food science* **2010,** *75*, (1), R43-R49.
9. Dastjerdi, R.; Montazer, M., A review on the application of inorganic nano-structured materials in the modification of textiles: focus on anti-microbial properties. *Colloids and Surfaces B: Biointerfaces* **2010,** *79*, (1), 5-18.
10. Zhang, L.; Gu, F.; Chan, J.; Wang, A.; Langer, R.; Farokhzad, O., Nanoparticles in medicine: therapeutic applications and developments. *Clinical Pharmacology & Therapeutics* **2007,** *83*, (5), 761-769.
11. Mauter, M. S.; Elimelech, M., Environmental applications of carbon-based nanomaterials. *Environ. Sci. Technol.* **2008,** *42*, (16), 5843-5859.
12. Aich, N.; Plazas-Tuttle, J.; Lead, J.; Saleh, N., A Critical Review of Nanohybrids: Synthesis, Applications, and Environmental Implications. *Environmental Chemistry* **2014,** *11*, 609-623.
13. Usui, T. *World budget of platinum*; Stanford University: 2010.
14. Wilburn, D. R.; Bleiwas, D. I. *Platinum-group metals-world supply and demand* U.S. Geological Survey: 2004.
15. Nguyen, M. T.; Nguyen, C. K.; Vu, T. M. P.; Van Duong, Q.; Pham, T. L.; Nguyen, T. C., A study on carbon nanotube titanium dioxide hybrids: experiment and calculation. *Advances in Natural Sciences: Nanoscience and Nanotechnology* **2014,** *5*, (4), 045018.

16. Eder, D.; Windle, A. H., Carbon–inorganic hybrid materials: the carbon-nanotube/TiO2 interface. *Advanced Materials* **2008,** *20*, (9), 1787-1793.
17. Yang, C.-F.; Hsu, W.-C.; Wu, S.-M.; Su, C.-C., Elucidating how surface functionalization of multiwalled carbon nanotube affects nanostructured MWCNT/titania hybrid materials. *Journal of Nanomaterials* **2015,** *2015*.
18. Haldorai, Y.; Rengaraj, A.; Lee, J.-B.; Huh, Y. S.; Han, Y.-K., Highly efficient hydrogen production via water splitting using Pt@ MWNT/TiO 2 ternary hybrid composite as a catalyst under UV–visible light. *Synth. Met.* **2015,** *199*, 345-352.
19. Jitianu, A.; Cacciaguerra, T.; Berger, M.-H.; Benoit, R.; Béguin, F.; Bonnamy, S., New carbon multiwall nanotubes–TiO 2 nanocomposites obtained by the sol–gel method. *Journal of non-crystalline solids* **2004,** *345*, 596-600.
20. Ding, M.; Sorescu, D. C.; Star, A., Photoinduced Charge Transfer and Acetone Sensitivity of Single-Walled Carbon Nanotube–Titanium Dioxide Hybrids. *Journal of the American Chemical Society* **2013,** *135*, (24), 9015-9022.
21. Zarezade, M.; Ghasemi, S.; Gholami, M. R., The effect of multiwalled carbon nanotubes and activated carbon on the morphology and photocatalytic activity of TiO 2/C hybrid materials. *Catalysis Science & Technology* **2011,** *1*, (2), 279-284.
22. Khanderi, J.; Hoffmann, R. C.; Gurlo, A.; Schneider, J. J., Synthesis and sensoric response of ZnO decorated carbon nanotubes. *Journal of Materials Chemistry* **2009,** *19*, (28), 5039-5046.
23. Song, W.-L.; Cao, M.-S.; Wen, B.; Hou, Z.-L.; Cheng, J.; Yuan, J., Synthesis of zinc oxide particles coated multiwalled carbon nanotubes: Dielectric properties, electromagnetic interference shielding and microwave absorption. *Materials Research Bulletin* **2012,** *47*, (7), 1747-1754.
24. Byrappa, K.; Dayananda, A.; Sajan, C.; Basavalingu, B.; Shayan, M.; Soga, K.; Yoshimura, M., Hydrothermal preparation of ZnO: CNT and TiO2: CNT composites and their photocatalytic applications. *Journal of Materials Science* **2008,** *43*, (7), 2348-2355.
25. Dai, K.; Zhang, X.; Fan, K.; Peng, T.; Wei, B., Hydrothermal synthesis of single-walled carbon nanotube–TiO 2 hybrid and its photocatalytic activity. *Applied Surface Science* **2013,** *270*, 238-244.
26. Liu, C.; Chen, H.; Dai, K.; Xue, A.; Chen, H.; Huang, Q., Synthesis, characterization, and its photocatalytic activity of double-walled carbon nanotubes-TiO 2 hybrid. *Materials Research Bulletin* **2013,** *48*, (4), 1499-1505.
27. Saleh, T. A.; Gondal, M.; Drmosh, Q., Preparation of a MWCNT/ZnO nanocomposite and its photocatalytic activity for the removal of cyanide from water using a laser. *Nanotechnology* **2010,** *21*, (49), 495705.
28. Tian, L. H.; Ye, L. Q.; Deng, K. J.; Zan, L., TiO2/carbon nanotube hybrid nanostructures: Solvothermal synthesis and their visible light photocatalytic activity. *Journal of Solid State Chemistry* **2011,** *184*, (6), 1465-1471.
29. Gomathi, A.; Vivekchand, S.; Govindaraj, A.; Rao, C., Chemically bonded ceramic oxide coatings on carbon nanotubes and inorganic nanowires. *Advanced Materials* **2005,** *17*, (22), 2757-2761.

30. Ikuno, T.; Yasuda, T.; Honda, S.-i.; Oura, K.; Katayama, M.; Lee, J.-G.; Mori, H., Coating carbon nanotubes with inorganic materials by pulsed laser deposition. *Journal of applied physics* **2005,** *98*, (11), 114305.
31. Xie, X.; Gao, L., Characterization of a manganese dioxide/carbon nanotube composite fabricated using an in situ coating method. *Carbon* **2007,** *45*, (12), 2365-2373.
32. Green, J. M.; Dong, L.; Gutu, T.; Jiao, J.; Conley Jr, J. F.; Ono, Y., ZnO-nanoparticle-coated carbon nanotubes demonstrating enhanced electron field-emission properties. *Journal of applied physics* **2006,** *99*, (9), 094308.
33. Guo, G.; Guo, J.; Tao, D.; Choy, W.; Zhao, L.; Qian, W.; Wang, Z., A Simple method to prepare multi-walled carbon nanotube/ZnO nanoparticle composites. *Applied Physics A* **2007,** *89*, (2), 525-528.
34. Kim, B. C.; Kim, S.; Chung, J.; Chen, J.; Park, S.; Wallace, G. G., Charge storage in carbon nanotube–TiO 2 hybrid nanoparticles. *Synth. Met.* **2012,** *162*, (7), 650-654.
35. Yan, X. M.; Pan, D. Y.; Li, Z.; Zhao, B.; Zhang, J. C.; Wu, M. H., Facile synthesis of solution-disposable carbon nanotube-TiO2 hybrids in organic media. *Materials Letters* **2010,** *64*, (15), 1694-1697.
36. Ueda, T.; Takahashi, K.; Mitsugi, F.; Ikegami, T., Preparation of single-walled carbon nanotube/TiO 2 hybrid atmospheric gas sensor operated at ambient temperature. *Diamond and Related Materials* **2009,** *18*, (2), 493-496.
37. Du, Y.; Hao, C.; Wang, G., Preparation of floral-patterned ZnO/MWCNT heterogeneity structure using microwave irradiation heating method. *Materials Letters* **2008,** *62*, (1), 30-32.
38. Mo, C. B.; Cha, S. I.; Kim, K. T.; Lee, K. H.; Hong, S. H., Fabrication of carbon nanotube reinforced alumina matrix nanocomposite by sol–gel process. *Materials Science and Engineering: A* **2005,** *395*, (1), 124-128.
39. Li, Y.; Ding, J.; Chen, J.; Xu, C.; Wei, B.; Liang, J.; Wu, D., Preparation of ceria nanoparticles supported on carbon nanotubes. *Materials Research Bulletin* **2002,** *37*, (2), 313-318.
40. Wu, R.-J.; Wu, J.-G.; Yu, M.-R.; Tsai, T.-K.; Yeh, C.-T., Promotive effect of CNT on Co 3 O 4–SnO 2 in a semiconductor-type CO sensor working at room temperature. *Sensors and Actuators B: Chemical* **2008,** *131*, (1), 306-312.
41. Fan, Z.; Chen, J.; Cui, K.; Sun, F.; Xu, Y.; Kuang, Y., Preparation and capacitive properties of cobalt–nickel oxides/carbon nanotube composites. *Electrochimica Acta* **2007,** *52*, (9), 2959-2965.
42. Kahram, M.; Asnavandi, M.; Dolati, A., Synthesis and electrochemical characterization of sol–gel-derived RuO2/carbon nanotube composites. *Journal of Solid State Electrochemistry* **2014,** *18*, (4), 993-1003.
43. Attari, S. G.; Bahrami, A.; Shahna, F. G.; Heidari, M., Single-walled carbon nanotube/silica composite as a novel coating for solid-phase microextraction fiber based on sol-gel technology. *Journal of analytical chemistry* **2015,** *70*, (10), 1192-1198.
44. Gong, J.; Sun, J.; Chen, Q., Micromachined sol–gel carbon nanotube/SnO 2 nanocomposite hydrogen sensor. *Sensors and Actuators B: Chemical* **2008,** *130*, (2), 829-835.

45. Abbas, N.; Shao, G. N.; Haider, M. S.; Imran, S. M.; Park, S. S.; Jeon, S.-J.; Kim, H. T., Inexpensive sol-gel synthesis of multiwalled carbon nanotube-TiO 2 hybrids for high performance antibacterial materials. *Materials Science and Engineering: C* **2016,** *68*, 780-788.
46. Köse, H.; Karaal, Ş.; Aydın, A. O.; Akbulut, H., A facile synthesis of zinc oxide/multiwalled carbon nanotube nanocomposite lithium ion battery anodes by sol–gel method. *Journal of Power Sources* **2015,** *295*, 235-245.
47. Bi, S.; Su, X.; Hou, G.; Gu, G.; Xiao, Z., Microstructural characterization of alumina-coated multi-walled carbon nanotubes synthesized by hydrothermal crystallization. *Physica B: Condensed Matter* **2010,** *405*, (16), 3312-3315.
48. Kalubarme, R. S.; Kim, Y.-H.; Park, C.-J., One step hydrothermal synthesis of a carbon nanotube/cerium oxide nanocomposite and its electrochemical properties. *Nanotechnology* **2013,** *24*, (36), 365401.
49. Yu, Y.; Ma, L.-L.; Huang, W.-Y.; Du, F.-P.; Jimmy, C. Y.; Yu, J.-G.; Wang, J.-B.; Wong, P.-K., Sonication assisted deposition of Cu 2 O nanoparticles on multiwall carbon nanotubes with polyol process. *Carbon* **2005,** *43*, (3), 670-673.
50. Chen, C.-S.; Chen, X.-H.; Yi, B.; Zhang, G.-B.; Li, F.-J.; Luo, H.-S., Modified multi-walled carbon nanotubes with nano-europium oxide. *Transactions of Nonferrous Metals Society of China* **2007,** *17*, (s1B), s704-s707.
51. Matsui, K.; Kyotani, T.; Tomita, A., Hydrothermal synthesis of nano-sized iron oxide crystals in the cavity of carbon nanotubes. *Molecular Crystals and Liquid Crystals* **2002,** *387*, (1), 1-5.
52. Sun, Z.; Liu, Z.; Han, B.; Miao, S.; Du, J.; Miao, Z., Microstructural and electrochemical characterization of RuO 2/CNT composites synthesized in supercritical diethyl amine. *Carbon* **2006,** *44*, (5), 888-893.
53. Liu, H.; Huang, J.; Li, X.; Liu, J.; Zhang, Y., One-step hydrothermal synthesis of flower-like SnO2/carbon nanotubes composite and its electrochemical properties. *Journal of Sol-Gel Science and Technology* **2012,** *63*, (3), 569-572.
54. Wang, A.; Wang, Y.; Yu, W.; Huang, Z.; Fang, Y.; Long, L.; Song, Y.; Cifuentes, M. P.; Humphrey, M. G.; Zhang, L., TiO 2–multi-walled carbon nanotube nanocomposites: hydrothermal synthesis and temporally-dependent optical properties. *Rsc Advances* **2016,** *6*, (24), 20120-20127.
55. Li, H.; Zhang, X.; Zhu, Y.; Li, R.; Chen, H.; Gao, P.; Zhang, Y.; Li, T.; Liu, Y.; Li, Q., Hydrothermal deposition of a zinc oxide nanorod array on a carbon nanotube film as a piezoelectric generator. *Rsc Advances* **2014,** *4*, (82), 43772-43777.
56. Garmendia, N.; Bilbao, L.; Muñoz, R.; Imbuluzqueta, G.; García, A.; Bustero, I.; Calvo-Barrio, L.; Arbiol, J.; Obieta, I., Zirconia coating of carbon nanotubes by a hydrothermal method. *Journal of Nanoscience and Nanotechnology* **2008,** *8*, (11), 5678-5683.
57. Zhao, L.; Chen, X.; Wang, X.; Zhang, Y.; Wei, W.; Sun, Y.; Antonietti, M.; Titirici, M. M., One-Step Solvothermal Synthesis of a Carbon@ TiO2 Dyade Structure Effectively Promoting Visible-Light Photocatalysis. *Advanced Materials* **2010,** *22*, (30), 3317-3321.

58. Zhang, D.; Pan, C.; Zhang, J.; Shi, L., Solvothermal synthesis of necklace-like carbon nanotube/ceria composites. *Materials Letters* **2008,** *62*, (23), 3821-3823.
59. Keshri, A. K.; Huang, J.; Singh, V.; Choi, W.; Seal, S.; Agarwal, A., Synthesis of aluminum oxide coating with carbon nanotube reinforcement produced by chemical vapor deposition for improved fracture and wear resistance. *Carbon* **2010,** *48*, (2), 431-442.
60. Fan, Z.; Chen, J.; Wang, M.; Cui, K.; Zhou, H.; Kuang, Y., Preparation and characterization of manganese oxide/CNT composites as supercapacitive materials. *Diamond and Related Materials* **2006,** *15*, (9), 1478-1483.
61. Yu, K.-l.; Zou, J.-j.; Ben, Y.-h.; Zhang, Y.-p.; Liu, C.-j., Synthesis of NiO-embedded carbon nanotubes using corona discharge enhanced chemical vapor deposition. *Diamond and Related Materials* **2006,** *15*, (9), 1217-1222.
62. Min, Y. S.; Bae, E. J.; Jeong, K. S.; Cho, Y. J.; Lee, J. H.; Choi, W. B.; Park, G. S., Ruthenium oxide nanotube arrays fabricated by atomic layer deposition using a carbon nanotube template. *Advanced Materials* **2003,** *15*, (12), 1019-1022.
63. Turano, S.; Flicker, J.; Ready, W., Nanoscale coaxial cables produced from vertically aligned carbon nanotube arrays grown via chemical vapor deposition and coated with indium tin oxide via ion assisted deposition. *Carbon* **2008,** *46*, (5), 723-728.
64. Zhang, R.; Zhang, Y.; Zhang, Q.; Xie, H.; Wang, H.; Nie, J.; Wen, Q.; Wei, F., Optical visualization of individual ultralong carbon nanotubes by chemical vapour deposition of titanium dioxide nanoparticles. *Nature communications* **2013,** *4*, 1727.
65. Javey, A.; Kim, H.; Brink, M.; Wang, Q.; Ural, A.; Guo, J.; McIntyre, P.; McEuen, P.; Lundstrom, M.; Dai, H., High-κ dielectrics for advanced carbon-nanotube transistors and logic gates. *Nature materials* **2002,** *1*, (4), 241-246.
66. Ikuno, T.; Katayama, M.; Kamada, K.; Honda, S.-i.; Lee, J.-G.; Mori, H.; Oura, K., Insulator-coated carbon nanotubes synthesized by pulsed laser deposition. *Japanese journal of applied physics* **2003,** *42*, (11B), L1356.
67. Pan, L.; Konishi, Y.; Tanaka, H.; Chakrabarti, S.; Hokushin, S.; Akita, S.; Nakayama, Y., Effect of MgO coating on field emission of a stand-alone carbon nanotube. *Journal of Vacuum Science & Technology B* **2007,** *25*, (5), 1581-1583.
68. Fang, W.-C.; Chyan, O.; Sun, C.-L.; Wu, C.-T.; Chen, C.-P.; Chen, K.-H.; Chen, L.-C.; Huang, J.-H., Arrayed CN x NT–RuO 2 nanocomposites directly grown on Ti-buffered Si substrate for supercapacitor applications. *Electrochemistry Communications* **2007,** *9*, (2), 239-244.
69. Fan, W.; Gao, L., Silica nanobeads-decorated multi-walled carbon nanotubes by vapor-phase method. *Chemistry Letters* **2005,** *34*, (7), 954-955.
70. Borkar, T.; Chang, W. S.; Hwang, J. Y.; Shepherd, N. D.; Banerjee, R., Microstructural and optical properties of nanocrystalline ZnO deposited onto vertically aligned carbon nanotubes by physical vapor deposition. *Materials Research Bulletin* **2012,** *47*, (10), 2756-2759.
71. Nguyen, V. H.; Ren, Y.; Lee, Y. R.; Tuma, D.; Min, B.-K.; Shim, J.-J., Microwave-Assisted Synthesis of Carbon Nanotube-TiO2 Nanocomposites in Ionic Liquid for the Photocatalytic Degradation of Methylene Blue. *Synthesis and Reactivity in Inorganic, Metal-Organic, and Nano-Metal Chemistry* **2012,** *42*, (2), 296-301.

72. Motshekga, S. C.; Pillai, S. K.; Sinha Ray, S.; Jalama, K.; Krause, R. W. M., Recent Trends in the Microwave-Assisted Synthesis of Metal Oxide Nanoparticles Supported on Carbon Nanotubes and Their Applications. *Journal of Nanomaterials* **2012,** *2012*, 15.
73. Hernadi, K.; Couteau, E.; Seo, J. W.; Forró, L., Al (OH) 3/multiwalled carbon nanotube composite: homogeneous coverage of Al (OH) 3 on carbon nanotube surfaces. *Langmuir* **2003,** *19*, (17), 7026-7029.
74. Georgakilas, V.; Tzitzios, V.; Gournis, D.; Petridis, D., Attachment of magnetic nanoparticles on carbon nanotubes and their soluble derivatives. *Chemistry of Materials* **2005,** *17*, (7), 1613-1617.
75. Eder, D.; Windle, A. H., Morphology control of CNT-TiO2 hybrid materials and rutile nanotubes. *J. Mater. Chem.* **2008,** *18*, (17), 2036-2043.
76. Sun, Z.; Zhang, X.; Na, N.; Liu, Z.; Han, B.; An, G., Synthesis of ZrO2− Carbon Nanotube Composites and Their Application as Chemiluminescent Sensor Material for Ethanol. *The Journal of Physical Chemistry B* **2006,** *110*, (27), 13410-13414.
77. Bottini, M.; Tautz, L.; Huynh, H.; Monosov, E.; Bottini, N.; Dawson, M. I.; Bellucci, S.; Mustelin, T., Covalent decoration of multi-walled carbon nanotubes with silica nanoparticles. *Chemical Communications* **2005**, (6), 758-760.
78. Sainsbury, T.; Fitzmaurice, D., Templated assembly of semiconductor and insulator nanoparticles at the surface of covalently modified multiwalled carbon nanotubes. *Chemistry of Materials* **2004,** *16*, (19), 3780-3790.
79. Mahajan, S.; Hasan, S.; Cho, J.; Shaffer, M.; Boccaccini, A.; Dickerson, J., Carbon nanotube–nanocrystal heterostructures fabricated by electrophoretic deposition. *Nanotechnology* **2008,** *19*, (19), 195301.
80. Chou, S.-L.; Wang, J.-Z.; Chew, S.-Y.; Liu, H.-K.; Dou, S.-X., Electrodeposition of MnO 2 nanowires on carbon nanotube paper as free-standing, flexible electrode for supercapacitors. *Electrochemistry Communications* **2008,** *10*, (11), 1724-1727.
81. Nørskov, J. K.; Bligaard, T.; Logadottir, A.; Kitchin, J.; Chen, J. G.; Pandelov, S.; Stimming, U., Trends in the exchange current for hydrogen evolution. *Journal of the Electrochemical Society* **2005,** *152*, (3), J23-J26.
82. Jiang, L. C.; Zhang, W. D., Electrodeposition of TiO2 nanoparticles on multiwalled carbon nanotube arrays for hydrogen peroxide sensing. *Electroanalysis* **2009,** *21*, (8), 988-993.
83. Moriguchi, I.; Hidaka, R.; Yamada, H.; Kudo, T.; Murakami, H.; Nakashima, N., A Mesoporous Nanocomposite of TiO2 and Carbon Nanotubes as a High-Rate Li-Intercalation Electrode Material. *Advanced Materials* **2006,** *18*, (1), 69-73.
84. Sun, J.; Gao, L.; Iwasa, M., Noncovalent attachment of oxide nanoparticles onto carbon nanotubes using water-in-oil microemulsions. *Chemical Communications* **2004**, (7), 832-833.
85. Lowry, G. V.; Gregory, K. B.; Apte, S. C.; Lead, J. R., Transformations of nanomaterials in the environment. In ACS Publications: 2012.
86. Nowack, B.; Ranville, J. F.; Diamond, S.; Gallego-Urrea, J. A.; Metcalfe, C.; Rose, J.; Horne, N.; Koelmans, A. A.; Klaine, S. J., Potential scenarios for nanomaterial release

and subsequent alteration in the environment. *Environmental Toxicology and Chemistry* **2012,** *31*, (1), 50-59.
87. Afrooz, A. N.; Khan, I. A.; Hussain, S. M.; Saleh, N. B., Mechanistic heteroaggregation of gold nanoparticles in a wide range of solution chemistry. *Environmental science & technology* **2013,** *47*, (4), 1853-1860.
88. Afrooz, A. R. M. N.; Sivalapalan, S. T.; Murphy, C. J.; Hussain, S. M.; Schlager, J. J.; Saleh, N. B., Spheres vs. rods: the shape of gold nanoparticles influences aggregation and deposition behavior. *Chemosphere* **2013,** *91*, (1), 93-98.
89. Aich, N.; Boateng, L. K.; Sabaraya, I. V.; Das, D.; Flora, J. R.; Saleh, N. B., Aggregation kinetics of higher order fullerene clusters in aquatic systems. *Environmental science & technology* **2016,** *50*, (7), 3562-3571.
90. Khan, I. A.; Afrooz, A. R. M. N.; Flora, J. R. V.; Schierz, P. A.; Ferguson, P. L.; Sabo-Attwood, T.; Saleh, N. B., Chirality affects aggregation kinetics of single-walled carbon nanotubes. *Environmental science & technology* **2013,** *47*, (4), 1844-1852.
91. Saleh, N. B.; Pfefferle, L. D.; Elimelech, M., Aggregation kinetics of multiwalled carbon nanotubes in aquatic systems: measurements and environmental implications. *Environmental Science & Technology* **2008,** *42*, (21), 7963-7969.
92. Saleh, N. B.; Pfefferle, L. D.; Elimelech, M., Influence of biomacromolecules and humic acid on the aggregation kinetics of single-walled carbon nanotubes. *Environmental Science & Technology* **2010,** *44*, (7), 2412-2418.
93. Hua, Z.; Zhang, J.; Bai, X.; Ye, Z.; Tang, Z.; Liang, L.; Liu, Y., Aggregation of TiO 2–graphene nanocomposites in aqueous environment: Influence of environmental factors and UV irradiation. *Science of the Total Environment* **2016,** *539*, 196-205.
94. Saleh, N. B.; Aich, N.; Lead, J.; Plazas-Tuttle, J.; Lowry, G. V., Research strategy to determine when novel nanohybrids pose unique environmental risks. *Environmental Science: Nano* **2015,** *2*, 11-18 (Cover Article).
95. Plazas-Tuttle, J. Nano-Enabled Water Disinfection Technology Development that Harnesses the Power of Microwaves. The University of Texas at Austin, Austin, Texas, 2017.

Chapter 2:

1. Aich, N.; Plazas-Tuttle, J.; Lead, J.; Saleh, N., A Critical Review of Nanohybrids: Synthesis, Applications, and Environmental Implications. *Environmental Chemistry* **2014,** *11*, 609-623.
2. Saleh, N. B.; Aich, N.; Lead, J.; Plazas-Tuttle, J.; Lowry, G. V., Research strategy to determine when novel nanohybrids pose unique environmental risks. *Environmental Science: Nano* **2015,** *2*, 11-18 (Cover Article).
3. Eder, D.; Windle, A. H., Carbon–inorganic hybrid materials: the carbon-nanotube/TiO2 interface. *Advanced Materials* **2008,** *20*, (9), 1787-1793.
4. Alley, N. J.; Liao, K. S.; Andreoli, E.; Dias, S.; Dillon, E. P.; Orbaek, A. W.; Barron, A. R.; Byrne, H. J.; Curran, S. A., Effect of carbon nanotube-fullerene hybrid additive on P3HT:PCBM bulk-heterojunction organic photovoltaics. *Synth. Met.* **2012,** *162*, (1-2), 95-101.
5. Llobet, E.; Espinosa, E.; Sotter, E.; Ionescu, R.; Vilanova, X.; Torres, J.; Felten, A.; Pireaux, J.-J.; Ke, X.; Van Tendeloo, G., Carbon nanotube–TiO2 hybrid films for detecting traces of O2. *Nanotechnology* **2008,** *19*, (37), 375501.
6. Liu, Z.; Wang, J.; Xie, D.; Chen, G., Polyaniline-Coated Fe3O4 Nanoparticle–Carbon-Nanotube Composite and its Application in Electrochemical Biosensing. *Small* **2008,** *4*, (4), 462-466.
7. Zhu, Y.; Elim, H. I.; Foo, Y. L.; Yu, T.; Liu, Y.; Ji, W.; Lee, J. Y.; Shen, Z.; Wee, A. T.-S.; Thong, J. T.-L., Multiwalled carbon nanotubes beaded with ZnO nanoparticles for ultrafast nonlinear optical switching. *Advanced Materials* **2006,** *18*, (5), 587-592.
8. Rigdon, W. A.; Huang, X., Carbon monoxide tolerant platinum electrocatalysts on niobium doped titania and carbon nanotube composite supports. *Journal of Power Sources* **2014,** *272*, (0), 845-859.
9. Pehnt, M., Life-cycle analysis of fuel cell system components. *Handbook of Fuel Cells* **2003**.
10. Saleh, N. B.; Afrooz, A.; Bisesi Jr, J. H.; Aich, N.; Plazas-Tuttle, J.; Sabo-Attwood, T., Emergent properties and toxicological considerations for nanohybrid materials in aquatic systems. *Nanomaterials* **2014,** *4*, (2), 372-407.
11. Saleh, N. B.; Aich, N.; Plazas-Tuttle, J.; Lead, J. R.; Lowry, G. V., Research strategy to determine when novel nanohybrids pose unique environmental risks. *Environmental Science: Nano* **2015,** *2*, (1), 11-18.
12. Aich, N.; Plazas-Tuttle, J.; Lead, J. R.; Saleh, N. B., A critical review of nanohybrids: synthesis, applications and environmental implications. *Environmental Chemistry* **2014,** *11*, (6), 609-623.
13. Fernández-García, M.; Rodriguez, J. A., Metal oxide nanoparticles. *Encyclopedia of Inorganic and Bioinorganic Chemistry* **2011**.
14. Eder, D., Carbon Nanotube−Inorganic Hybrids. *Chemical Reviews* **2010,** *110*, (3), 1348-1385.
15. Lee, S. H.; Lee, D. H.; Lee, W. J.; Kim, S. O., Tailored assembly of carbon nanotubes and graphene. *Advanced Functional Materials* **2011,** *21*, (8), 1338-1354.

16. Bergin, I. L.; Witzmann, F. A., Nanoparticle toxicity by the gastrointestinal route: evidence and knowledge gaps. *J Biomedical Nanosci and Nanotechnol* **2013,** *3*, 163-210.
17. Cheng, J.; Cheng, S. H., Influence of carbon nanotube length on toxicity to zebrafish embryos. *Int J Nanomedicine* **2012,** *7*, 3731-3739.
18. Diniz, M. S.; de Matos, A. P.; Lourenço, J.; Castro, L.; Peres, I.; Mendonça, E.; Picado, A., Liver alterations in two freshwater fish species (Carassius auratus and Danio rerio) following exposure to different TiO_2 nanoparticle concentrations. *Microsc Microanal* **2013,** *19*, 1131-1140.
19. Chen, H.; Wang, B.; Gao, D.; Guan, M.; Zheng, L.; Ouyang, H.; Chai, Z.; Zhao, Y.; Feng, W., Broad-Spectrum Antibacterial Activity of Carbon Nanotubes to Human Gut Bacteria. *Small* **2013,** *9*, (16), 2735-2746.
20. Kang, S.; Herzberg, M.; Rodrigues, D. F.; Elimelech, M., Antibacterial Effects of Carbon Nanotubes: Size Does Matter! *Langmuir* **2008,** *24*, (13), 6409-6413.
21. Adams, L. K.; Lyon, D. Y.; Alvarez, P. J., Comparative eco-toxicity of nanoscale TiO 2, SiO 2, and ZnO water suspensions. *Water research* **2006,** *40*, (19), 3527-3532.
22. Xia, T.; Kovochich, M.; Liong, M.; Mädler, L.; Gilbert, B.; Shi, H.; Yeh, J. I.; Zink, J. I.; Nel, A. E., Comparison of the Mechanism of Toxicity of Zinc Oxide and Cerium Oxide Nanoparticles Based on Dissolution and Oxidative Stress Properties. *ACS nano* **2008,** *2*, (10), 2121-2134.
23. Saleh, N. B.; Milliron, D. J.; Aich, N.; Katz, L. E.; Liljestrand, H. M.; Kirisits, M. J., Importance of Doping, Dopant Distribution, and Nano-Scale Defects on Electronic Band Structure
Alteration of Metal Oxide Nanoparticles: Implications for Reactive Oxygen Species Generation. *Science of the Total Environment (In Press)* **2016**.
24. Xiong, D.; Fang, T.; Yu, L.; Sima, X.; Zhu, W., Effects of nano-scale TiO2, ZnO and their bulk counterparts on zebrafish: Acute toxicity, oxidative stress and oxidative damage. *Science of the Total Environment* **2011,** *409*, (8), 1444-1452.
25. Balázs, N.; Mogyorósi, K.; Srankó, D. F.; Pallagi, A.; Alapi, T.; Oszkó, A.; Dombi, A.; Sipos, P., The effect of particle shape on the activity of nanocrystalline TiO2 photocatalysts in phenol decomposition. *Applied Catalysis B: Environmental* **2008,** *84*, (3–4), 356-362.
26. Mogyorosi, K.; Balazs, N.; Sranko, D. F.; Tombacz, E.; Dekany, I.; Oszko, A.; Sipos, P.; Dombi, A., The effect of particle shape on the activity of nanocrystalline TiO2 photocatalysts in phenol decomposition. Part 3: The importance of surface quality. *Applied Catalysis B-Environmental* **2010,** *96*, (3-4), 577-585.
27. Sayes, C. M.; Wahi, R.; Kurian, P. A.; Liu, Y.; West, J. L.; Ausman, K. D.; Warheit, D. B.; Colvin, V. L., Correlating Nanoscale Titania Structure with Toxicity: A Cytotoxicity and Inflammatory Response Study with Human Dermal Fibroblasts and Human Lung Epithelial Cells. *Toxicological Sciences* **2006,** *92*, (1), 174-185.
28. Jung, K.-h.; Hong, J. S.; Vittal, R.; Kim, K.-J., Enhanced Photocurrent of Dye-Sensitized Solar Cells by Modification of TiO2 with Carbon Nanotubes. *Chemistry Letters* **2002**, (8), 864-865.

29. Dai, K.; Dawson, G.; Yang, S.; Chen, Z.; Lu, L., Large scale preparing carbon nanotube/zinc oxide hybrid and its application for highly reusable photocatalyst. *Chemical Engineering Journal* **2012,** *191*, 571-578.
30. Hua, Z.; Zhang, J.; Bai, X.; Ye, Z.; Tang, Z.; Liang, L.; Liu, Y., Aggregation of TiO 2–graphene nanocomposites in aqueous environment: Influence of environmental factors and UV irradiation. *Science of the Total Environment* **2016,** *539*, 196-205.
31. Nguyen, M. T.; Nguyen, C. K.; Vu, T. M. P.; Van Duong, Q.; Pham, T. L.; Nguyen, T. C., A study on carbon nanotube titanium dioxide hybrids: experiment and calculation. *Advances in Natural Sciences: Nanoscience and Nanotechnology* **2014,** *5*, (4), 045018.
32. Yang, C.-F.; Hsu, W.-C.; Wu, S.-M.; Su, C.-C., Elucidating how surface functionalization of multiwalled carbon nanotube affects nanostructured MWCNT/titania hybrid materials. *Journal of Nanomaterials* **2015,** *2015*.
33. Haldorai, Y.; Rengaraj, A.; Lee, J.-B.; Huh, Y. S.; Han, Y.-K., Highly efficient hydrogen production via water splitting using Pt@ MWNT/TiO 2 ternary hybrid composite as a catalyst under UV–visible light. *Synth. Met.* **2015,** *199*, 345-352.
34. Jitianu, A.; Cacciaguerra, T.; Berger, M.-H.; Benoit, R.; Béguin, F.; Bonnamy, S., New carbon multiwall nanotubes–TiO 2 nanocomposites obtained by the sol–gel method. *Journal of non-crystalline solids* **2004,** *345*, 596-600.
35. Ding, M.; Sorescu, D. C.; Star, A., Photoinduced Charge Transfer and Acetone Sensitivity of Single-Walled Carbon Nanotube–Titanium Dioxide Hybrids. *Journal of the American Chemical Society* **2013,** *135*, (24), 9015-9022.
36. Zarezade, M.; Ghasemi, S.; Gholami, M. R., The effect of multiwalled carbon nanotubes and activated carbon on the morphology and photocatalytic activity of TiO 2/C hybrid materials. *Catalysis Science & Technology* **2011,** *1*, (2), 279-284.
37. Khanderi, J.; Hoffmann, R. C.; Gurlo, A.; Schneider, J. J., Synthesis and sensoric response of ZnO decorated carbon nanotubes. *Journal of Materials Chemistry* **2009,** *19*, (28), 5039-5046.
38. Song, W.-L.; Cao, M.-S.; Wen, B.; Hou, Z.-L.; Cheng, J.; Yuan, J., Synthesis of zinc oxide particles coated multiwalled carbon nanotubes: Dielectric properties, electromagnetic interference shielding and microwave absorption. *Materials Research Bulletin* **2012,** *47*, (7), 1747-1754.
39. Byrappa, K.; Dayananda, A.; Sajan, C.; Basavalingu, B.; Shayan, M.; Soga, K.; Yoshimura, M., Hydrothermal preparation of ZnO: CNT and TiO2: CNT composites and their photocatalytic applications. *Journal of Materials Science* **2008,** *43*, (7), 2348-2355.
40. Dai, K.; Zhang, X.; Fan, K.; Peng, T.; Wei, B., Hydrothermal synthesis of single-walled carbon nanotube–TiO 2 hybrid and its photocatalytic activity. *Applied Surface Science* **2013,** *270*, 238-244.
41. Liu, C.; Chen, H.; Dai, K.; Xue, A.; Chen, H.; Huang, Q., Synthesis, characterization, and its photocatalytic activity of double-walled carbon nanotubes-TiO 2 hybrid. *Materials Research Bulletin* **2013,** *48*, (4), 1499-1505.
42. Saleh, T. A.; Gondal, M.; Drmosh, Q., Preparation of a MWCNT/ZnO nanocomposite and its photocatalytic activity for the removal of cyanide from water using a laser. *Nanotechnology* **2010,** *21*, (49), 495705.

43. Tian, L. H.; Ye, L. Q.; Deng, K. J.; Zan, L., TiO2/carbon nanotube hybrid nanostructures: Solvothermal synthesis and their visible light photocatalytic activity. *Journal of Solid State Chemistry* **2011,** *184*, (6), 1465-1471.
44. Guo, G.; Guo, J.; Tao, D.; Choy, W.; Zhao, L.; Qian, W.; Wang, Z., A Simple method to prepare multi-walled carbon nanotube/ZnO nanoparticle composites. *Applied Physics A* **2007,** *89*, (2), 525-528.
45. Kim, B. C.; Kim, S.; Chung, J.; Chen, J.; Park, S.; Wallace, G. G., Charge storage in carbon nanotube–TiO 2 hybrid nanoparticles. *Synth. Met.* **2012,** *162*, (7), 650-654.
46. Yan, X. M.; Pan, D. Y.; Li, Z.; Zhao, B.; Zhang, J. C.; Wu, M. H., Facile synthesis of solution-disposable carbon nanotube-TiO2 hybrids in organic media. *Materials Letters* **2010,** *64*, (15), 1694-1697.
47. Ueda, T.; Takahashi, K.; Mitsugi, F.; Ikegami, T., Preparation of single-walled carbon nanotube/TiO 2 hybrid atmospheric gas sensor operated at ambient temperature. *Diamond and Related Materials* **2009,** *18*, (2), 493-496.
48. Du, Y.; Hao, C.; Wang, G., Preparation of floral-patterned ZnO/MWCNT heterogeneity structure using microwave irradiation heating method. *Materials Letters* **2008,** *62*, (1), 30-32.
49. Green, J. M.; Dong, L.; Gutu, T.; Jiao, J.; Conley Jr, J. F.; Ono, Y., ZnO-nanoparticle-coated carbon nanotubes demonstrating enhanced electron field-emission properties. *Journal of applied physics* **2006,** *99*, (9), 094308.
50. Jassby, D.; Farner Budarz, J.; Wiesner, M., Impact of aggregate size and structure on the photocatalytic properties of TiO2 and ZnO nanoparticles. *Environmental science & technology* **2012,** *46*, (13), 6934-6941.
51. Wilkinson, L. L. Visible and infrared emission from Er_2O_3 nanoparticles, and Ho^{+3}, Tm^{+3}, and Sm^{+3} doped in AlN for optical and biomedical applications. Ball State University, Muncie, Indiana, 2012.
52. Afrooz, A. N.; Das, D.; Murphy, C. J.; Vikesland, P.; Saleh, N. B., Co-transport of gold nanospheres with single-walled carbon nanotubes in saturated porous media. *Water Research* **2016,** *99*, 7-15.
53. Aich, N.; Boateng, L. K.; Sabaraya, I. V.; Das, D.; Flora, J. R.; Saleh, N. B., Aggregation kinetics of higher order fullerene clusters in aquatic systems. *Environmental science & technology* **2016,** *50*, (7), 3562-3571.
54. Afrooz, A. N.; Khan, I. A.; Hussain, S. M.; Saleh, N. B., Mechanistic heteroaggregation of gold nanoparticles in a wide range of solution chemistry. *Environmental science & technology* **2013,** *47*, (4), 1853-1860.
55. Khan, I. A.; Afrooz, A. R. M. N.; Flora, J. R. V.; Schierz, P. A.; Ferguson, P. L.; Sabo-Attwood, T.; Saleh, N. B., Chirality affects aggregation kinetics of single-walled carbon nanotubes. *Environmental science & technology* **2013,** *47*, (4), 1844-1852.
56. Khan, I. A.; Aich, N.; Afrooz, A. R. M. N.; Flora, J. R. V.; ferguson, L.; sabo-Attwood, T.; Saleh, N. B., Fractal structures of single-walled carbon nanotubes in biologically relevant conditions: role of chirality vs. media conditions. *Chemosphere* **2013** *93*, (9), 1997-2003.

57. Khan, I. A.; Flora, J. R. V.; Afrooz, A. R. M. N.; Aich, N.; Schierz, P. A.; Ferguson, P. L.; Sabo-Attwood, T.; Saleh, N. B., Change in chirality of semiconducting single-walled carbon nanotubes can overcome anionic surfactant stabilisation: a systematic study of aggregation kinetics. *Environmental Chemistry* **2015,** *12*, (6), 652-661.
58. Saleh, N. B.; Pfefferle, L. D.; Elimelech, M., Aggregation kinetics of multiwalled carbon nanotubes in aquatic systems: measurements and environmental implications. *Environmental Science & Technology* **2008,** *42*, (21), 7963-7969.
59. Mansfield, E.; Kar, A.; Hooker, S. A., Applications of TGA in quality control of SWCNTs. *Analytical and Bioanalytical Chemistry* **2010,** *396*, (3), 1071-1077.
60. Afrooz, A. R. M. N.; Khan, I. A.; Hussain, S. M.; Saleh, N. B., Mechanistic heteroaggregation of gold nanoparticles in a wide range of solution chemistry. *Environmental Science & Technology* **2013,** *47*, (4), 1853-1860.
61. Afrooz, A. R. M. N.; Sivalapalan, S. T.; Murphy, C. J.; Hussain, S. M.; Schlager, J. J.; Saleh, N. B., Spheres vs. rods: the shape of gold nanoparticles influences aggregation and deposition behavior. *Chemosphere* **2013,** *91*, (1), 93-98.
62. Rigdon, W. A.; Huang, X., Carbon monoxide tolerant platinum electrocatalysts on niobium doped titania and carbon nanotube composite supports. *Journal of Power Sources* **2014,** *272*, 845-859.
63. Miritello, M.; Savio, R. L.; Piro, A.; Franzo, G.; Priolo, F.; Iacona, F.; Bongiorno, C., Optical and structural properties of Er2O3 films grown by magnetron sputtering. *Journal of applied physics* **2006,** *100*, (1), 013502.
64. Hassan, M. S.; Akhtar, M. S.; Shim, K.-B.; Yang, O.-B., Morphological and electrochemical properties of crystalline praseodymium oxide nanorods. *Nanoscale research letters* **2010,** *5*, (4), 735.
65. Wepasnick, K. A.; Smith, B. A.; Bitter, J. L.; Fairbrother, D. H., Chemical and structural characterization of carbon nanotube surfaces. *Analytical and bioanalytical chemistry* **2010,** *396*, (3), 1003-1014.
66. Naumkin, A. V.; Kraut-Vass, A.; Gaarenstroom, S. W.; Powell, C. J., NIST X-ray Photoelectron Spectroscopy Database *NIST Standard Reference Database 20, Version 4.1* **2012**.
67. Naumkin, A. V.; Kraut-Vass, A.; Gaarenstroom, S. W.; Powell, C. J., NIST X-ray Photoelectron Spectroscopy Database In 2012.
68. Aksel, S.; Eder, D., Catalytic effect of metal oxides on the oxidation resistance in carbon nanotube–inorganic hybrids. *J. Mater. Chem.* **2010,** *20*, (41), 9149-9154.
69. Eder, D.; Windle, A. H., Morphology control of CNT-TiO 2 hybrid materials and rutile nanotubes. *Journal of Materials Chemistry* **2008,** *18*, (17), 2036-2043.
70. Aich, N.; Boateng, L. K.; Flora, J. R.; Saleh, N. B., Preparation of non-aggregating aqueous fullerenes in highly saline solutions with a biocompatible non-ionic polymer. *Nanotechnology* **2013,** *24*, (39), 395602.
71. Khan, I. A.; Flora, J. R.; Afrooz, A. N.; Aich, N.; Schierz, P. A.; Ferguson, P. L.; Sabo-Attwood, T.; Saleh, N. B., Change in chirality of semiconducting single-walled carbon nanotubes can overcome anionic surfactant stabilisation: a systematic study of aggregation kinetics. *Environmental Chemistry* **2015,** *12*, (6), 652-661.

72. Yi, P.; Chen, K. L., Influence of surface oxidation on the aggregation and deposition kinetics of multiwalled carbon nanotubes in monovalent and divalent electrolytes. *Langmuir* **2011,** *27*, (7), 3588-3599.
73. Smith, B.; Wepasnick, K.; Schrote, K. E.; Cho, H.-H.; Ball, W. P.; Fairbrother, D. H., Influence of surface oxides on the colloidal stability of multi-walled carbon nanotubes: a structure-property relationship. *Langmuir* **2009,** *25*, (17), 9767-9776.
74. Smith, B.; Wepasnick, K.; Schrote, K. E.; Bertele, A. R.; Ball, W. P.; O'Melia, C.; Fairbrother, D. H., Colloidal Properties of Aqueous Suspensions of Acid-Treated, Multi-Walled Carbon Nanotubes. *Environmental Science & Technology* **2009,** *43*, (3), 819-825.
75. Saleh, N. B.; Pfefferle, L. D.; Elimelech, M., Influence of biomacromolecules and humic acid on the aggregation kinetics of single-walled carbon nanotubes. *Environmental Science & Technology* **2010,** *44*, (7), 2412-2418.
76. Sano, M.; Okamura, J.; Shinkai, S., Colloidal nature of single-walled carbon nanotubes in electrolyte solution: the Schulze-Hardy rule. *Langmuir* **2001,** *17*, (22), 7172-7173.
77. Chowdhury, I.; Duch, M. C.; Mansukhani, N. D.; Hersam, M. C.; Bouchard, D., Colloidal properties and stability of graphene oxide nanomaterials in the aquatic environment. *Environmental Science & Technology* **2013,** *47*, (12), 6288-6296.
78. Lanphere, J. D.; Luth, C. J.; Walker, S. L., Effects of solution chemistry on the transport of graphene oxide in saturated porous media. *Environmental Science & Technology* **2013,** *47*, (9), 4255-4261.

Chapter 3:

1. Rao, C. N. R.; Müller, A.; Cheetham, A. K., *The chemistry of nanomaterials: synthesis, properties and applications*. John Wiley & Sons: 2006.
2. Vorkapic, D.; Matsoukas, T., Effect of temperature and alcohols in the preparation of titania nanoparticles from alkoxides. *Journal of the American Ceramic Society* 1998, *81*, (11), 2815-2820.
3. Raveendran, P.; Fu, J.; Wallen, S. L., Completely "green" synthesis and stabilization of metal nanoparticles. *Journal of the American Chemical Society* 2003, *125*, (46), 13940-13941.
4. He, F.; Zhao, D., Manipulating the size and dispersibility of zerovalent iron nanoparticles by use of carboxymethyl cellulose stabilizers. *Environmental science & technology* 2007, *41*, (17), 6216-6221.
5. Bom, D.; Andrews, R.; Jacques, D.; Anthony, J.; Chen, B.; Meier, M. S.; Selegue, J. P., Thermogravimetric analysis of the oxidation of multiwalled carbon nanotubes: evidence for the role of defect sites in carbon nanotube chemistry. *Nano Letters* 2002, *2*, (6), 615-619.
6. Das, D.; Plazas-Tuttle, J.; Sabaraya, I. V.; Jain, S. S.; Sabo-Attwood, T.; Saleh, N. B., An elegant method for large scale synthesis of metal oxide-carbon nanotube nanohybrids for nano-environmental application and implication studies. *Environmental Science: Nano* 2017, *4*, (1), 60-68.
7. Mulfinger, L.; Solomon, S. D.; Bahadory, M.; Jeyarajasingam, A. V.; Rutkowsky, S. A.; Boritz, C., Synthesis and study of silver nanoparticles. *J. Chem. Educ* 2007, *84*, (2), 322.
8. Mo, C. B.; Cha, S. I.; Kim, K. T.; Lee, K. H.; Hong, S. H., Fabrication of carbon nanotube reinforced alumina matrix nanocomposite by sol–gel process. *Materials Science and Engineering: A* 2005, *395*, (1), 124-128.
9. Sun, J.; Gao, L.; Li, W., Colloidal processing of carbon nanotube/alumina composites. *Chemistry of Materials* 2002, *14*, (12), 5169-5172.
10. Kumari, L.; Zhang, T.; Du, G.; Li, W.; Wang, Q.; Datye, A.; Wu, K., Synthesis, microstructure and electrical conductivity of carbon nanotube–alumina nanocomposites. *Ceramics International* 2009, *35*, (5), 1775-1781.
11. Zhang, D.; Shi, L.; Fu, H.; Fang, J., Ultrasonic-assisted preparation of carbon nanotube/cerium oxide composites. *Carbon* 2006, *44*, (13), 2853-2855.
12. Kalubarme, R. S.; Kim, Y.-H.; Park, C.-J., One step hydrothermal synthesis of a carbon nanotube/cerium oxide nanocomposite and its electrochemical properties. *Nanotechnology* 2013, *24*, (36), 365401.
13. Lang, J.; Yan, X.; Xue, Q., Facile preparation and electrochemical characterization of cobalt oxide/multi-walled carbon nanotube composites for supercapacitors. *Journal of Power Sources* 2011, *196*, (18), 7841-7846.
14. Wang, G.; Shen, X.; Yao, J.; Wexler, D.; Ahn, J.-h., Hydrothermal synthesis of carbon nanotube/cobalt oxide core-shell one-dimensional nanocomposite and application

as an anode material for lithium-ion batteries. *Electrochemistry Communications* 2009, *11*, (3), 546-549.
15. Yang, H.; Zhang, D.; Shi, L.; Fang, J., Synthesis and strong red photoluminescence of europium oxide nanotubes and nanowires using carbon nanotubes as templates. *Acta materialia* 2008, *56*, (5), 955-967.
16. Chuansheng, C.; Tiangui, L.; Xiaohua, C.; Bin, Y.; Zhenwu, N.; Zhenwu, N.; Can, Z.; Chenchong, H., Preparation of Multi-Walled Carbon Nanotubes/Europium Oxide Composite. *RARE METAL MATERIALS AND ENGINEERING* 2009, *38*, 477-480.
17. Chen, C.; Hu, J.; Shao, D.; Li, J.; Wang, X., Adsorption behavior of multiwall carbon nanotube/iron oxide magnetic composites for Ni (II) and Sr (II). *Journal of hazardous materials* 2009, *164*, (2), 923-928.
18. Hu, J.; Shao, D.; Chen, C.; Sheng, G.; Li, J.; Wang, X.; Nagatsu, M., Plasma-induced grafting of cyclodextrin onto multiwall carbon nanotube/iron oxides for adsorbent application. *The Journal of Physical Chemistry B* 2010, *114*, (20), 6779-6785.
19. Chen, C.; Wang, X.; Nagatsu, M., Europium adsorption on multiwall carbon nanotube/iron oxide magnetic composite in the presence of polyacrylic acid. *Environmental science & technology* 2009, *43*, (7), 2362-2367.
20. Wang, Q.; Li, J.; Chen, C.; Ren, X.; Hu, J.; Wang, X., Removal of cobalt from aqueous solution by magnetic multiwalled carbon nanotube/iron oxide composites. *Chemical Engineering Journal* 2011, *174*, (1), 126-133.
21. Ikuno, T.; Yasuda, T.; Honda, S.-i.; Oura, K.; Katayama, M.; Lee, J.-G.; Mori, H., Coating carbon nanotubes with inorganic materials by pulsed laser deposition. *Journal of applied physics* 2005, *98*, (11), 114305.
22. Ikuno, T.; Katayama, M.; Kamada, K.; Honda, S.-i.; Lee, J.-G.; Mori, H.; Oura, K., Insulator-coated carbon nanotubes synthesized by pulsed laser deposition. *Japanese journal of applied physics* 2003, *42*, (11B), L1356.
23. Pan, L.; Konishi, Y.; Tanaka, H.; Chakrabarti, S.; Hokushin, S.; Akita, S.; Nakayama, Y., Effect of MgO coating on field emission of a stand-alone carbon nanotube. *Journal of Vacuum Science & Technology B* 2007, *25*, (5), 1581-1583.
24. Wang, M. Y.; Li, J. H.; Cui, K. Z., Preparation of Pt-MoOx/CNT Electrode and Its Electrocatalytic Property for Ethanol Electrooxidation. *Chinese Journal of Chemistry* 2006, *24*, (7), 881-886.
25. Roro, K. T.; Tile, N.; Mwakikunga, B.; Yalisi, B.; Forbes, A., Solar absorption and thermal emission properties of multiwall carbon nanotube/nickel oxide nanocomposite thin films synthesized by sol–gel process. *Materials Science and Engineering: B* 2012, *177*, (8), 581-587.
26. Wen, B.; Cao, M.-S.; Hou, Z.-L.; Song, W.-L.; Zhang, L.; Lu, M.-M.; Jin, H.-B.; Fang, X.-Y.; Wang, W.-Z.; Yuan, J., Temperature dependent microwave attenuation behavior for carbon-nanotube/silica composites. *Carbon* 2013, *65*, 124-139.
27. Sivakumar, R.; Guo, S.; Nishimura, T.; Kagawa, Y., Thermal conductivity in multi-wall carbon nanotube/silica-based nanocomposites. *Scripta Materialia* 2007, *56*, (4), 265-268.

28. Bottini, M.; Tautz, L.; Huynh, H.; Monosov, E.; Bottini, N.; Dawson, M. I.; Bellucci, S.; Mustelin, T., Covalent decoration of multi-walled carbon nanotubes with silica nanoparticles. *Chemical Communications* 2005, (6), 758-760.
29. Wongchoosuk, C.; Wisitsoraat, A.; Tuantranont, A.; Kerdcharoen, T., Portable electronic nose based on carbon nanotube-SnO 2 gas sensors and its application for detection of methanol contamination in whiskeys. *Sensors and Actuators B: Chemical* 2010, *147*, (2), 392-399.
30. Eder, D.; Windle, A. H., Carbon–inorganic hybrid materials: the carbon-nanotube/TiO2 interface. *Advanced Materials* 2008, *20*, (9), 1787-1793.
31. Ding, M.; Sorescu, D. C.; Star, A., Photoinduced Charge Transfer and Acetone Sensitivity of Single-Walled Carbon Nanotube–Titanium Dioxide Hybrids. *Journal of the American Chemical Society* 2013, *135*, (24), 9015-9022.
32. Wu, G.-M.; Wang, A.-R.; Zhang, M.-X.; Yang, H.-Y.; Zhou, B.; Shen, J., Investigation on properties of V2O5–MWCNTs composites as cathode materials. *Journal of Sol-Gel Science and Technology* 2008, *46*, (1), 79-85.
33. Green, J. M.; Dong, L.; Gutu, T.; Jiao, J.; Conley Jr, J. F.; Ono, Y., ZnO-nanoparticle-coated carbon nanotubes demonstrating enhanced electron field-emission properties. *Journal of applied physics* 2006, *99*, (9), 094308.
34. Sun, Z.; Zhang, X.; Na, N.; Liu, Z.; Han, B.; An, G., Synthesis of ZrO2− Carbon Nanotube Composites and Their Application as Chemiluminescent Sensor Material for Ethanol. *The Journal of Physical Chemistry B* 2006, *110*, (27), 13410-13414.
35. Gao, C.; Li, W.; Jin, Y. Z.; Kong, H., Facile and large-scale synthesis and characterization of carbon nanotube/silver nanocrystal nanohybrids. *Nanotechnology* 2006, *17*, (12), 2882.
36. Rahman, G.; Guldi, D. M.; Zambon, E.; Pasquato, L.; Tagmatarchis, N.; Prato, M., Dispersable carbon nanotube/gold nanohybrids: evidence for strong electronic interactions. *Small* 2005, *1*, (5), 527-530.
37. Wu, B.; Kuang, Y.; Zhang, X.; Chen, J., Noble metal nanoparticles/carbon nanotubes nanohybrids: synthesis and applications. *Nano Today* 2011, *6*, (1), 75-90.
38. Jawale, D. V.; Gravel, E.; Boudet, C.; Shah, N.; Geertsen, V.; Li, H.; Namboothiri, I. N.; Doris, E., Room temperature Suzuki coupling of aryl iodides, bromides, and chlorides using a heterogeneous carbon nanotube-palladium nanohybrid catalyst. *Catalysis Science & Technology* 2015, *5*, (4), 2388-2392.
39. Kecsenovity, E.; Endrődi, B.; Pápa, Z.; Hernádi, K.; Rajeshwar, K.; Janáky, C., Decoration of ultra-long carbon nanotubes with Cu 2 O nanocrystals: a hybrid platform for enhanced photoelectrochemical CO 2 reduction. *Journal of Materials Chemistry A* 2016, *4*, (8), 3139-3147.
40. Chen, L.; Tsang, S. C., Ag doped WO 3-based powder sensor for the detection of NO gas in air. *Sensors and Actuators B: Chemical* 2003, *89*, (1), 68-75.
41. Sohrabi, M. R.; Mansouriieh, N.; Khosravi, M.; Zolghadr, M., Removal of diazo dye Direct Red 23 from aqueous solution using zero-valent iron nanoparticles immobilized on multi-walled carbon nanotubes. *Water Science and Technology* 2015, *71*, (9), 1367-1374.

42. Khan, I. A.; Aich, N.; Afrooz, A. R. M. N.; Flora, J. R. V.; ferguson, L.; sabo-Attwood, T.; Saleh, N. B., Fractal structures of single-walled carbon nanotubes in biologically relevant conditions: role of chirality vs. media conditions. *Chemosphere* 2013 *93*, (9), 1997-2003.
43. Wepasnick, K. A.; Smith, B. A.; Bitter, J. L.; Fairbrother, D. H., Chemical and structural characterization of carbon nanotube surfaces. *Analytical and bioanalytical chemistry* 2010, *396*, (3), 1003-1014.
44. Jia, B.; Gao, L.; Sun, J., Self-assembly of magnetite beads along multiwalled carbon nanotubes via a simple hydrothermal process. *Carbon* 2007, *45*, (7), 1476-1481.
45. Li, P.; Xu, Z. P.; Hampton, M. A.; Vu, D. T.; Huang, L.; Rudolph, V.; Nguyen, A. V., Control preparation of zinc hydroxide nitrate nanocrystals and examination of the chemical and structural stability. *The Journal of Physical Chemistry C* 2012, *116*, (18), 10325-10332.
46. Li, C.; Liu, H.; Yang, J., A facile hydrothermal approach to the synthesis of nanoscale rare earth hydroxides. *Nanoscale research letters* 2015, *10*, (1), 1-6.
47. Losurdo, M.; Giangregorio, M. M.; Capezzuto, P.; Bruno, G.; Toro, R. G.; Malandrino, G.; Fragalà, I. L.; Armelao, L.; Barreca, D.; Tondello, E., Multifunctional nanocrystalline thin films of Er2O3: Interplay between nucleation kinetics and film characteristics. *Advanced Functional Materials* 2007, *17*, (17), 3607-3612.
48. Hassan, M. S.; Akhtar, M. S.; Shim, K.-B.; Yang, O.-B., Morphological and electrochemical properties of crystalline praseodymium oxide nanorods. *Nanoscale research letters* 2010, *5*, (4), 735.
49. Sun, Y.; Xia, Y., Shape-controlled synthesis of gold and silver nanoparticles. *Science* 2002, *298*, (5601), 2176-2179.
50. Ghodselahi, T.; Vesaghi, M.; Shafiekhani, A.; Baghizadeh, A.; Lameii, M., XPS study of the Cu@ Cu 2 O core-shell nanoparticles. *Appl. Surf. Sci.* 2008, *255*, (5), 2730-2734.
51. Pastoriza-Santos, I.; Liz-Marzán, L. M., Formation and stabilization of silver nanoparticles through reduction by N, N-dimethylformamide. *Langmuir* 1999, *15*, (4), 948-951.
52. Lowry, R. W.; Dickman, D., The ABC's of ORP—Clearing up some of the mystery of Oxidation-Reduction Potential. *Service Industry News* 2010.

Chapter 4:

1. Chen, W.; Xu, N. F.; Xu, L. G.; Wang, L. B.; Li, Z. K.; Ma, W.; Zhu, Y. Y.; Xu, C. L.; Kotov, N. A., Multifunctional Magnetoplasmonic Nanoparticle Assemblies for Cancer Therapy and Diagnostics (Theranostics). *Macromolecular Rapid Communications* **2010,** *31*, (2), 228-236.
2. Fan, Z.; Shelton, M.; Singh, A. K.; Senapati, D.; Khan, S. A.; Ray, P. C., Multifunctional plasmonic shell–magnetic core nanoparticles for targeted diagnostics, isolation, and photothermal destruction of tumor cells. *Acs Nano* **2012,** *6*, (2), 1065-1073.
3. Chen, J. H.; Mao, S.; Wen, Z. H. One-Pot Fabrication of Crumpled Graphene-Based Nanohybrids for Supercapacitors. 2013.
4. Alley, N. J.; Liao, K. S.; Andreoli, E.; Dias, S.; Dillon, E. P.; Orbaek, A. W.; Barron, A. R.; Byrne, H. J.; Curran, S. A., Effect of carbon nanotube-fullerene hybrid additive on P3HT:PCBM bulk-heterojunction organic photovoltaics. *Synth. Met.* **2012,** *162*, (1-2), 95-101.
5. Zhu, P.; Nair, A. S.; Yang, S.; Peng, S.; Elumalai, N. K.; Ramakrishna, S., Rice grain-shaped TiO2-CNT composite-A functional material with a novel morphology for dye-sensitized solar cells. *Journal of Photochemistry and Photobiology a-Chemistry* **2012,** *231*, (1), 9-18.
6. Park, D.-H.; Jeon, Y.; Ok, J.; Park, J.; Yoon, S.-H.; Choy, J.-H.; Shul, Y.-G., Pt Nanoparticle-Reduced Graphene Oxide Nanohybrid for Proton Exchange Membrane Fuel Cells. *Journal of Nanoscience and Nanotechnology* **2012,** *12*, (7), 5669-5672.
7. Muszynski, R.; Seger, B.; Kamat, P. V., Decorating graphene sheets with gold nanoparticles. *J. Phys. Chem. C* **2008,** *112*, (14), 5263-5266.
8. Liu, J. M.; Wang, X. X.; Cui, M. L.; Lin, L. P.; Jiang, S. L.; Jiao, L.; Zhang, L. H., A promising non-aggregation colorimetric sensor of AuNRs-Ag+ for determination of dopamine. *Sensors and Actuators B-Chemical* **2013,** *176*, 97-102.
9. Saleh, N. B.; Aich, N.; Lead, J.; Plazas-Tuttle, J.; Lowry, G. V., Research strategy to determine when novel nanohybrids pose unique environmental risks. *Environmental Science: Nano* **2015,** *2*, 11-18 (Cover Article).
10. Saleh, N. B.; Afrooz, A.; Bisesi Jr, J. H.; Aich, N.; Plazas-Tuttle, J.; Sabo-Attwood, T., Emergent properties and toxicological considerations for nanohybrid materials in aquatic systems. *Nanomaterials* **2014,** *4*, (2), 372-407.
11. Kim, S.; Shin, D. H.; Kim, C. O.; Hwang, S. W.; Choi, S. H.; Ji, S.; Koo, J. Y., Enhanced ultraviolet emission from hybrid structures of single-walled carbon nanotubes/ZnO films. *Applied Physics Letters* **2009,** *94*, (21).
12. Li, F. S.; Cho, S. H.; Son, D. I.; Kim, T. W.; Lee, S. K.; Cho, Y. H.; Jin, S. H., UV photovoltaic cells based on conjugated ZnO quantum dot/multiwalled carbon nanotube heterostructures. *Applied Physics Letters* **2009,** *94*, (11).
13. Gund, G. S.; Dubal, D. P.; Shinde, S. S.; Lokhande, C. D., Architectured Morphologies of Chemically Prepared NiO/MWCNTs Nanohybrid Thin Films for High Performance Supercapacitors. *Acs Applied Materials & Interfaces* **2014,** *6*, (5), 3176-3188.

14. Wen, Z. H.; Ci, S. Q.; Mao, S.; Cui, S. M.; Lu, G. H.; Yu, K. H.; Luo, S. L.; He, Z.; Chen, J. H., TiO2 nanoparticles-decorated carbon nanotubes for significantly improved bioelectricity generation in microbial fuel cells. *Journal of Power Sources* **2013,** *234*, 100-106.
15. Sealy, C., The problem with platinum. *Materials Today* **2008,** *11*, (12), 65-68.
16. Tang, Z.; Chua, D. H. C., Investigation of Pt/CNT-Based Electrodes in Proton Exchange Membrane Fuel Cells Using AC Impedance Spectroscopy. *Journal of The Electrochemical Society* **2010,** *157*, (6), B868.
17. Akalework, N. G.; Pan, C.-J.; Su, W.-N.; Rick, J.; Tsai, M.-C.; Lee, J.-F.; Lin, J.-M.; Tsai, L.-D.; Hwang, B.-J., Ultrathin TiO2-coated MWCNTs with excellent conductivity and SMSI nature as Pt catalyst support for oxygen reduction reaction in PEMFCs. *Journal of Materials Chemistry* **2012,** *22*, (39), 20977.
18. Jiang, Z.-Z.; Gu, D.-M.; Wang, Z.-B.; Qu, W.-L.; Yin, G.-P.; Qian, K.-J., Effects of anatase TiO2 with different particle sizes and contents on the stability of supported Pt catalysts. *Journal of Power Sources* **2011,** *196*, (20), 8207-8215.
19. Xia, B. Y.; Ding, S.; Wu, H. B.; Wang, X.; Wen, X., Hierarchically structured Pt/CNT@TiO2 nanocatalysts with ultrahigh stability for low-temperature fuel cells. *Rsc Advances* **2012,** *2*, (3), 792.
20. Usui, T. *World budget of platinum*; Stanford University: 2010.
21. Wilburn, D. R.; Bleiwas, D. I. *Platinum-group metals-world supply and demand* U.S. Geological Survey: 2004.
22. Pehnt, M., Life-cycle analysis of fuel cell system components. *Handbook of Fuel Cells* **2003**.
23. Brunelli, A.; Zabeo, A.; Semenzin, E.; Hristozov, D.; Marcomini, A., Extrapolated long-term stability of titanium dioxide nanoparticles and multi-walled carbon nanotubes in artificial freshwater. *Journal of Nanoparticle Research* **2016,** *18*, (5), 1-13.
24. Saleh, N. B.; Pfefferle, L. D.; Elimelech, M., Aggregation kinetics of multiwalled carbon nanotubes in aquatic systems: measurements and environmental implications. *Environmental Science & Technology* **2008,** *42*, (21), 7963-7969.
25. Saleh, N. B.; Pfefferle, L. D.; Elimelech, M., Influence of biomacromolecules and humic acid on the aggregation kinetics of single-walled carbon nanotubes. *Environmental Science & Technology* **2010,** *44*, (7), 2412-2418.
26. Liu, X.; Chen, G.; Su, C., Effects of material properties on sedimentation and aggregation of titanium dioxide nanoparticles of anatase and rutile in the aqueous phase. *Journal of Colloid and Interface Science* **2011,** *363*, (1), 84-91.
27. Yi, P.; Chen, K. L., Influence of surface oxidation on the aggregation and deposition kinetics of multiwalled carbon nanotubes in monovalent and divalent electrolytes. *Langmuir* **2011,** *27*, (7), 3588-3599.
28. Smith, B.; Wepasnick, K.; Schrote, K. E.; Cho, H.-H.; Ball, W. P.; Fairbrother, D. H., Influence of surface oxides on the colloidal stability of multi-walled carbon nanotubes: a structure-property relationship. *Langmuir* **2009,** *25*, (17), 9767-9776.

29. Smith, B.; Wepasnick, K.; Schrote, K. E.; Bertele, A. R.; Ball, W. P.; O'Melia, C.; Fairbrother, D. H., Colloidal Properties of Aqueous Suspensions of Acid-Treated, Multi-Walled Carbon Nanotubes. *Environmental Science & Technology* **2009,** *43*, (3), 819-825.
30. Khan, I. A.; Afrooz, A. R. M. N.; Flora, J. R. V.; Schierz, P. A.; Ferguson, P. L.; Sabo-Attwood, T.; Saleh, N. B., Chirality affects aggregation kinetics of single-walled carbon nanotubes. *Environmental science & technology* **2013,** *47*, (4), 1844-1852.
31. Khan, I. A.; Flora, J. R. V.; Afrooz, A. R. M. N.; Aich, N.; Schierz, P. A.; Ferguson, P. L.; Sabo-Attwood, T.; Saleh, N. B., Change in chirality of semiconducting single-walled carbon nanotubes can overcome anionic surfactant stabilisation: a systematic study of aggregation kinetics. *Environmental Chemistry* **2015,** *12*, (6), 652-661.
32. Shih, Y. H.; Liu, W. S.; Su, Y. F., Aggregation of stabilized TiO2 nanoparticle suspensions in the presence of inorganic ions. *Environmental Toxicology and Chemistry* **2012,** *31*, (8), 1693-1698.
33. Hua, Z.; Zhang, J.; Bai, X.; Ye, Z.; Tang, Z.; Liang, L.; Liu, Y., Aggregation of TiO2–graphene nanocomposites in aqueous environment: Influence of environmental factors and UV irradiation. *Science of The Total Environment* **2016,** *539*, 196-205.
34. Rigdon, W. A.; Huang, X., Carbon monoxide tolerant platinum electrocatalysts on niobium doped titania and carbon nanotube composite supports. *Journal of Power Sources* **2014,** *272*, 845-859.
35. Yang, D.; Velamakanni, A.; Bozoklu, G.; Park, S.; Stoller, M.; Piner, R. D.; Stankovich, S.; Jung, I.; Field, D. A.; Ventrice, C. A., Chemical analysis of graphene oxide films after heat and chemical treatments by X-ray photoelectron and Micro-Raman spectroscopy. *Carbon* **2009,** *47*, (1), 145-152.
36. Afrooz, A. N.; Das, D.; Murphy, C. J.; Vikesland, P.; Saleh, N. B., Co-transport of gold nanospheres with single-walled carbon nanotubes in saturated porous media. *Water Research* **2016,** *99*, 7-15.
37. Aich, N.; Boateng, L. K.; Sabaraya, I. V.; Das, D.; Flora, J. R.; Saleh, N. B., Aggregation kinetics of higher order fullerene clusters in aquatic systems. *Environmental science & technology* **2016,** *50*, (7), 3562-3571.
38. Afrooz, A. N.; Khan, I. A.; Hussain, S. M.; Saleh, N. B., Mechanistic heteroaggregation of gold nanoparticles in a wide range of solution chemistry. *Environmental science & technology* **2013,** *47*, (4), 1853-1860.
39. Khan, I. A.; Aich, N.; Afrooz, A. R. M. N.; Flora, J. R. V.; ferguson, L.; sabo-Attwood, T.; Saleh, N. B., Fractal structures of single-walled carbon nanotubes in biologically relevant conditions: role of chirality vs. media conditions. *Chemosphere* **2013** *93*, (9), 1997-2003.
40. Afrooz, A. R. M. N.; Khan, I. A.; Hussain, S. M.; Saleh, N. B., Mechanistic Heteroaggregation of Gold Nanoparticles in a Wide Range of Solution Chemistry. *Environ. Sci. Technol.* **2013,** *47*, (4), 1853-1860.
41. Afrooz, A. R. M. N.; Sivalapalan, S. T.; Murphy, C. J.; Hussain, S. M.; Schlager, J. J.; Saleh, N. B., Spheres vs. rods: the shape of gold nanoparticles influences aggregation and deposition behavior. *Chemosphere* **2013,** *91*, (1), 93-98.

42. Chen, K. L.; Elimelech, M., Aggregation and deposition kinetics of fullerene (C60) nanoparticles. *Langmuir* **2006,** *22*, (26), 10994-11001.
43. Huynh, K. A.; McCaffery, J. M.; Chen, K. L., Heteroaggregation of multiwalled carbon nanotubes and hematite nanoparticles: Rates and mechanisms. *Environmental Science & Technology* **2012,** *46*, (11), 5912-5920.
44. Benjamin, M. M.; Lawler, D. F., *Water quality engineering: physical/chemical treatment processes*. John Wiley & Sons: 2013.
45. Wepasnick, K. A.; Smith, B. A.; Bitter, J. L.; Fairbrother, D. H., Chemical and structural characterization of carbon nanotube surfaces. *Analytical and bioanalytical chemistry* **2010,** *396*, (3), 1003-1014.
46. Naumkin, A. V.; Kraut-Vass, A.; Gaarenstroom, S. W.; Powell, C. J., NIST X-ray Photoelectron Spectroscopy Database In 2012.
47. Yang, H. G.; Sun, C. H.; Qiao, S. Z.; Zou, J.; Liu, G.; Smith, S. C.; Cheng, H. M.; Lu, G. Q., Anatase TiO2 single crystals with a large percentage of reactive facets. *Nature* **2008,** *453*, (7195), 638-641.
48. Sano, M.; Okamura, J.; Shinkai, S., Colloidal nature of single-walled carbon nanotubes in electrolyte solution: the Schulze-Hardy rule. *Langmuir* **2001,** *17*, (22), 7172-7173.
49. Chowdhury, I.; Duch, M. C.; Mansukhani, N. D.; Hersam, M. C.; Bouchard, D., Colloidal properties and stability of graphene oxide nanomaterials in the aquatic environment. *Environmental Science & Technology* **2013,** *47*, (12), 6288-6296.
50. Lanphere, J. D.; Luth, C. J.; Walker, S. L., Effects of solution chemistry on the transport of graphene oxide in saturated porous media. *Environmental Science & Technology* **2013,** *47*, (9), 4255-4261.
51. Liao, D. L.; Wu, G. S.; Liao, B. Q., Zeta potential of shape-controlled TiO2 nanoparticles with surfactants. *Colloids and Surfaces A: Physicochemical and Engineering Aspects* **2009,** *348*, (1–3), 270-275.
52. Long, T. C.; Saleh, N.; Tilton, R. D.; Lowry, G. V.; Veronesi, B., Titanium dioxide (P25) produces reactive oxygen species in immortalized brain microglia (BV2): implications for nanoparticle neurotoxicity. *Environmental Science & Technology* **2006,** *40*, (14), 4346-4352.
53. Suresh, L.; Walz, J. Y., Direct measurement of the effect of surface roughness on the colloidal forces between a particle and flat plate. *Journal of Colloid and Interface Science* **1997,** *196*, (2), 177-190.
54. Bouyer, F.; Robben, A.; Yu, W. L.; Borkovec, M., Aggregation of colloidal particles in the presence of oppositely charged polyelectrolytes: effect of surface charge heterogeneities. *Langmuir* **2001,** *17*, (17), 5225-5231.
55. Behrens, S. H.; Christl, D. I.; Emmerzael, R.; Schurtenberger, P.; Borkovec, M., Charging and aggregation properties of carboxyl latex particles: Experiments versus DLVO theory. *Langmuir* **2000,** *16*, (6), 2566-2575.
56. Kihira, H.; Ryde, N.; Matijević, E., Kinetics of heterocoagulation. Part. 2—The effect of the discreteness of surface charge. *Journal of the Chemical Society, Faraday Transactions* **1992,** *88*, (16), 2379-2386.

57. Suresh, L.; Walz, J. Y., Effect of Surface Roughness on the Interaction Energy between a Colloidal Sphere and a Flat Plate. *Journal of Colloid and Interface Science* **1996,** *183,* (1), 199-213.

Appendix B:

1. Vanysek, P., Electrochemical series. *CRC handbook of chemistry and physics* **1998,** *87*.